LARGE DEVIATIONS FOR DYNAMICAL SYSTEMS

WITH SMALL NOISE

A Dissertation

Presented to

the Faculty of the Department of Mathematics

University of Houston

In Partial Fulfillment

of the Requirements for the Degree

Doctor of Philosophy

By

Brett Geiger

April 2017

LARGE DEVIATIONS FOR DYNAMICAL SYSTEMS

WITH SMALL NOISE

_____

Brett Geiger

APPROVED:

_____

Prof. Robert Azencott, Advisor

_____

Dr. William Ott, Advisor

_____

Prof. Ilya Timofeyev, Advisor

_____

Dr. Ricardo Azevedo

_____

Dean, College of Natural Sciences and Mathematics

Acknowledgements

I would like to Dr. Azencott, Dr. Ott, and Dr. Timofeyev for agreeing to work with me over these past few years en route to completing my dissertation. Their constant support, encouragement, humor, and understanding along with their criticisms have been paramount in my success as a graduate student at the University of Houston. Even during the weeks in which progress was slow or I was discouraged, they continued to push and encourage me to keep going forward while remaining sympathetic to my struggles. A special thanks goes to Dr. Ott for agreeing to be my advisor initially and introducing me to Dr. Azencott and Dr. Timofeyev, which began the work in this dissertation.

The moment I knew I wanted to pursue a career in a mathematical field was back in 2004, my senior year of high school, where I took a Calculus class with Mrs. Marsha Poole. Her passion and knowledge of mathematics was truly an inspiration to me. I knew I wanted to emulate her style and approach to mathematics, which had been completely new to me at the time. This pushed me to major in mathematics at Nicholls State University in Thibodaux, LA. The rest, as they say, is history. A heartfelt thanks goes out to Mrs. Poole.

My parents Benjamin and Rose Geiger instilled in me and my siblings the importance of education from an early age, which is the root of my love for mathematics and thirst for education. My entire family, including siblings, aunts, uncles, and cousins, have been very supportive of my educational endeavors. After long and arduous semesters of work, they have always provided an opportunity f0r me to briefly escape from work to enjoy good company and good food back in Louisiana, which is

my home away from home. I owe everything in this world to my family, especially my parents, who have fought tooth and nail to allow me this educational opportunity.

Last, but certainly not least, I want to thank my numerous friends and colleagues. I have learned so much from all of them, and I have been able to truly enjoy my time here at the University of Houston because of them. I have had the utmost pleasure from sharing many mathematical and personal experiences with all of them which I will cherish for my entire life. I look forward to hopefully sharing many more with them.

LARGE DEVIATIONS FOR DYNAMICAL SYSTEMS
WITH SMALL NOISE

An Abstract of a Dissertation

Presented to

the Faculty of the Department of Mathematics

University of Houston

In Partial Fulfillment

of the Requirements for the Degree

Doctor of Philosophy

By

Brett Geiger

April 2017

Abstract

Dynamical systems with small noise can exhibit important rare events on long timescales. For systems driven by stochastic differential equations (SDEs) with small noise and no delay, classical large deviations theory quantifies rare events which are difficult to evaluate through direct simulation such as escapes from nominally stable fixed points. Near such fixed points, one can approximate nonlinear SDEs by linear SDEs. When delay is introduced, the situation is quite similar where nonlinear *delay* SDEs can be approximated by linear *delay* SDEs near metastable states.

For genetic evolution of bacterial populations of E. Coli modeled by discrete Markov chains with small mutation rates and random dilution, radical shifts in the genetic composition of large cell populations are *rare events* with quite low probabilities. Direct simulations generally fail to evaluate these events accurately. Large deviations theory then becomes a natural approach in order to quantify transition pathways linking a fixed initial population state to a desired target state.

In this dissertation, we first develop a fully explicit large deviations framework for (necessarily Gaussian) processes X_t driven by linear delay SDEs with small diffusion coefficients. Our approach enables fast numerical computation of the action functional controlling rare events for X_t and of the most likely paths transitioning from $X_0 = p$ to $X_T = q$. Via linear noise local approximations, we can then compute most likely routes of escape from metastable states for nonlinear delay SDEs. We apply our methodology to the detailed dynamics of a genetic regulatory circuit, namely the co-repressive toggle switch, which may be described by a nonlinear chemical Langevin SDE with delay. Second, we develop an applicable large deviations framework for a class of Markov chains used to model genetic evolution of E. Coli bacteria.

Finally, we apply this framework using realistic parameter sets in order to solve several difficult numerical and mathematical questions of high biological interest, such as computing the most likely evolutionary path linking two given population states in the fitness landscape and evaluating transition probabilities between successive genotype fixations.

Contents

ix

List of Figures

List of Tables

Chapter 1

Introduction

1.1 Broad Outline

Dynamical processes are often influenced by small random fluctuations acting on a variety of spatiotemporal scales. Small noise can dramatically affect the underlying deterministic dynamics by transforming stable states into metastable states and giving positive probability to *rare events* of high interest, such as excursions away from nominally stable states, transitions between metastable states, and fixations of genotypes in cell populations. These rare events play important functional roles in a wide range of applied settings, including genetic circuits [16], molecular dynamics, turbulent flows [7] and other systems with multiple timescales [6].

Populations of *bacteria* or *viruses* exhibit strong genetic adaptivity through emergence and fixation of beneficial mutations. Predictive studies of these evolutions

have strong potential impact on questions such as bacterial resistance to antibiotics or emergence of viral strains transferable from animal to humans. However, existing stochastic dynamic models for these populations still lack applicable algorithmic tools to quantify genetic evolution trajectories in the fitness landscape. Current analysis tends to rely on intensive simulations, which are not efficient to evaluate key rare events such as specific chains of beneficial genotype fixations.

Large deviations approaches then become natural tools to obtain quantitative information on rare events of interest. Their numerical applicability is still quite unexploited in concrete models, including cell population experiments and nonlinear stochastic differential equations (SDEs). In this dissertation, we will focus our theoretical and computational study on two stochastic models: genetic evolution of bacterial populations with concrete applications to the analysis of long-term laboratory experiments on Escherichia Coli and Gaussian diffusions with delay with a focus on applications to biochemical systems.

In the bacterial experiments (see [12, 22]), on day n, the current cell population pop_n has a fixed large size N and grows freely until nutrients exhaustion. At any time during this phase, the cells have a small chance of mutating. One then extracts (by dilution or otherwise) a random sample of roughly N cells, which constitutes the next day population pop_{n+1}. Therefore, many widely used genetic evolution models involve a succession of fixed duration growth phases with Poisson distributed mutations, alternating with random selection of a fixed size subsample. Typically, at the start of growth phase n, the population pop_n has then a roughly stable large size $N \geq 10^5$.

For Gaussian diffusions with delay, we are motivated in part by the importance of delay for the dynamics of genetic regulatory circuits. Many of these circuits can be modeled by a nonlinear delay SDE of Langevin type. Near metastable states, genetic circuits can be approximated by Gaussian diffusions with delay, which are linear delay SDEs, using Taylor expansions based at the stable state.

For bacterial populations, our first goal will be to develop, for a large population size N, a rigorous large deviations theory for population trajectories in the fitness landscape, where the state of pop_n is identified by the histogram H_n describing the g genotype frequencies. We will hence study the random histograms trajectories $\mathbf{H}(0, T) = [H_1 \, H_2 \, \ldots \, H_T]$ of arbitrary length T, which live on the path spaces S^T, where $S \subset \mathbb{R}^g$ is the compact convex set of histograms. We will derive an *explicit* large deviations cost function $\lambda(\mathbf{w}, T) \geq 0$ verifying $P(\mathbf{H}(0, T) = \mathbf{w}) \sim \exp(-N\lambda(\mathbf{w}, T))$ for all paths $w \in S^T$.

Our second goal will be, for any given histograms H and G, to characterize the histogram paths $\mathbf{w}^*$ which minimize the cost $\lambda(\mathbf{w}, T)$ over all histogram paths $\mathbf{w}$ starting at $w_1 = H$ and reaching $w_T = G$ at some finite time T. We will prove that for large N, these "cost geodesics" $\mathbf{w}^* = \mathbf{w}^*(H, G)$ are indeed the most likely population trajectories between the initial state H and terminal state G. We will derive a new and *explicit* second order recurrence equation satisfied by these "cost geodesics", which essentially solve in $\mathbb{R}^g$ the discretized Hamilton-Jacobi-Bellmann partial differential equations verified by the cost function $\lambda(\mathbf{w}, T)$.

Our third goal will be to develop feasible algorithms to solve the cost geodesics' second-order difference equation by geodesic shooting in reverse time. For genotype

3

numbers $g \leq 8$, this innovative approach will enable us to numerically compute in reasonable time the most likely population trajectories linking any two successive genotype fixations and to estimate the probabilities of these long term transitions. In doing so, we will also obtain the approximate time needed to complete this transition. We will apply our new computational techniques to analyze the genotypic data gathered by T. Cooper in his long term experiments on Escherichia Coli [11, 12], which deepen and extend the celebrated Lenski experiments [26, 27].

For Gaussian diffusions with delay, we rigorously develop and implement a *fully explicit* large deviations framework enabling fast numerical computation of optimal transition paths along with probabilistic estimates of such transitions occurring. We thus center our study on the Itô delay SDE

$$\begin{cases} \mathrm{d}X_t^\varepsilon = (a + BX_t^\varepsilon + CX_{t-\tau}^\varepsilon)\,\mathrm{d}t + \varepsilon\Sigma\,\mathrm{d}W_t, \\ X_t^\varepsilon = \gamma(t) \text{ for } t \in [-\tau, 0]. \end{cases} \tag{1.1}$$

Here $X_t^\varepsilon \in \mathbb{R}^d$, t denotes time, $\tau \geqslant 0$ is the delay, $a \in \mathbb{R}^d$, B and C are real $d \times d$ matrices, W_t denotes standard n-dimensional Brownian motion, $\Sigma \in \mathbb{R}^{d \times n}$ denotes the diffusion matrix, and $\varepsilon > 0$ is a small noise parameter. The initial history of the process is given by the Lipschitz continuous curve $\gamma : [-\tau, 0] \to \mathbb{R}^d$. We work with fixed delay to simplify the presentation – all of our results apply just as well to multiple delays and to random delay distributed over a finite time interval. We demonstrate the utility of our approach by computing optimal escape trajectories from a small neighborhood of a metastable state for the co-repressive toggle switch, a bistable genetic circuit driven by a nonlinear delay Langevin equation.

1.2   Outline of Each Chapter

This dissertation will focus on applications of large deviations principles. The chapters to follow will discuss the systems in biochemistry and bacterial evolution to which the principles will be applied, as stated in the outline above.

In Chapter 2, we discuss the biology background in relation to the systems we study. In Section 2.1, we discuss the concept of excitability in biochemical systems. We note the importance of cellular noise and transcriptional delay in influencing the dynamics of genetic regulatory networks where bistability becomes a characteristic of interest. These dynamical networks can be described by chemical Langevin equations, which are nonlinear delay SDEs, where the delay and noise appear explicitly. In Section 2.1.1, we discuss how these systems can be simplified and linearized through a linear noise approximation, which involves Taylor expansions. Doing so yields a linear delay SDE with additive noise called a *Gaussian diffusion with delay*. In Section 2.2, we present a particular biochemical system known as the corepressive toggle switch which models two protein species who represses the production of each other along with the resulting linearization in Section 2.2.1.

Once this is completed, we move on to discuss evolution of bacterial populations in Section 2.3. We focus on populations of E. Coli in Section 2.3.1 where we discuss characteristics of E. Coli cells. We also discuss relevant experiments conducted to analyze the behavior of these populations as well as estimate systems parameters such as mutation rates, growth rates, et cetera. Motivated by these experiments, we end this chapter by presenting the stochastic model used to study E. Coli populations,

which is a discrete Markov chain consisting of daily cycles involving growth, mutation, and dilution.

With the necessary background and stochastic models presented, we shift to some probabilistic and statistical calculations in Chapter 3 that will be relevant in our later large deviations study. We begin with the mean and covariance of Gaussian diffusions with delay in Section 3.1. We justify that a Gaussian diffusion with delay is indeed a Gaussian process. Therefore, it is reasonable to expect that the mean and covariance become key elements in the large deviations analysis to follow. Since a Gaussian diffusion with delay has such a nice form, we can write a delay ODE for the mean, which is presented in Section 3.1.1. Later large deviations principles apply only to centered processes (mean zero), so by writing a centered version of the Gaussian diffusion with delay X_t, we get another Gaussian diffusion with delay Z_t that is centered. Thus, the covariance of this centered process becomes useful. In Section 3.1.3, we derive a first-order nonhomogeneous linear delay ODE for the covariances of Z_t. The nonhomogeneous term also satisfies a linear delay ODE so that we may discuss the analytical solutions of these equations, which appears in Sections 3.1.4 and 3.1.5. These types of differential equations can be solved using a natural step-by-step approach that reduces the delay ODE into a sequence of nonhomogeneous ODEs with no delay where the nonhomogeneous term involves the delay term in the equation.

In Section 3.2, we derive the relevant formulas and probabilities associated to

6

genetic evolution of E. Coli. In Sections 3.2.1-3.2.3, we present formulas and probabilities associated to deterministic growth, independent Poisson mutations, and random selection. This immediately yields the one-step transition probability, given in Section 3.2.4, which describes the probability of transitioning from one histogram to another during a daily cycle. Since we will state a large deviations principle for random histogram trajectories associated to the Markov chain, this probability will be important in the large deviations analysis. Section 3.2.5 ends the chapter by deriving the mean trajectory of genetic evolution of E. Coli. This trajectory will represent the most likely evolutionary track that the system will take when cell populations become very large.

We move on to Chapter 4 where we discuss large deviations theory and background that will be applicable to the models that we have described. In Section 4.1, we present the formal large deviations problem stated in terms of empirical distributions, which was the main focus of study for the classical Cramer-Chernoff large deviations study. Large deviations can be thought of as a study of the tails of distributions. This often reveals quantitative information on rare events. We present the classical Cramer-Chernoff theorem in Section 4.2. The central items that reveal asymptotic decay rates of probabilities is the Cramer transform and Cramer set functional. We define these explicitly. We end the section by providing an intuitive interpretation of Cramer transforms in terms of the Cramer-Chernoff theorem. We also discuss the connection of the Cramer transform to the Laplace transform of a probability μ.

In Section 4.3, we discuss the general large deviations principles and framework

for Gaussian measures and processes, which will be relevant to Gaussian diffusions with delay. The Cramer transform in this case, which is for centered Gaussian processes, reveals the importance of the covariance since it is defined in terms of the covariance operator. In fact, we compare the Cramer transform associated to Gaussian processes as an energy functional. Indeed, when we consider the classical Gaussian process known as Brownian motion, the Cramer transform associated to Brownian paths is given as the kinetic energy formula.

In Section 4.4, we present the large deviations principles for one-step transition probabilities and random histogram trajectories associated to E. Coli evolution. We show a complete derivation of the one-step cost function in Section 4.4.1. This calculation makes use of Taylor expansions in terms of the mutation rates, which are assumed to be small. Once the one-step cost is derived, we immediately get the cost function of an evolutionary trajectory written as a sum of one-step costs. This leads to a large deviations principle for random histogram trajectories, which is stated in Section 4.4.2.

Establishing large deviations principles allows one to consider applications of said principles. We accomplish this in Chapter 5 with Gaussian diffusions with delay and genetic evolution of E. Coli populations. In both cases, we seek to find the most likely path which links an initial point to a desired target point. In Section 5.1, we accomplish this for Gaussian diffusions with delay by minimizing the Cramer transform for Gaussian processes. This minimizing path is explicit in terms of the mean of the process X_t, covariance of the centered process Z_t, and the target point. In Section 5.2, we numerically minimize the cost function. Most likely evolutionary

trajectories in this setting are shown to be completely determined by their final two points.

In Chapter 6, we discuss implementation of the results from Chapter 5. Section 6.1 focuses on simulating the relevant delay ODEs for Gaussian diffusions with delay. With the step-by-step method described previously, we can essentially simulate these equations using classical numerical ODE schemes. We then discuss the numerical minimization of the Cramer transform and calculation of exit paths from neighborhoods of stable stationary states.

In Section 6.2, we design methods to generate most likely evolutionary trajectories linking and initial histogram to a desired target histogram. We use a reverse shooting algorithm which generates trajectories recursively in reverse time. We then discuss numerical challenges associated to this approach in Section 6.2.3. The reverse shooting method will depend heavily on the penultimate histogram; therefore, many computational issues arise relating to algorithm efficiency. We present three conjectures which can be used efficiently generate optimal trajectories. The chapter concludes with analysis of these conjectures using the case of three genotypes. In this setting, we can let every histogram be a possible penultimate point so that we can analyze which points may yield optimal paths.

With the algorithms now explicitly described, we calculate most likely trajectories for the corepressive toggle switch and E. Coli populations with four genotypes in Chapter 7. For the corepressive toggle switch, we calculate optimal escape trajectories from a neighborhood of a stable state. For E. Coli populations, we calculate three most likely trajectories linking a fixed initial state to desired target states near

the boundaries. We then provide brief analyses and predictions for higher dimensions (more genotypes). The dissertation then concludes with Chapter 8 which contains a summary and plans for future work.

Chapter 2

Biochemical and Biological Background and Models

The interplay between genetic regulatory networks and genetic evolution provide many interesting applications of large deviations principles in order to study the persistence of cellular populations over time. Charles Darwin's theory of evolution through natural selection states that organisms adjust to environmental challenges through favorable mutations. These favorable mutations, which occur in DNA and genes, then spread to the entire population over several generations. This creates a population in which the fittest organisms survive, essentially exterminating weaker organisms and creating an improved, evolved population. Genetic regulatory networks are responsible for translating these beneficial mutations to create a stronger organism. In this section, we will briefly discuss background material relating to the dynamics of gene networks and genetic evolution along with important rare events

that manifest in these settings. We will then present a biochemical model used to describe the concentration of two protein species and a stochastic model used to describe evolution of E. Coli cells.

2.1   Excitable systems from biochemistry

Translation of a cell's genetic configuration (genotype) to observable characteristics (phenotype) is a key function of gene regulatory networks. Gene regulatory networks control gene expression in order to provide cells with a way to battle environmental challenges in order to prolong its existence. These dynamics are naturally affected by many factors which can create delay in protein production, noise, et cetera. Therefore, creating accurate models for gene networks becomes key in mathematical biology. We begin by explaining the importance of noise, delay, and metastability for the dynamics of genetic regulatory circuits. Such circuits may be described by delay SDEs [8,20] and represent a significant class of systems to which our large deviations framework for Gaussian diffusions with delay can be applied.

Cellular noise and transcriptional delay shape the dynamics of genetic regulatory circuits. Stochasticity within cellular processes arises from a variety of sources. Sequences of chemical reactions at low molecule numbers produce an intrinsic form of noise. Multiple other types of variability affect dynamics across spatial and temporal scales. Examples include fluctuations in environmental conditions, metabolic processes, energy availability, et cetera. Noise functions constructively in both microbial

and eukaryotic cells and on multiple timescales. It enables probabilistic differentiation strategies for cell populations, such as stochastic state-switching in bistable circuits and transient cellular differentiation in excitable circuits (*e.g.* [14, 16, 38]).

Certain circuit architectures such as toggle switches and excitable circuits enable noise-induced rare events. These architectures allow cellular populations to probabilistically switch states in response to environmental fluctuations [16].

Bistability is a central characteristic of biological switches. It is essential in the determination of cell fate in multicellular organisms [24], the regulation of cell cycle oscillations during mitosis [21], and the maintenance of epigenetic traits in microbes [35]. Metastable states can be created by positive feedback loops. Once a trajectory enters a metastable state, it will typically remain there for a considerable amount of time before noise induces a transition [16, 25]. This phenomenon has been studied in many contexts, including the lysis/lysogeny switch of bacteriophage λ [1, 40], bacterial persistence [4], and synthetically constructed positive feedback loops [18, 34].

Many biological systems exhibit excitability [15, 33, 38]. Excitable systems commonly feature a single metastable state bordered by a sizable, active region of phase space. When stochastic fluctuations cause a trajectory to exit the basin of attraction of this metastable state, the trajectory will make a large excursion before returning to the basin. Transient differentiation into a genetically competent state in *Bacillus subtilis*, for example, is enabled by an excitable circuit architecture. Positive feedback controls the threshold for competent event initiation, while a slower negative feedback loop controls the duration of competence events [9, 29, 30, 37, 38]. Rare

events in such excitable systems manifest as bursts of activity.

2.1.1   General linear noise approximations (LNAs)

We explain how Gaussian diffusions driven by delay SDEs such as (1.1) arise from linear noise approximations of nonlinear delay SDEs in a neighborhood of a metastable state, which we apply to the co-repressive toggle switch to obtain our local model in which our large deviations results will apply. Brett and Galla [8] introduced linear noise approximations for chemical Langevin equations modeling biochemical reaction networks.

Consider the delay SDE

$$\mathrm{d}x_t = f(x(t), x(t-\tau))\,\mathrm{d}t + \frac{1}{\sqrt{N}}g(x(t), x(t-\tau))\,\mathrm{d}W_t. \tag{2.1}$$

Here $f : \mathbb{R}^d \times \mathbb{R}^d \to \mathbb{R}^d$, $g : \mathbb{R}^d \times \mathbb{R}^d \to \mathbb{R}^{d\times n}$, W_t denotes standard n-dimensional Brownian motion, and $N > 0$ denotes system size (characteristic number of molecules in a biochemical system). Notice that we allow both the drift and the diffusion to depend on the past. Suppose $x^\infty(t)$ solves the deterministic limit of (2.1); that is, $x^\infty(t)$ solves

$$\mathrm{d}x_t = f(x(t), x(t-\tau))\,\mathrm{d}t. \tag{2.2}$$

As we have indicated in our introduction, around a stable point z of the limit ODE as N tends to infinity, one can approximate such a system by a Gaussian diffusion with delay and small diffusion matrix $\frac{1}{\sqrt{N}}\Sigma$. Define $\xi(t)$ by

$$x(t) = x^\infty(t) + \xi(t).$$

14

Substituting this ansatz into (2.1) and performing Taylor expansions of f and g based at the deterministic trajectory yields the linear noise approximation

$$
\begin{aligned}
\mathrm{d}\xi_t = {} & [D_1 f(x^\infty(t), x^\infty(t-\tau))\xi(t) + D_2 f(x^\infty(t), x^\infty(t-\tau))\xi(t-\tau)]\,\mathrm{d}t \\
& + \frac{1}{\sqrt{N}} g(x^\infty(t), x^\infty(t-\tau))\,\mathrm{d}W_t.
\end{aligned}
\tag{2.3}
$$

Here D_1 and D_2 denote differentiation with respect to the first and second sets of d arguments, respectively. If $x^\infty(t)$ happens to be a stable fixed point of (2.2), say $x^\infty(t) \equiv z$, then (2.3) becomes

$$
\mathrm{d}\xi_t = [D_1 f(z, z)\xi(t) + D_2 f(z, z)\xi(t-\tau)]\,\mathrm{d}t + \frac{1}{\sqrt{N}} g(z, z)\,\mathrm{d}W_t.
$$

This is (1.1) with $a = \mathbf{0}$, $B = D_1 f(z, z)$, $C = D_2 f(z, z)$, $\Sigma = g(z, z)$, and $\varepsilon = \frac{1}{\sqrt{N}}$.

2.2 Corepressive Toggle Switch

The genetic toggle switch we study consists of two protein species, each of which represses the production of the other. We model the switch using the chemical Langevin equation

$$
\mathrm{d}x = \left(\frac{\beta}{1 + y(t-\tau)^2/k} - \gamma x \right) \mathrm{d}t + \frac{1}{\sqrt{N}} \left(\frac{\beta}{1 + y(t-\tau)^2/k} + \gamma x \right)^{\frac{1}{2}} \mathrm{d}W_1
\tag{2.4a}
$$

$$
\mathrm{d}y = \left(\frac{\beta}{1 + x(t-\tau)^2/k} - \gamma y \right) \mathrm{d}t + \frac{1}{\sqrt{N}} \left(\frac{\beta}{1 + x(t-\tau)^2/k} + \gamma y \right)^{\frac{1}{2}} \mathrm{d}W_2,
\tag{2.4b}
$$

where x and y denote the concentrations of the two protein species, β denotes maximal protein production rate, k is the protein level at which production is cut in half, γ is the dilution rate, N denotes system size, and W_1 and W_2 are independent

standard Brownian motions. Notice that (2.4) is a symmetric system. In the deter-ministic limit as $N \to \infty$, the co-repressive toggle switch is described by the reaction rate equations

$$\mathrm{d}x = \left(\frac{\beta}{1 + y(t-\tau)^2/k} - \gamma x \right) \mathrm{d}t \tag{2.5a}$$

$$\mathrm{d}y = \left(\frac{\beta}{1 + x(t-\tau)^2/k} - \gamma y \right) \mathrm{d}t. \tag{2.5b}$$

System (2.5) has two stable stationary states, $(x_{\text{low}}, y_{\text{high}})$ and $(x_{\text{high}}, y_{\text{low}})$, as well as a saddle stationary state (x_s, y_s). See [20, Figure 7] or [39, Figure 3A, inset] for a phase portrait of (2.5).

In the stochastic $(N < \infty)$ regime, a typical trajectory of the co-repressive toggle switch will spend most of its time near the metastable states, occasionally hopping from one to the other [39, Figure 3A]. Such rare events raise interesting questions. For large N, is the co-repressive toggle switch well-approximated by a two-state Markov chain on long timescales? If so, what are the transition rates? To determine these rates, one would need to compute both a quasipotential and a formula of Eyring-Kramers type.

2.2.1 Approximation by Gaussian Diffusions with delays

We study an approximation of (2.4) by Gaussian diffusions with delay that is valid in a neighborhood of $(x_{\text{low}}, y_{\text{high}}) =: (v, w)$. We note that we chose the stable stationary state $(x_{\text{low}}, y_{\text{high}})$ without loss of generality as we easily would get symmetric results

had we chosen the stable state $(x_{\text{high}}, y_{\text{low}}) = (w, v)$. Writing

$$x(t) = v + \xi_1(t), \qquad y(t) = w + \xi_2(t),$$

the Gaussian diffusion with delay is given by

$$d\xi_1(t) = \left(-\gamma\xi_1(t) - \frac{2\beta w}{k[1 + w^2/k]^2}\xi_2(t - \tau) \right) dt + \frac{1}{\sqrt{N}} \left(\frac{\beta}{1 + w^2/k} + \gamma v \right)^{1/2} dW_1(t),$$

$$d\xi_2(t) = \left(-\gamma\xi_2(t) - \frac{2\beta v}{k[1 + v^2/k]^2}\xi_1(t - \tau) \right) dt + \frac{1}{\sqrt{N}} \left(\frac{\beta}{1 + v^2/k} + \gamma w \right)^{1/2} dW_2(t).$$

$$(2.6)$$

The system (2.6) represents a local approximation of the co-repressive toggle switch near the stable state (v, w).

2.3   Genetic Evolution of Bacterial Populations

Because of the prominence of mutations and cell fitness in adaptive evolution of bacterial and viral populations, many genetic evolution experiments are driven towards mutation rate and selective advantage estimations. Once these parameters are sufficiently understood, one can use realistic models in order to better understand the genetic evolution of cell populations. A comprehensive study of these parameters has been carried out by Zhang, et. al. [41] for E. Coli populations. We briefly describe the experiments used to study the genetic evolution of E. Coli. Then, we fully describe the class of Markov chains used to model random bacterial evolutions.

2.3.1   Genetic evolution experiments for E. Coli bacteria

E. Coli bacteria colonize mammal or human digestive tracks, where each E. Coli cell splits into 2 cells roughly 20 to 40 minutes after its birth depending on cell genotype and nutrients availability. Cell divisions may be randomly affected by gene mutations with very small occurrence rates in the 10^{-8} to 10^{-6} range. These mutations may occur at any time over a cell's lifespan and often improve a cell's selective advantage; that is, mutations are usually unidirectional and irreversible. Mutations with strong selective advantage (linked to faster rates of exponential growth) seem to only affect a small set of well-identified genes sites. When nutrients are exhausted, exponential growth stops and cells enter into a stasis regime. A few times per day in the host digestive system, E. Coli colonies are also submitted to abrupt intensive population reduction to a roughly stable large size N. The evolution of these large cell populations thus involves a sequence of cycles where exponential growth and random mutation alternate with random selection.

Laboratory experiments on E. Coli evolution [11, 12, 22, 26, 27] emulate these cycles. Fresh cell colonies of fixed size N are extracted daily (by fixed-rate dilution or otherwise) from previous day colonies and then injected into test wells filled with glucose solutions containing always the same amount of nutrients. After a roughly fixed time τ such as 8 to 12 hours, each such new colony grows to a large fairly stable saturation size $N_{sat} >> N$ determined by the initial amount of nutrients. The population is then diluted at roughly fixed rate N/N_{sat} the next day to generate new colonies of size N. These daily random selections have a strong *bottleneck effect* [22, 36, 41] on the emergence and persistence of new genotypes since very few

new mutants born during a daily cycle are transferred to the next day's population.

For the E. Coli evolution experiments in [12], one has $N \sim 50,000$, $8\,\text{hours} \leq \tau \leq 10\,\text{hours}$, $N_{sat} \sim 10^7$, and the daily growth factors F_j range from 200 to 400. Several mutation rates are equal to 0 since "regressive" mutations where $F_j < F_k$ are often impossible. The non-zero mutation rates range from 10^{-8} to 10^{-6}. For the E. Coli experiments in [22], the situation is quite similar, but the stable population size $N \sim 10^8$ is much larger. In actual experiments, useful biological inferences can be derived from "short" genotype descriptions involving only a few well identified genes, typically less than 5 key genes, so that the number g of observable genotypes remains moderate with $g \leq 32$. Over a thousand daily cycles, each initial colony of pure "ancestor" genotype will generate at most 6 to 8 successive genotype fixations so that for experiments spanning 3 years, useful models can already be built with as few as $g = 8$ genotypes.

2.3.2   Stochastic models for bacterial evolution experiments

To model the main features of random bacterial evolutions, the following class of Markov chains has often been used [22, 36, 41] and will be called *locked box* models here. The finite set of distinct genotypes is denoted $\Gamma = \{1, 2, \ldots, g\}$. Cells of genotype j (called *j-cells* here) have rate of exponential growth $f_j > 0$, called the *fitness* of genotype j.

Genetic evolution is modeled as a sequence of cycles, called here "daily" cycles as is the case for many experimental contexts. The nth cycle starts with a population

pop_n of fixed large size N and involves three successive steps to generate pop_{n+1}:

(1) Deterministic growth with no mutations: The size of each j-cell colony in pop_n is multiplied by the *growth factor* $F_j = \exp(\tau f_j)$ where τ is a fixed growth duration parameter.

(2) Independent random mutations: For any two distinct genotypes (j, k), a random number $R_{j,k}$ of j-cells mutate into k-cells. Let $siz_n(j)$ be the j-cells colony size after growth step 1. The random variable $R_{j,k}$ has a Poisson distribution with mean $siz_n(j)M_{j,k}$ where the mutation rates $M_{j,k}$ are fixed and very small.

(3) Random Selection: After step 2, the population has reached a saturation size N_{sat} much larger than N, and one extracts a random sample of fixed size N, which constitutes pop_{n+1}.

The stochastic transition $pop_n \to pop_{n+1}$ is then a Markov chain on a state space of finite but very large size g^N. In laboratory evolution experiments, observable data systematically come from the populations pop_n of fixed size N with a specific focus on successive genotype fixations. The key model parameters are the number g of genotypes, the fixed size N of all daily initial populations pop_n, the multiplicative growth factors $F_j = e^{\tau f_j}$, and the $(g \times g)$ matrix M of mutation rates $M_{j,k}$.

Chapter 3

Probabilistic and Statistical Calculations

The linear delay SDE we call a Gaussian diffusion with delay can be viewed as a small random perturbation of a deterministic system. The underlying deterministic system in this case is precisely the mean trajectory. When the noise level (randomness) approaches 0, the system converges to the mean trajectory. For stochastic evolution of E. Coli populations, the population size N becomes the main parameter that controls the randomness of the system so that when N approaches ∞, the system approaches the deterministic mean trajectory. The large deviations principles that we discuss in Section 4 essentially show that the probabilities of the occurrences of events other than the mean converge exponentially quickly to 0 when the noise level approaches 0 or population size approaches ∞. In the case of Gaussian diffusions with delay, this exponential decay rate involves the mean of the process X_t verifying (1.1),

which we will show is a Gaussian process, and the covariance of a centered process Z_t defined by $X_t = m(t) + \varepsilon Z_t$, which is also a Gaussian diffusion with delay. While this is not the case for stochastic evolution of E. Coli, the mean trajectory is of interest since this is the underlying deterministic system. The mean trajectory will also be utilized in the method used to generate most likely trajectories in Section 5.2. In addition, since random histogram trajectories $\mathbf{H}(0, T) \equiv \mathbf{H} = [H_0 \, H_1 \, \ldots \, H_T]$ describing the evolution of E. Coli populations up to day T are composed of daily transitions $H_n \to H_{n+1}$, the one-step transition probability becomes paramount in establishing and applying large deviations principles to $\mathbf{H}$. Thus, we will calculate the mean trajectory and one-step transition probability explicitly. In the case of Gaussian diffusions with delay, the mean and covariance under consideration are described by delay ODEs which we solve analytically and numerically.

3.1 Mean and Covariance of Gaussian Diffusions with Delay

Recall that a Gaussian diffusion with delay is defined by the linear delay SDE given by (1.1). Notice that we have not yet established that a process verifying this system is Gaussian. Thus, we first show that (1.1) defines a Gaussian process by first discretizing and then taking an L^2-limit.

Proposition 3.1.1. *The delay SDE* (1.1) *has a unique strong solution X_t, which is a Gaussian process.*

Proof of Proposition 3.1.1. The existence of a unique strong solution X_t is classical (see *e.g.* [31]). To see that X_t is Gaussian, we consider Euler-Maruyama discretizations [23]. For positive integers N, let $\Delta = \tau/N$ denote time step size. The Euler-Maruyama approximate solution $Y_t^{(\Delta)}$ to (1.1) is defined first at nonnegative integer multiples of Δ by

$$Y_{(k+1)\Delta}^{(\Delta)} = Y_{k\Delta}^{(\Delta)} + (a + BY_{k\Delta}^{(\Delta)} + CY_{k\Delta-\tau}^{(\Delta)})\Delta + \varepsilon\Sigma(W_{(k+1)\Delta} - W_{k\Delta})$$

and then on $[0, T]$ by interpolation. Much is known about the convergence of EM schemes for delay SDEs (see *e.g.* [3, 32]). In particular, we have

$$\lim_{\Delta \to 0} \mathbb{E}\left[\sup_{0 \leqslant t \leqslant T} |Y_t^{(\Delta)} - X_t|^2\right] = 0$$

by Theorem 2.1 of [32]. Since $Y_t^{(\Delta)}$ is Gaussian by construction, this L^2-convergence implies that X_t is Gaussian as well. $\qquad\square$

Since the process X_t is Gaussian, it is completely determined by its mean and covariance. First, we write a delay ODE that is verified by the mean of X_t.

3.1.1   Delay ODE for the mean of X_t

Writing (1.1) in integral form, we have

$$X_t = X_0 + \int_0^t (a + BX_z + CX_{z-\tau})\, \mathrm{d}z + \varepsilon\Sigma W_t. \tag{3.1}$$

Taking the expectation of (3.1) and applying Fubini gives

$$m(t) = m(0) + \int_0^t (a + Bm(z) + Cm(z - \tau))\, \mathrm{d}z,$$

or, in differential form, a delay ODE for $m(t)$:

$$\begin{cases} m'(t) = a + Bm(t) + Cm(t - \tau) \\ m(t) = \gamma(t) \text{ for } t \in [-\tau, 0]. \end{cases} \tag{3.2}$$

We note that our eventual goal will be to apply large deviations principles to the Gaussian process X_t (see Section 4.3.2). These principles assume that the process X_t is centered, which is not true in general. Thus, we need to define a process that is a centered version of X_t so that we can apply these principles.

3.1.2 The centered Gaussian process Z_t

Given a Gaussian diffusion with delay X_t, the process Z_t defined by $X_t = m(t) + \varepsilon Z_t$ is a centered Gaussian diffusion with delay. Since X_t verifies (1.1) and $m(t)$ verifies (3.2), elementary algebra shows that Z_t verifies the delay SDE

$$\begin{cases} \mathrm{d}Z_t = (BZ_t + CZ_{t-\tau})\,\mathrm{d}t + \Sigma\,\mathrm{d}W_t, \\ Z_t = 0 \text{ for } t \in [-\tau, 0] \end{cases} \tag{3.3}$$

Note that this delay ODE *does not depend on* ε. This is a crucial point further on because our key large deviations estimates will be stated in path space for the centered Gaussian process εZ_t . In Section 5.1, our large deviations computations will essentially involve the deterministic mean path of X_t and the covariance function $\rho(s, t)$ of the process Z_t. The importance of the mean and covariance in our large deviations computations is not surprising since these statistics characterize Gaussian processes.

3.1.3 Delay ODEs for the covariances of Z_t

We now find delay ODEs for the covariance of Z_t. Denote A^* the matrix transpose of A, and let

$$\rho(s,t) = \mathbb{E}[Z_s Z_t^*]$$

be the covariance matrix of Z_s and Z_t. Since the history of Z_t anterior to $t = 0$ is deterministic, $\rho(s,t) = 0$ when either s or t are in $[-\tau, 0]$. Fix $t \in [0, T]$, and let s vary. We have

$$\mathbb{E}[Z_s Z_t^*] = \int_0^s \left(B\mathbb{E}[Z_u Z_t^*] + C\mathbb{E}[Z_{u-\tau} Z_t^*] \right) \mathrm{d}u + \Sigma\mathbb{E}[W_s Z_t^*].$$

We thus obtain

$$\rho(s,t) = \int_0^s \left(B\rho(u,t) + C\rho(u-\tau,t) \right) \mathrm{d}u + \Sigma\mathbb{E}[W_s Z_t^*]. \tag{3.4}$$

Let $G(s,t) = \mathbb{E}[W_s Z_t^*]$. Differentiating $\rho(s,t)$ with respect to s gives

$$\frac{\partial \rho}{\partial s}(s,t) = B\rho(s,t) + C\rho(s-\tau,t) + \Sigma\frac{\partial G}{\partial s}(s,t), \tag{3.5}$$

which is a first-order delay ODE in s for each fixed t. To close (3.5), we compute a differential equation for $\frac{\partial G}{\partial s}(s,t)$. Proceeding as just done for (3.4), one checks that the function $G(s,t)$ satisfies the ODE

$$\frac{\partial G}{\partial t}(s,t) = \begin{cases} G(s,t)B^* + G(s,t-\tau)C^* + \Sigma^* & (t \leq s); \\ G(s,t)B^* + G(s,t-\tau)C^* & (t > s), \end{cases} \tag{3.6}$$

where $G(s,t) = 0$ for $t \in [-\tau, 0]$. Let $H(x)$ denote the Heaviside function

$$H(x) = \begin{cases} 0 & x < 0 \\ 1 & x \geq 0 \end{cases}.$$

We can rewrite (3.6) as

$$\frac{\partial G}{\partial t}(s,t) = G(s,t)B^* + G(s,t-\tau)C^* + \Sigma^* H(s-t). \tag{3.7}$$

Note that the partial derivative of the Heaviside distribution $H(s-t)$ is classically given by

$$\frac{\partial H}{\partial s}(s-t) = \delta(s-t),$$

where the distribution $x \to \delta(x)$ is the Dirac point mass concentrated at $x = 0$. By definition of $G(s,t)$ and by (3.7), the function $G(s,t)$ is continuous for all s and t and differentiable in s and t for $s \neq t$. We will denote, for $s \neq t$,

$$F(s,t) := \frac{\partial G}{\partial s}(s,t) \tag{3.8}$$

so that F verifies the initial condition $F(s,t) = 0$ for $s \neq t$ and $t \in [-\tau, 0]$.

Differentiating (3.7) in s for $s \neq t$ and switching the order of partial derivatives yields a linear delay ODE in $t > 0$ for $F(s,t)$, namely

$$\frac{\partial F}{\partial t}(s,t) = F(s,t)B^* + F(s,t-\tau)C^* + \Sigma^* \delta(s-t) \tag{3.9}$$

with initial condition $F(s,t) = 0$ for all $t \in [-\tau, 0]$.

Once $F(s,t)$ is determined, the covariance $\rho(s,t)$ for each fixed $t \in [0,T]$ will be computed by solving the delay ODE

$$\frac{\partial \rho}{\partial s}(s,t) = B\rho(s,t) + C\rho(s-\tau,t) + \Sigma F(s,t). \tag{3.10}$$

We now describe how to successively solve the delay ODEs driving $m(t), F(s,t)$, and $\rho(s,t)$.

26

3.1.4 Analytical solution of the delay ODE verified by the mean

First-order delay ODEs can be analytically solved by a natural stepwise approach, sometimes called "method of steps," a terminology which we will avoid since it is has a different meaning in classical numerical analysis. The basic idea is to convert each one of our delay ODE into a finite sequence of nonhomogeneous ODEs in which the delay terms successively become known terms. Consider first the delay ODE (3.2) for $m(t)$ with $t \in [-\tau, T]$. The delay term $Cm(t - \tau)$ is unknown for $t \in (\tau, T]$ but is known for $t \in [0, \tau]$. So we can solve the delay ODE (analytically or numerically) on the interval $[0, \tau]$ as a linear non-homogeneous first-order ODE. Then, for $t \in [\tau, 2\tau]$, the delay ODE turns again into a linear non-homogeneous first-order ODE where the delay term has actually just been computed. One can thus successively solve the delay ODE on intervals $[k\tau, (k+1)\tau]$ to get a full step-by-step solution on all of $[0, T]$.

We first describe the explicit solution of the mean $m(t)$ on $[-\tau, T]$. For $x \in \mathbb{R}$, denote $\lfloor x \rfloor$ as the greatest integer less than or equal to x. Partition the interval $[-\tau, T]$ into closed subintervals of the form $[(k-1)\tau, k\tau]$ where $k = 0, 1, 2, \ldots, \lfloor \frac{T}{\tau} \rfloor$ with final partition interval $\left[\lfloor \frac{T}{\tau} \rfloor \tau, T \right]$. Let $m_k(t)$ denote the solution to the DDE on the interval $[(k-1)\tau, k\tau]$ and $m_{\lfloor \frac{T}{\tau} \rfloor + 1}(t)$ denote the solution of $m(t)$ on the final partition interval. When $k = 0$, we have $m_0(t) = \gamma(t)$. Now, when $k = 1$, the intial

condition gives the following ODE for $m_1(t)$, the solution of $m(t)$ on $[0, \tau]$:

$$\begin{cases} m_1'(t) = a + Bm_1(t) + C\gamma(t - \tau) \\ m_1(0) = \gamma(0). \end{cases}$$

We can write the solution $m_1(t)$ as

$$m_1(t) = e^{tB} \int_0^t e^{-uB} \left(a + C\gamma(u - \tau) \right) \, \mathrm{d}u + e^{tB}\gamma(0).$$

Call $m_k(t)$ the solution $m(t)$ on the interval $J_k = [(k-1)\tau, k\tau]$ for $k = 0, 1, 2, \dots, \lfloor \frac{T}{\tau} \rfloor$.
Given $m_{k-1}(t)$ for t in J_{k-1}, we can similarly compute $m_k(t)$ by

$$m_k(t) = e^{(t-(k-1)\tau)B} \int_{(k-1)\tau}^t e^{-uB} \left(a + Cm_{k-1}(u - \tau) \right) \, \mathrm{d}u + e^{(t-(k-1)\tau)B} m_{k-1}((k-1)\tau).$$

Finally, piecing together all the $m_k(t)$ yields the full solution $m(t)$ on all of $[-\tau, T]$.
Note that many characteristics of the initial segment γ, such as continuity, differen-
tiability, discontinuities, etc., will essentially propagate through to the solution $m(t)$
at each step. More precisely, if γ is of class C^q on $[-\tau, 0]$ for some integer $q \geq 0$, then
$m(t)$ will be of class $q + 1$ for all t except possibly at integer multiples of τ. Since we
assume here that γ is Lipschitz continuous, $m(t)$ will be differentiable except possibly
at integer multiples of τ.

3.1.5 Analytical solutions of the delay ODEs verified by $F(s, t)$ and $\rho(s, t)$

We can extend the preceding method to the ODE in s verified by $F(s, t)$ for each
fixed s and then to the ODE in t verified by $\rho(s, t)$. We first focus on $F(s, t)$. Fix

28

$s \in [0, T]$. Due to the delay ODE (3.9), the distribution ϕ_s defined on R^+ by

$$\phi_s(t) = F(s,t) + \Sigma^* H(s-t)$$

clearly verifies the delay ODE

$$\frac{\partial \phi_s}{\partial t}(t) - \phi_s(t)B^* - \phi_s(t-\tau)C^* = -\Sigma^* H(s-t)B^* - \Sigma^* H(s-t+\tau)C^* \quad (3.11)$$

with initial condition

$$\phi_s(t) = \Sigma^* H(s-t) \text{ for all } t \in [-\tau, 0].$$

Note that for each fixed $s > 0$ this initial condition is a bounded and continuous function of $t \in [-\tau, 0]$. For each fixed s, the right hand side of equation (3.11) is the function θ_s defined for $t \geq 0$ by

$$\theta_s(t) = -\Sigma^* H(s-t)B^* - \Sigma^* H(s-t+\tau)C^*$$

which is uniformly bounded in t, and is continuous in t except for the two points $t = s$ and $t = s + \tau$. As was done above for $m(t)$, one can perform the iterative analysis of the delay ODE (3.11) on successive time intervals $J_k = [(k-1)\tau, k\tau]$. Since both the initial condition and the right-hand side θ_s are known, the kth step of this iterative construction amounts to solving a first order linear ODE with constant coefficients and known right-hand side. So this construction is essentially stepwise explicit and proves by recurrence on k that the distribution $\phi_s(t)$ is actually a bounded function of t which is differentiable except maybe at the points $t = k\tau$ and $t = s + k\tau$.

For each $s \geq 0$, once the full solution ϕ_s has been constructed for $t \in [-\tau, T]$ as just outlined, we immediately obtain $F(s,t) = \phi_s(t) - \Sigma^* H(s-t)$.

29

At this stage $F(s, t)$ is theoretically known for all $s \geq 0$ and $t \in [-\tau, T]$ and can be plugged into the delay ODE in s verified by $\rho(s, t)$ for each fixed t, with initial conditions $\rho(s, t) = 0$ for $(s, t) \in [-\tau, 0] \times [-\tau, 0]$. For each fixed $t \in [0, T]$, this delay ODE for $s \to \rho(s, t)$ can again be solved iteratively on the successive time intervals J_k.

The preceding approaches can easily be numerically implemented to derive explicit solution to the three types of delay ODEs involved. Each reduction to a succession of roughly T/τ linear ODEs enables the use of classical numerical schemes to compute $m(t)$ and $\rho(s, t)$. We have used the approach of [5], which implements the step-wise analysis presented above, along with standard numerical ODE methods. This numerical implementation is described explicitly in Section 6.1.1.

The key role played below by $m(t)$ and $\rho(s, t)$ is that these two functions essentially determine the rate functional of large deviations theory for the Gaussian diffusion with delay X_t. The general rate functional for Gaussian processes is given in Section 4.3.2. The rate functional for transition pathways linking an initial state to a desired target state is given in Section 5.1.1. These formulas determine the exponential decay rates of the probabilities associated to the Gaussian diffusion with delay X_t.

3.2   Genetic Evolution Probabilities and Statistics

In the case of Gaussian diffusions with delay, previously established large deviations principles for Gaussian processes [2] can provide probabilistic estimates in terms of

the mean and covariance and without the direct use of the probability associated to the Gaussian process. For stochastic evolution of E. Coli, we will need to establish a large deviations principle for probabilities associated to random histogram trajectories. The key probability will be the one-step transition probability which describes the probability of transitioning to a histogram H on some day $n+1$ given that histogram on day n is G. Recall that a population of E. Coli cells at the beginning of day n undergoes deterministic growth, independent Poisson mutations, and random selection in order to generate a population on day $n+1$. Therefore, we first calculate the formulas and probabilities involved in each of these three steps. Then, we will give an explicit formula for the one-step transition probability. Finally, we end the section by giving the mean of the random histogram trajectory $\mathbf{H}$, which is given recursively by the conditional expectation.

3.2.1 Deterministic Growth

For any histogram $H = (H(1), H(2), \ldots, H(g))$, we assume that the genotypes are arranged in ascending order of fitness so that if $i < j$, then $F_i < F_j$. In particular, genotype 1 is the ancestor and genotype g is the fittest. During deterministic growth and before mutation, pop_n becomes a population P_n. The number of cells with genotype j grows from $NH_n(j)$ to $siz_n(j) := NH_n(j)F_j$ so that the size of the population P_n is $N\langle F, H_n \rangle$ where $\langle \cdot, \cdot \rangle$ is the standard inner product on $\mathbb{R}^g$. The frequency of cells with genotype j in the population P_n is given by $G_n(j) = F_j H_n(j)/\langle F, H_n \rangle$. Let $S \subset \mathbb{R}^g$ denote the simplex of histograms. Hence, the deterministic growth

stage transforms the histogram H_n to the histogram $G_n = \Phi(H_n)$ via the deterministic function $\Phi : S \to S$ defined on the entirety of the compact, convex space of histograms S by

$$\Phi_j(H) = \frac{F_j H(j)}{\langle F, H \rangle}.$$

3.2.2 Random Mutations

After changing the time unit, we can assume that the fixed duration of free growth periods is $\tau = 1$. Even though mutations can occur randomly at any time throughout the day, we assume that all mutations occur simultaneously at the end of each growth period, which has minimal impact for large values of N (see e.g. [41]). These random independent Poisson mutations are described by the $(g \times g)$ matrix of mutation rates, written as $M_{j,k} = mQ_{j,k}$ where m is the mutation rate ranging between 10^{-8} and 10^{-6}. The entry $M_{j,k}$ represents the mutation rate of E. Coli cells from genotype j to genotype k.

Let $X_{j,k}$ denote the number of mutants of genotype j changing into genotype k at time step n where all the $X_{j,k}$ are independent and $X_{j,j} = 0$. Since the $X_{j,k}$ are assumed to be Poisson, we have

$$P(X_{j,k} = R_{j,k}) = \exp(-siz_n(j)M_{j,k}) \frac{(siz_n(j)M_{j,k})^{R_{j,k}}}{R_{j,k}!}, \quad j \neq k$$

$$\mathbb{E}[X_{j,k}] = siz_n(j)M_{j,k}, \quad j \neq k.$$

After growth of pop_n to a population P_n, these mutations represent a random perturbation of the deterministic population P_n to a new (random) intermediary population

P_n^{mut} where the number of individuals of genotype j is given by

$$siz_n(j) - \sum_{k=1}^{g} X_{j,k} + \sum_{k=1}^{g} X_{k,j}.$$

For the cells of genotype j, let the number of emigrants and immigrants be denoted as

$$O_n(j) = \sum_{k=1}^{g} X_{j,k}, \quad I_n(j) = \sum_{k=1}^{g} X_{k,j},$$

respectively. Since the $X_{j,k}$ are independent Poisson random variables for all indices $j \neq k$, the emigrants $O_n(j)$ and immigrants $I_n(j)$ are Poisson distributions with means given by

$$\mathbb{E}[O_n(j)] = siz_n(j)\left(\sum_{k \neq j} M_{j,k}\right), \qquad \mathbb{E}[I_n(j)] = \sum_{k \neq j} siz_n(k) M_{k,j},$$

respectively. The intermediary population P_n^{mut} after the mutation step has g groups of sizes $U_n(j)$ for $1 \leq j \leq g$ where

$$U_n(j) = siz_n(j) - O_n(j) + I_n(j).$$

Clearly, the total number of cells in P_n^{mut} is equal to the number of cells after growth, which is $N\langle F, H_n \rangle$. Therefore, if $G_n = \Phi(H_n)$ is the histogram after deterministic growth and G_n^{mut} is the random histogram after mutation, we have that

$$G_n^{\mathrm{mut}} = \frac{U_n}{N\langle F, H_n \rangle}. \tag{3.12}$$

3.2.3 Random Selection

After deterministic growth and random mutation of a population pop_n, the population pop_{n+1} is generated by extracting a random sample of size N from the intermediary population P_n^{mut}. This intermediate population is described precisely by the

histogram G_n^{mut} given in (3.12).

Let $V_n(j)$ be the number of j-cells present in pop_{n+1} at time $n+1$ after random selection. We then have $\sum_j V_n(j) = N$, and the new population histogram becomes $H_{n+1} = V_n/N$. Since the intermediate population before selection is described by (3.12), the random vector V_n has a multinomial distribution $\mu(N)$ with g occurrences which are given by the coordinates of the histogram (3.12). More precisely, $\mu(N)$ is given by the formula

$$\mu(N) := P(H_{n+1} = G \,|\, G_n^{\mathrm{mut}} = p) = P(V_n = V \,|\, G_n^{\mathrm{mut}} = p) = \frac{N!}{\prod_{i=1}^{g} V(i)!} \prod_{i=1}^{g} p_i^{V(i)}.$$

(3.13)

We note that the choice of notation $\mu(N)$ is for simplicity in the calculations of the one-step cost function in Section 4.4.1 which involves direct analysis of $\frac{1}{N} \log \mu(N)$ for large N. However, this probability clearly depends on the mutation step preceding random selection as well as the population size N.

3.2.4   One-Step Transition Probability

In order to generate the new population pop_{n+1}, we have one deterministic step (growth) and two probabilistic steps (mutation and random selection). The concatenated probability of this sequence is given by the transition probability

$$\Theta(H, G) = P(H_{n+1} = G \,|\, H_n = H) = \sum_{R_{j,k} \neq 0} \prod_{j,k | j \neq k} P(X_{j,k} = R_{j,k} \,|\, H_n = H)\mu(N).$$

(3.14)

34

Notice that $\sum_k X_{j,k}$ represents the number of cells mutating from genotype j to any other genotype $i \neq j$. Since $siz_n(j)$ is the number of cells of genotype j after growth, we must have that $X_{j,k} \geq 0$ and $\sum_k X_{j,k} \leq siz_n(j)$, which is dependent on the histogram H_n. Thus, the conditioning in (3.14) apriori is necessary. However, we will show that $P(X_{j,k} = R_{j,k} \mid H_n = H) \approx P(X_{j,k} = R_{j,k})$. To this end, let

$$Q(R, H, N) = \prod_{j,k \mid j \neq k} P(X_{j,k} = R_{j,k} \mid H_n = H).$$

We have that

$$Q(R, H, N) = \prod_{j,k \mid j \neq k} P(X_{j,k} = R_{j,k} \mid H_n = H, X_{j,k} \leq siz_n(j))$$

$$= \prod_{j,k \mid j \neq k} P(X_{j,k} = R_{j,k} \mid H_n = H, X_{j,k} \leq NF_j H_n(j))$$

$$= \prod_{j,k \mid j \neq k} P(X_{j,k} = R_{j,k} \mid X_{j,k} \leq NF_j H_j).$$

Now,

$$P(X_{j,k} = R_{j,k} \mid X_{j,k} \leq NF_j H_j) = \frac{P(X_{j,k} = R_{j,k}, X_{j,k} \leq NF_j H_j)}{P(X_{j,k} \leq NF_j H_j)}$$

$$= \frac{P(X_{j,k} = R_{j,k}, X_{j,k} \leq NF_j H_j)}{1 - P(X_{j,k} > NF_j H_j)}.$$

Recall that $X_{j,k}$ are assumed to be Poisson with mean $\mathbb{E}[X_{j,k}] = siz_n(j)M_{j,k} = NF_j H j M_{j,k}$. In our stochastic model, mutation rates are assumed to be at most order 10^{-6}, which implies that $\mathbb{E}[X_{j,k}] \approx 10^{-6} NF_j H_j$. We will show that

$$P(X_{j,k} \leq NF_j H_j) = 1 - P(X_{j,k} > NF_j H_j) \approx 1$$

using the following lemma.

Lemma 3.2.1. *If X is a Poisson random variable with mean λ, then for $a > 0$,*

$$P(X > a\lambda) < e^{\lambda(e^t - 1 - at)}$$

for all $t > 0$.

Proof. For $a > 0$, we know that

$$P(X > a\lambda) = P(e^{tX} > e^{at\lambda}) \tag{3.15}$$

for all $t > 0$. Since e^{tX} is a positive random variable, Markov's inequality yields for any $b > 0$

$$P(e^{tX} \geq b) \leq \frac{\mathbb{E}[e^{tX}]}{b}.$$

Take $b = e^{at\lambda}$. Since X is Poisson and $\mathbb{E}[e^{tX}]$ is the moment-generating function for X, using (3.15) gives

$$\begin{aligned}
P(X > a\lambda) &= P(e^{tX} > e^{at\lambda}) \\
&< \frac{\mathbb{E}[e^{tX}]}{e^{at\lambda}} \\
&= \frac{e^{\lambda(e^t - 1)}}{e^{at\lambda}} \\
&= e^{\lambda(e^t - 1 - at)}.
\end{aligned}$$

$\square$

Using Lemma 3.2.1 to analyze $P(X_{j,k} > NF_jH_j)$, assuming $X_{j,k} \neq 0$, let $\lambda = M_{j,k}NF_jH_j$ and $a = 1/M_{j,k} \simeq 10^6$. We have

$$\begin{aligned}
P(X_{j,k} > NF_jH_j) &< e^{M_{j,k}NF_jH_j\left(e^t - 1 - \frac{1}{M_{j,k}}t\right)} \\
&\simeq e^{10^{-6}NF_jH_j(e^t - 1 - 10^6 t)}.
\end{aligned}$$

The function $e^t - 1 - 10^6 t$ attains its minimum at $t = \log 10^6$ so that

$$P(X_{j,k} > NF_j H_j) < e^{10^{-6} NF_j H_j (10^6 - 1 - 10^6 \log 10^6)}$$

$$= e^{NF_j H_j (1 - 10^{-6} - 6 \log 10)}.$$

If $H_j = 0$, then $X_{j,k} = 0$ and $P(X_{j,k} > NF_j H_j) = 0$. If $H_j \neq 0$, then $H_j \geq 1/N$, implying that $NF_j H_j$ is of order F_j. For E. Coli experiments, growth factors are assumed to be at least 200. Therefore,

$$P(X_{j,k} > NF_j H_j) < e^{200(1 - 10^{-6} - 6 \log 10)} \approx 0.$$

Finally, we have $P(X_{j,k} \leq NF_j H_j) \approx 1$ so that

$$Q(R, H, N) = \prod_{j,k|j \neq k} P(X_{j,k} = R_{j,k}).$$

Letting $Q(R, H, N) := \prod_{j,k} P(X_{j,k} = R_{j,k})$, we now have our one-step transition probability $\Theta(H, G)$ as

$$\Theta(H, G) = \sum_{R_{j,k} \neq 0} Q(R, H, N)\mu(N), \qquad (3.16)$$

$$Q(R, H, N) = \prod_{j,k|j \neq k} \exp(-siz_n(j)M_{j,k}) \frac{(siz_n(j)M_{j,k})^{R_{j,k}}}{R_{j,k}!},$$

where $\mu(N)$ is given by (3.13). This formula will be useful in Section 4.4.1 when completing a large deviations calculation for one-step probabilities.

3.2.5 Mean of Genetic Evolution of E. Coli

Consider the Markov chain H_n of histograms associated above to the successive cell populations pop_n of fixed size N. Stochastic genotype evolution is driven by the

growth factors $F_1 < F_2 < \cdots < F_g$, ordered by increasing fitness, and by the $g \times g$ matrix $M = (M_{j,k})$ of mutation rates. Let $M_{j,\cdot}$ and $M_{\cdot,k}$ be the jth row sum and the kth column sum for M.

The genotype frequencies reached after any daily growth starting with a population histogram $H \in S$ are given by $q(j) = F_j H(j)/ < F, H >$ where the brackets $< \cdot, \cdot >$ denote the scalar product in $\mathbb{R}^g$. For any fixed population size N, the mean behavior, which constitutes our underlying deterministic system, of the chain H_n is analyzed in the next theorem.

Theorem 3.2.2. *For any H in S, define the histogram $\Psi(H)$ by*

$$\Psi_j(H) = \mathbb{E}[H_{n+1}(j) \mid H_n = H] = (1 - M_{j,\cdot})q(j) + \sum_k q(k)M_{k,j}.$$

For any initial population histogram $H_0 = Y_0$, the successive mean vectors $Y_n = \mathbb{E}[H_n]$ of the histograms Markov chain H_n are given iteratively by $Y_{n+1} = \Psi(Y_n)$. Then, as $n \to \infty$, if the nonzero mutation matrix $M_{j,k} = mQ_{j,k}$ is such that $M_{g,\cdot} = 0$ (the fittest genotype can not mutate into a weaker genotype), then the mean histogram (Y_n) converges at exponential speed to the deterministic histogram for which the fittest genotype g is fully dominant, i.e has frequency 100%. Otherwise, the mean histogram (Y_n) converges at exponential speed to the deterministic histogram in which the fittest genotype is highly dominant, i.e. has frequency of order $1 - m$.

Proof. Let $X_{j,k}$ be the Poisson random variable which denotes the number of mutants of genotype j changing into genotype k at time step n where all the $X_{j,k}$ are independent and $X_{j,j} = 0$. Notice that since the population at the next time step $n + 1$ involves random selection, the expected histogram H_{n+1} given that $H_n = H$

will be given by the expected histogram after growth and mutation. The random histogram after deterministic growth and mutation during day n, denoted as MH_n, is given by the formula

$$MH_n(j) = \frac{NF_j H_n(j) - \sum_{k=1}^g X_{j,k} + \sum_{k=1}^g X_{k,j}}{N\langle F, H_n \rangle}$$

for each genotype $j = 1, \ldots, g$. Since $\mathbb{E}[X_{j,k} \mid H_n = H] = NF_j H(j) M_{j,k}$, direct calculation of the conditional expectation yields

$$\mathbb{E}[H_{n+1}(j) \mid H_n = H] = \mathbb{E}[MH_n(j) \mid H_n = H]$$

$$= \frac{1}{N\langle F, H \rangle} \left(NF_j H(j) - NF_j H(j) \sum_{k=1}^g M_{j,k} + \sum_{k=1}^g NF_k H(k) M_{k,j} \right)$$

$$= (1 - M_{j,.})q(j) + \sum_{k=1}^g q(k) M_{k,j}.$$

Denote the above conditional expectation for genotype j as $\Psi_j(H)$. For a fixed initial population histogram H_0, the expected histogram of the Markov chain H_n on day n is given by $\Psi^n(H_0)$ where Ψ^n represents the n-fold composition of the vector-valued function Ψ. We analyze inductively the behavior of the mean $\Psi_g^n(H_0)$ for the fittest genotype on day n for all positive integer values of n. On day 1, the expected concentration of cells of genotype j is given by

$$\Psi_j^1(H_0) = (1 - M_{j,.})\frac{F_j H_0(j)}{\langle F, H_0 \rangle} + \sum_{k=1}^g \frac{F_k H_0(k)}{\langle F, H_0 \rangle} M_{k,j}.$$

Notice that the order of $\Psi_j^1(H_0)$ is roughly given by $(1 - M_{j,.})F_j/F_g + M_{l,j}F_l/F_g$ where l is the largest index such that $M_{l,j} \neq 0$. On day 2, the expected concentration of cells of genotype j is given by

$$\Psi_j^2(H_0) = (1 - M_{j,.})\frac{F_j \Psi_j^1(H_0)}{\langle F, \Psi^1(H_0) \rangle} + \sum_{k=1}^g \frac{F_k \Psi_k^1(H_0)}{\langle F, \Psi^1(H_0) \rangle} M_{k,j}.$$

A similar calculation shows that the order of $\Psi_j^2(H_0)$ is roughly given by $(1 - M_{j,.})(F_j/F_g)^2 + M_{l,j}(F_l/F_g)^2$. Proceeding inductively, we have that $\Psi_j^n(H_0)$ has order $(1 - M_{j,.})(F_j/F_g)^n + M_{l,j}(F_l/F_g)^n$. In particular, for the strongest genotype g, we have that the order of $\Psi_g^n(H_0)$ is $(1 - M_{g,.}) + M_{i,g}(F_i/F_g)^n$ where $i < g$ is the largest index such that $M_{i,g} \neq 0$. We conclude that as $n \to \infty$, if $M_{g,.} \neq 0$, the mean histogram $\Psi^n(H_0)$ converges at exponential speed to a fixed histogram in which the fittest genotype has frequency of order $1 - m$. Otherwise, the mean converges to the histogram in which the fittest genotype is fully dominant. $\square$

In the mean trajectory, dominance of the strongest genotype in a population will occur exponentially quickly given an initial state. Consequently, the appearance of other genotypes over long time scales and large populations become rare events with probabilities vanishing exponentially fast. A large deviations principle roughly gives the exponential decay rate of the probabilities $P(\mathbf{H} \in A)$ for generic sets of trajectories. Since the Markov chain trajectory $\mathbf{H} = [H_0\, H_1\, \ldots\, H_T]$ is formed by a finite sequence of one-step transitions $H_n \to H_{n+1}$ for $n < T$, a large deviations principle for $\mathbf{H}$ first requires a detailed analysis of the exponential behavior of the one-step transition probabilities $P(H_{n+1} = G \,|\, H_n = H)$, which is given in Section 4.4.1.

Chapter 4

Large Deviations Theory and Background

Large deviations is largely thought of as a study of rare events. Many natural systems are influenced by small random perturbations or large population sizes which have some underlying deterministic system. When a small noise parameter approaches 0 or a population size approaches ∞, the probability that the system takes a large excursion away from the deterministic system decays exponentially fast. Large deviations theory reveals this exponential decay rate in terms of an explicit *rate function*. To make this discussion more rigorous, we will formally describe the large deviations problem. Then, we will discuss the first landmark theorem in large deviations known as the Cramer-Chernoff Theorem. Finally, we will discuss large deviations results relevant to Gaussian diffusions with delay and stochastic evolution of bacterial populations.

4.1 Formal Large Deviations Problem

To describe the large deviations problem generally, let X_n be a sequence of independent random vectors taking values in a vector space E and having the same probability distribution μ. For $n \in \mathbb{N}$, denote the empirical means by $\bar{X}_n = (X_1 + \cdots + X_n)/n$. For any set $A \subset E$, we study the exponential decay rate of the probabilities $P(\bar{X}_n \in A)$ as $n \to \infty$.

For $E = \mathbb{R}^k$ and when $\int_E |x| \, d\mu(x) < \infty$, the law of large numbers implies that if A contains a neighborhood of the theoretical mean $m = \int_E x \, d\mu(x)$, then $\lim_{n \to \infty} P(\bar{X}_n \in A) = 1$. Denoting the closure of the set A as $\bar{A}$, if $m \notin \bar{A}$, then $\lim_{n \to \infty} P(\bar{X}_n \in A) = 0$. Therefore, when $m \notin \bar{A}$, the occurrence of the event $(\bar{X}_n \in A)$ becomes a rare event as $n \to \infty$ where the rate of decay is of particular interest. Thus, if we fix a large n in this situation, the occurrence of the event $(\bar{X}_n \in A)$ represents a *large deviation with respect to the law of large numbers*. Cramer and Chernoff [10, 13] study the case when $E = \mathbb{R}$. They focus on computing $\lim_{n \to \infty} \frac{1}{n} \log P(\bar{X}_n \in A)$ when A is a half-line which gives an explicit exponential decay rate in terms of the crucial Cramer transform, also called a rate function. These so-called "rate functions" become paramount in obtaining explicit decay rates which is obtained via a "large deviations principle," which we formally define below.

Definition 4.1.1 (Rate function and large deviations principle)**.** Let E be a vector space endowed with its Borel σ-algebra $\mathcal{B}(E)$. Let $(X_n)_{n=1}^{\infty}$ be a sequence of independent and identically distributed (i.i.d) random vectors taking values in E such that $\bar{X}_n$ is measurable for all $n \in \mathbb{N}$. A function $\lambda : E \to \mathbb{R}$ is called a *rate function* if

- $0 \leq \lambda(x) \leq \infty$ for all $x \in E$,

- λ is lower semi-continuous on E,

- the level sets $\{x \in E : \lambda(x) \leq c\}$ are compact sets in E.

The sequence (X_n) is said to obey a *large deviations principle with rate function* λ if

- For every closed set $K \subset E$

$$\limsup_{n \to \infty} \frac{1}{n} \log P(\bar{X}_n \in K) \leq - \inf_{x \in K} \lambda(x), \tag{4.1}$$

- For every open set $G \subset E$

$$\liminf_{n \to \infty} \frac{1}{n} \log P(\bar{X}_n \in G) \geq - \inf_{x \in G} \lambda(x). \tag{4.2}$$

If condition (4.1) holds only for compact sets, the sequence (X_n) obeys a *weak form of the large deviations principle.*

For $A \in \mathcal{B}(E)$, denote the interior of A as A°. In the large deviations principle above, notice that conditions (4.1) and (4.2) hold for $\bar{A}$ and A°, respectively. For a fixed Borel set A, it is natural to determine when the limit superior and limit inferior are equal so that the full limit exists. If A is a Borel set such that $\inf_{x \in A^\circ} \lambda(x) = \inf_{x \in \bar{A}} \lambda(x)$, which is necessarily the case when the closure of A° is equal to $\bar{A}$, we have

$$\lim_{n \to \infty} \frac{1}{n} \log P(\bar{X}_n \in A) = - \inf_{x \in A} \lambda(x).$$

43

Notation 4.1.2. In the large deviations principle, minimization of the rate function over a set in question becomes key in quantifying probabilistic estimates. Consequently, for a Borel set $A \in \mathcal{B}(E)$, we denote $\Lambda(A) := \inf_{x \in A} \lambda(x)$ and call $\Lambda(A)$ the *large deviations rate functional* or *Cramer set functional.*

In general, the vector space E and its topology influence the feasibility of this asymptotic study. For instance, given a generic sequence of i.i.d. random vectors X_n, the sum $X_1 + \cdots + X_n$ is not necessarily measurable with respect to the Borel σ-algebra $\mathcal{B}(E)$ so that the inequalities given by (4.1) and (4.2) would not make sense. This problem has been addressed rigorously in Chapters 2 and 3 in [2] where more details can be found. For now, we will focus on the case when $E = \mathbb{R}$ where the above problem is not relevant.

4.2   Classical Cramer-Chernoff Theorem

We begin by defining what will be the rate function for the large deviations principle on $\mathbb{R}$.

Definition 4.2.1. Let μ be a probability on $\mathbb{R}$ with Laplace transform $\hat{\mu} : \mathbb{R} \to (0, \infty]$ defined by $\hat{\mu}(t) := \mathbb{E}[e^{tx}] = \int_{\mathbb{R}} e^{tx} \, d\mu(x)$. Define the *Cramer transform* $\lambda : \mathbb{R} \to [0, \infty]$ of the probability μ by

$$\lambda(x) = \sup_{t \in \mathbb{R}}[tx - \log \hat{\mu}(t)]. \tag{4.3}$$

Notice the Cramer transform λ is necessarily convex and lower semi-continuous since it is the pointwise supremum of a family of continuous linear functions. In

fact, we will see shortly that the Cramer transform will be the rate function used to establish a large deviations principle. Furthermore, we can view the function $\lambda(x)$ and $\hat{\mu}(t)$ as dual functions in the Legendre duality framework between convex lower semi-continuous functions. The connection between $\hat{\mu}(t)$ and $\lambda(x)$ is given in Proposition 4.2.6. Notice that we have not excluded the possibility that $\lambda(x)$ or $\hat{\mu}(t)$ is infinite.

Before stating the Cramer-Chernoff Theorem, we will focus briefly on computing the Cramer transform in a few examples and providing some interpretation of the large deviations principle in connection with the Cramer transform.

4.2.1   Computing Cramer Transforms

When $\hat{\mu}(t)$ is finite for all $t \in \mathbb{R}$, the mean m and variance σ^2 of μ are both finite. Then, computation of $\lambda(x)$ for each fixed $x \in \mathbb{R}$ involves maximizing the function $tx - \log \hat{\mu}(t)$ as a function of t, as we will demonstrate below using some well-known distributions. Subsequently, one can verify that the Cramer transform $\lambda(x)$ is differentiable in a neighborhood of the mean m where $\lambda'(m) = 0$ and $\lambda''(m) = 1/\sigma^2$. This implies that $\lambda(x)$ reaches a minimum at $x = m$ with minimum value $\lambda(m) = 0$. An explicit form of the Cramer transform can be obtained in a few classical examples, which we illustrate below.

Example 4.2.2 (Gaussian distributions). When μ is Gaussian with mean m and variance σ^2, we have its density given by $\mathrm{d}\mu(x) = \frac{1}{\sqrt{2\pi\sigma^2}} \exp \frac{-(x-m)^2}{2\sigma^2} \, \mathrm{d}t$. This implies

that $\log \hat{\mu}(t) = tm + \frac{1}{2}\sigma^2 t^2$. Therefore, we have that

$$\lambda(x) = \sup_{t \in \mathbb{R}} \left[tx - tm - \frac{1}{2}\sigma^2 t^2 \right].$$

The maximizer of this function is given by $t = (x - m)/\sigma^2$. Plugging this value in for t gives the explicit formula of the Cramer transform

$$\lambda(x) = \frac{(x - m)^2}{2\sigma^2} \quad \text{for} \quad x \in \mathbb{R},$$

which is an infinitely differentiable quadratic function of x.

Example 4.2.3 (Binomial Distributions). Suppose $\mu = p\delta_u + (1 - p)\delta_v$ where $u < v$ and $0 < p < 1$. For all $x \in (u, v)$, we have $\mathrm{d}\mu(x) = p\,\mathrm{d}\delta_{x-u} + (1 - p)\,\mathrm{d}\delta_{v-x}$ so that the Laplace transform $\hat{\mu}(t)$ is given by evaluation of the exponential at $x = u$ and $x = v$. More precisely, we have that

$$\hat{\mu}(t) = pe^{tu} + (1 - p)e^{tv} = e^{tu}(p + (1 - p)e^{t(v-u)}).$$

The Cramer transform then takes the form

$$\lambda(x) = \sup_{t \in \mathbb{R}} \left[t(x - u) - \log\left(p + (1 - p)e^{t(v-u)}\right) \right].$$

The maximizer of this function is given by $t = \frac{1}{v-u}\log\frac{p(x-u)}{(1-p)(v-x)}$. Plugging this value in for t gives the explicit Cramer transform for all $x \in (u, v)$ as

$$\lambda(x) = \frac{x - u}{v - u}\log\frac{x - u}{1 - p} + \frac{v - x}{v - u}\log\frac{v - x}{p} - \log(v - u).$$

Notice that the maximizer in t is undefined when $x = u$ or $x = v$, which follows from the fact that $tu - \log\hat{\mu}(t)$ and $tv - \log\hat{\mu}(t)$ are strictly monotonic functions of t. We

analyze the Cramer transform for these boundary cases. Notice that

$$\lambda(u) = \sup_{t \in \mathbb{R}} \left[-\log \left(p + (1-p)e^{t(v-u)} \right) \right]$$

$$\lambda(v) = \sup_{t \in \mathbb{R}} \left[-\log \left(pe^{t(u-v)} + 1 - p \right) \right].$$

Because of monotonicity, the supremum in these two cases will be the value we obtain

as we let $t \to \infty$ or $t \to -\infty$. Notice that since $v - u > 0$, we have that

$$\lim_{t \to \infty} -\log \left(p + (1-p)e^{t(v-u)} \right) = -\infty$$

$$\lim_{t \to -\infty} -\log \left(p + (1-p)e^{t(v-u)} \right) = -\log p.$$

Therefore, we must have that $\lambda(u) = -\log p$. An analogous argument shows that

since $u - v > 0$, we must have that $\lambda(v) = -\log(1-p)$. Thus, the full Cramer

transform for the Binomial distribution is given as

$$\lambda(x) = \begin{cases} \frac{x-u}{v-u} \log \frac{x-u}{1-p} + \frac{v-x}{v-u} \log \frac{v-x}{p} - \log(v-u), & u < x < v \\ -\log p, & x = u \\ -\log(1-p), & x = v \\ \infty, & \text{otherwise,} \end{cases}$$

which is continuous on $[u, v]$ and differentiable on (u, v).

Example 4.2.4 (Exponential Densities). When μ has an exponential density given

by $d\mu(t) = 1_{[0,\infty)}(t)e^{-t}dt$. The Laplace transform is given by

$$\hat{\mu}(t) = \int_{-\infty}^{\infty} e^{tx} \, d\mu(x) = \int_0^{\infty} e^{(t-1)x} dx.$$

Notice that this integral is infinite for all $t \geq 1$ so that a maximum cannot be obtained

for these values of t. Therefore, suppose that $t < 1$. We then have that $\hat{\mu}(t) = \frac{-1}{t-1}$.

This implies that

$$\lambda(x) = \sup_{t \in (-\infty, 1)} [tx + \log(1 - t)].$$

The maximum of this function occurs at $t = 1 - 1/x$ so that the Cramer transform is given by

$$\lambda(x) = \begin{cases} x - 1 - \log x, & x > 0 \\ \infty, & x \leq 0, \end{cases}$$

which is continuously differentiable on $(0, \infty)$.

4.2.2 Probabilistic Interpretation of Cramer Transforms and the Cramer-Chernoff Theorem

The classic early results of Cramer and Chernoff show that for i.i.d. random variables $X_n \in L^1(\mathbb{R})$, the tails of the distribution of the sample mean $\bar{X}_n$ tend to zero at exponential speed as $n \to \infty$ with a rate completely determined by the Cramer transform λ of the common distribution μ. Suppose that we have a large deviations principle for a sequence of random variables $X_n \in L^1(\mathbb{R})$ with common distribution μ. Suppose further that $A \in \mathcal{B}(E)$ such that $\Lambda(A^\circ) = \Lambda(\bar{A})$ so that

$$\lim_{n \to \infty} \frac{1}{n} \log P(\bar{X}_n \in A) = -\Lambda(A).$$

Let $x \in A$ be an arbitrary point. The large deviations principle states then that observing $\bar{X}_n$ in a small neighborhood of x in A should be of order $e^{-n\lambda(x)}$ for large n. While this statement is not literally true, it still roughly summarizes the intuitive interpretation of the large deviations principle and its connection to the Cramer

transform. For large n, the probabilities of observing $\bar{X}_n$ in the vicinity of a point $x \in A$ such that $\lambda(x) > 0$ will vanish much more quickly when $\lambda(x)$ is large than when $\lambda(x)$ is small. Thus, this provides an intuitive reason why the exponential decay rates of the probabilities $P(\bar{X}_n \in A)$ are completely determined by $\lambda(x^*) = \Lambda(A)$ where $x^* \in A$ is the minimizer of $\lambda(x)$. Furthermore, this intuitively shows that if the event $(\bar{X}_n \in A)$ is to occur, then $\bar{X}_n$ is "most likely" going to be very close to the minimizer x^*. To make this precise, we now state the Cramer-Chernoff theorem without proof (see [2]).

Theorem 4.2.5 (Cramer-Chernoff). *Let X_n be a sequence of independent real-valued random variables with the same probability distribution μ, and let $\bar{X}_n = (X_1 + \cdots + X_n)/n$. Let λ be the Cramer transform of μ. We then have for all $a \in \mathbb{R}$ the lower bounds*

$$-\lambda(a) \leq \liminf_{n \to \infty} \frac{1}{n} \log P(\bar{X}_n \leq a)$$
$$-\lambda(a) \leq \liminf_{n \to \infty} \frac{1}{n} \log P(\bar{X}_n \geq a)$$

Now suppose that for each $n \in \mathbb{N}$ that $X_n \in L^1(\mathbb{R})$, and denote the mean as $m = \int_{\mathbb{R}} x \, d\mu(x)$. We then have the upper bounds

$$\frac{1}{n} \log P(\bar{X}_n \leq a) \leq -\lambda(a)$$
$$\frac{1}{n} \log P(\bar{X}_n \geq a) \leq -\lambda(a).$$

Finally, we have the following large deviations limits:

$$\lim_{n\to\infty} \frac{1}{n}\log P(\bar{X}_n \le a) = \begin{cases} -\lambda(a), & a \le m \\ 0, & a > m \end{cases},$$

$$\lim_{n\to\infty} \frac{1}{n}\log P(\bar{X}_n \ge a) = \begin{cases} 0, & a < m \\ -\lambda(a) & a \ge m \end{cases}.$$

With the Cramer transform being the key function in the Cramer-Chernoff theorem above, analysis of $\lambda(x)$ becomes helpful when explicitly utilizing this large deviations result. The following theorem links the behavior of $\lambda(x)$ as $|x| \to \infty$ to the finiteness of the Laplace transform $\hat{\mu}(t)$.

Proposition 4.2.6. *Let μ be a probability on $\mathbb{R}$ with $\int_{\mathbb{R}} |x|\, d\mu(x) < \infty$. The Cramer transform λ of μ has the following properties:*

- *$\hat{\mu}(t) = \infty$ for all $t \ne 0$ if and only if $\lambda(x) = 0$ for all $x \in \mathbb{R}$,*

- *$\hat{\mu}(t) < \infty$ for some $t \ne 0$ if and only if $\lim_{|x|\to\infty} \lambda(x)$ is infinite*

- *$\hat{\mu}(t) < \infty$ for all t if and only if $\lim_{|x|\to\infty} \frac{\lambda(x)}{x}$ is infinite.*

Large deviations principles like the one just stated often rely on regularity properties of the Cramer transform. Thus, for probabilities on $\mathbb{R}$, the following theorem clarifies the variations of λ on the support of μ. Let $[u, v]$ be the closed convex hull of support of μ, which may be bounded or unbounded.

Proposition 4.2.7. *Let μ be a probability on $\mathbb{R}$ with $\int_{\mathbb{R}} |x|\, d\mu(x) < \infty$ and $m = \int_{\mathbb{R}} x\, d\mu(x)$.*

- *The Cramer transform $\lambda(x)$ is finite, convex, and continuous for $u < x < v$ and $\lambda(x) = \infty$ for $x < u$ or $x > v$. When v is finite, $\lambda(x)$ is left continuous at $x = v$. When u is finite, $\lambda(x)$ is right continuous at $x = u$.*

- *The function λ decreases for $u < x \leq m$, reaches its minimum $\lambda(m) = 0$ at m, and increases for $m \leq x < v$.*

- *The integral $T(s) = \int_{\mathbb{R}} e^{s\lambda(x)} \, d\mu(x) < \infty$ for all $s < 1$. However, $T(1)$ can be infinite for a large class of probabilities μ.*

Naturally, the Cramer-Chernoff theorems were extended to random variables taking values in $E = \mathbb{R}^k$. As stated before, establishing analogous results in infinite-dimensional spaces is a bit more troublesome. However, this can be done for a large class of separable locally convex topological vector spaces, namely separable Frechet spaces, which is the content of Chapters 2 - 4 in [2]. The approach here was strongly influenced by the results of Donsker-Varadhan and is similar to the results of Bahadur-Zabell. In these chapters, the general Cramer transform (rate function) and Cramer set functional (large deviations rate functional) are defined, and a large deviations principle is established. The situation that will be of use when applying large deviations principles to Gaussian diffusions with delay will be when E is a separable Hilbert space, namely the space of vector-valued functions in L^2. We will describe the large deviations framework in this setting, which is the content of Chapter 6 in [2].

4.3 Large Deviations for Gaussian Measures and Processes

We present, without proof, a brief overview of large deviations theory of Gaussian measures and processes (refer to Chapter 6 in [2] for proofs of theorems). We will then apply these principles to Gaussian diffusions with delay. The following notations and definitions will be used throughout this section.

- H is any separable Hilbert space, with scalar product denoted $\langle t, x \rangle := t(x)$ for $t, x \in H$.

- μ is any probability on the Borel σ-algebra $\mathcal{B}(H)$.

- For $t \in H$, the image probability $t(\mu)$ is defined on $\mathbb{R}$ by $[t(\mu)](A) := \mu(t^{-1}(A))$ for all Borel subsets A of $\mathbb{R}$.

- μ is called *centered* iff $t(\mu)$ is centered for all $t \in H$.

- μ is called *Gaussian* iff for all $t \in H$, the image probability $t(\mu)$ is a Gaussian distribution on $\mathbb{R}$.

Large deviations concepts demand all $t(\mu)$ to have at least finite first-order moment. But most applicable results require all $t(\mu)$ to have some finite exponential moments since they depend on the Laplace tranform $\hat{\mu}(t)$ of μ, defined as follows for $t \in H$,

$$\hat{\mu}(t) = \int_H e^{\langle t, x \rangle} \, \mathrm{d}\mu(x).$$

For a full treatment of large deviations concepts for probabilities on general infinite dimensional Frechet vector spaces, refer to Chapters 2 and 3 of [2]. Here we only consider Borel probabilities μ on separable Hilbert spaces H. Later on below, H will be an L^2-space of process paths and μ will be Gaussian. Probabilities of rare events under μ can be estimated via a key non-negative functional defined for $x \in H$: the Cramer transform $\lambda(x)$ of μ. The following definition of $\lambda(x)$ is actually Theorem 3.2.1 in [2].

Definition 4.3.1. The *Cramer transform* λ of μ, also called the large deviations *rate functional* of μ, is defined for $x \in H$ by

$$\lambda(x) = \sup_{t \in H} \left[\langle t, x \rangle - \log \hat{\mu}(t) \right].$$

Note that $0 \leq \lambda(x) \leq +\infty$. The *Cramer set functional* $\Lambda(A)$ is then defined for all $A \subseteq H$ by

$$\Lambda(A) = \inf_{x \in A} \lambda(x).$$

The set functional $\Lambda(A)$ quantifies the probabilities of rare events by the following key large deviations inequalities initially formalized by S. Varadhan.

Theorem 4.3.2. *Let μ be a probability measure on a separable Hilbert space H. Let Z be an H-valued random variable with probability distribution μ. Let Λ be the Cramer set functional of μ. For every Borel subset A of H one has*

$$-\Lambda(A^\circ) \leq \liminf_{\varepsilon \to 0} \varepsilon^2 \log \mathbb{P}(\varepsilon Z \in A) \leq \limsup_{\varepsilon \to 0} \varepsilon^2 \log \mathbb{P}(\varepsilon Z \in A) \leq -\Lambda(\bar{A}). \quad (4.4)$$

where A° and $\bar{A}$ are resp. the interior and the closure of A.

Whenever $\Lambda(A^\circ) = \Lambda(\bar{A})$, which is necessarily the case when $\bar{A}$ is the closure of A°, then the limits in (4.4) exist and

$$-\Lambda(A) = \lim_{\varepsilon \to 0} \varepsilon^2 \log \mathbb{P}(\varepsilon Z \in A).$$

In particular for small ε, one has the rough estimate by

$$\log \mathbb{P}(\varepsilon Z \in A) \approx -\frac{\Lambda(A)}{\varepsilon^2}.$$

In our applications below, Z is the random path of a centered Gaussian diffusion with delay so that the probability distribution ν of Z will be a centered Gaussian probability on the Hilbert space $H = L^2[0, T]$. So we now focus on Gaussian probabilities on Hilbert spaces.

4.3.1 Gaussian probabilities on Hilbert spaces

Let H be a separable Hilbert space, and let ν be a centered Gaussian probability on the Borel subsets of H. With no loss of generality, we assume that the only closed vector subspace F of H such that $\nu(F) = 1$ is H itself. The *covariance kernel* $\mathrm{Cov}(s, t)$ of ν is defined for all $s, t \in H$ by

$$\mathrm{Cov}(s, t) = \int_H \langle s, x \rangle \langle t, x \rangle d\nu(x) = \langle s, \Gamma t \rangle = \langle \Gamma s, t \rangle,$$

where the linear operator $\Gamma : H \to H$ is known to be a bounded, positive, self-adjoint operator with finite trace. The positive operator $\sqrt{\Gamma}$ then exists and is unique. The following theorem gives a fairly concrete form for $\lambda(x)$. This result can be applied in

54

path space to centered Gaussian processes, once the covariance operator Γ has been computed.

Theorem 4.3.3. *Let ν be a centered Gaussian probability on a separable Hilbert space H. Let $\Gamma : H \to H$ be the self-adjoint covariance operator of ν. Let U be the orthogonal complement in H of the null space $\ker \Gamma = \ker \sqrt{\Gamma}$. The restriction S of $\sqrt{\Gamma}$ to U is injective and maps U onto $\sqrt{\Gamma}(H)$. Then the Cramer transform λ of ν is given by*

$$\lambda(x) = \begin{cases} \frac{1}{2} \left\| S^{-1} x \right\|^2 & x \in \sqrt{\Gamma}(H) \\ \\ \infty & \text{otherwise} \end{cases}.$$

4.3.2 Application to Gaussian processes

Let $Z_s : \Omega \to \mathbb{R}$ with $s \in [0, T]$ be a centered Gaussian stochastic process with almost surely continuous trajectories and continuous covariance function

$$\rho(s, t) = \int_\Omega Z_s(\omega) Z_t(\omega) \, d\mathbb{P}(\omega).$$

Call $C([0, T])$ the Banach space of continuous functions on $[0, T]$ endowed with its Borel σ-algebra. One can trivially construct a version of Z_s with surely continuous trajectories. This defines a $C([0, T])$-valued random path Z, where $Z(\omega)$ is the path $s \to Z_s(\omega)$ with $0 \le s \le T$. The probability distribution ν of the random path Z is then a centered Gaussian probability on the Borel sets of $C([0, T])$. We now state the main large deviations result used below, which is essentially an application of Theorem 4.3.3 to the separable Hilbert space $L^2[0, T]$ and appears as Proposition 6.3.7 in [2].

Proposition 4.3.4. *Consider a centered continuous Gaussian process $Z_s : \Omega \to \mathbb{R}$ defined for s in $[0, T]$ with continuous covariance function $\rho(s, t)$. The linear operator $R : L^2[0, T] \to L^2[0, T]$ defined by*

$$Rf(s) = \int_0^T \rho(s, u) f(u) \, du$$

takes values in $C([0, T])$. Moreover, R is self-adjoint, positive, compact, and has finite trace. Let $U = (\ker(R))^\perp \subset L^2([0, T])$ and let S be the restriction of $\sqrt{R}$ to U. Then $S : U \to L^2[0, T]$ is injective and maps U onto $\sqrt{R}(L^2[0, T])$. On the path space $C[0, T]$, the probability distribution ν induced by the process Z_t has Cramer transform λ defined for $f \in C[0, T]$ by

$$\lambda(f) = \begin{cases} \frac{1}{2} \|S^{-1} f\|^2_{L^2[0,T]}, & \text{if } f \in \sqrt{R}(L^2[0, T]); \\ \\ \infty, & \text{otherwise.} \end{cases}$$

Note that by duality, R also acts on the space of all bounded Radon measures π on $[0, T]$, via the natural formula

$$R\pi(s) = \int_0^T \rho(s, u) \, d\pi(u).$$

Since the integral operator R is positive and self-adjoint, the square-root operator $\sqrt{R}$ exists and is also an integral operator of the form

$$\sqrt{R}f(s) = \int_0^T k(s, u) f(u) \, du$$

where $k(s, u)$ is uniquely defined by the relation $\int_0^T k(s, u) k(u, v) \, du = \rho(s, v)$ for all $s, v \in [0, T]$.

The value $\lambda(f)$ of the Cramer transform can be viewed as the "energy" of the path f. In particular, for a small multiple εW_t of the Brownian motion W_t, the

Cramer transform is indeed the kinetic energy $\lambda(f) = \frac{1}{2} \|f'\|_{L^2[0,T]}^2$ (Proposition 6.3.8 in [2]). Further on, we will apply Proposition 4.3.4 to the centered Gaussian process $\varepsilon Z_t = X_t - m_t$ associated to the Gaussian diffusion with delay X_t. Indeed, since the mean trajectory m_t is deterministic, probability estimates for the random paths of Z_t immediately translate into probability estimates for the random paths of X_t.

4.4 Large Deviations for Bacterial Populations

For Gaussian diffusions with delay, previous results unveiled an explicit form of the Cramer transform (cost function) which we were able to exploit directly. For stochastic models of bacterial populations described in Section 2.3.2, our main goal is to derive an explicit form for the energy or cost function $\lambda(\mathbf{w}, T)$ for a histogram trajectory $\mathbf{w}$ of length T. Minimization of this cost function over a set of paths A will be directly linked to the behavior of $-\frac{1}{N} \log P(\mathbf{H} \in A)$ as the population size $N \to \infty$. However, in order to understand the asymptotic behavior of this probability, we must first understand the asymptotic behavior of the probabilities associated to daily transitions given by (3.16). In this section, we first complete a large deviations analysis of these one-step transition probabilities which will yield a formula for the *one-step cost function $C(H, G)$*. This will explicitly define the cost function $\lambda(\mathbf{w}, T)$, which is a sum of one-step costs. Next, we will use this explicit cost function to establish a large deviations principle for the random histogram trajectory $\mathbf{H}$. Finally, we apply this large deviations principle to state a well-known result for sets of paths that follow closely to an optimal path in A.

4.4.1 Large deviations for one-step transition probabilities

Just as the cost function $\lambda(\mathbf{w}, T)$ will be directly linked to exponential decay rates of probabilities associated to $\mathbf{H}$, the *one-step cost function* $C(H, G)$, which gives the "cost" of transitioning from a histogram H to a histogram G during a daily cycle, is directly linked by $C(H, G) = -\lim_{N \to \infty} \frac{1}{N} \log P(H_{n+1} = G \,|\, H_n = H)$. We derived an explicit form for the one-step transition probability given by (3.16), which involves two probabilistic steps: independent Poisson mutations and random selection. Thus, a large deviations analysis of the one-step transition involves a large deviations analysis of multinomial sampling and independent Poisson mutations.

Large deviations approximation for multinomial sampling

Let $U(i)$ denote the number of cells of genotype i present in the population before random selection by multinomial sampling. Let $V(i)$ denote the number of cells of genotype i chosen after random selection. We then have that $\sum_{i=1}^{g} U(i) = N \langle F, H \rangle = N_{sat}$ and $\sum_{i=1}^{g} V(i) = N$. Since the computation of $\frac{1}{N} \log(\mu(N))$ will involve logarithms of factorials, we will make use of Stirling's formula $\log(N!) \simeq N \log N - N$. This approximation is only valid for $N \geq 50$, so we need to introduce boundary cases. Thus, let $p_i = U(i)/N_{sat}$, and recall that $G(i) = V(i)/N$. We then have that the boundary cases will consist of genotypes i such that $0 \leq G(i) \leq \varepsilon$ where $\varepsilon = 50/N$. We now compute $\frac{1}{N} \log(\mu(N))$ under various boundary cases. Note that since we need $\sum_{i=1}^{g} G(i) = 1$, it is not feasible to have the case where $G(i) \leq \varepsilon$ for all genotypes i unless we allowed a significantly large number of genotypes ($N = 50,000$

would require at least 1000 genotypes).

Case 1: Assume that $G(i) \geq \varepsilon$; that is, $V(i) \geq 50$ for all genotypes i. We then have that

$$\mu(N) = \frac{N!}{\prod_{i=1}^{g} V(i)!} \prod_{i=1}^{g} p_i^{V(i)}. \tag{4.5}$$

Applying the logarithm to both sides, dividing by N, and applying Stirling's formula yields

$$
\begin{aligned}
\frac{1}{N}\log\mu(N) &= \frac{1}{N}\log(N!) - \frac{1}{N}\sum_{i=1}^{g}\log(V(i)!) + \sum_{i=1}^{g}\frac{V(i)}{N}\log p_i \\
&\simeq \frac{1}{N}(N\log N - N) - \frac{1}{N}\sum_{i=1}^{g}(V(i)\log V(i) - V(i)) + \sum_{i=1}^{g}\frac{V(i)}{N}\log p_i \\
&= \log N - 1 + \frac{1}{N}\sum_{i=1}^{g}V(i) - \frac{1}{N}\sum_{i=1}^{g}V(i)\log V(i) + \sum_{i=1}^{g}\frac{V(i)}{N}\log p_i \\
&= \log N - 1 + \sum_{i=1}^{g}G(i) - \frac{1}{N}\sum_{i=1}^{g}V(i)\log V(i) + \sum_{i=1}^{g}\frac{V(i)}{N}\log p_i \\
&= \sum_{i=1}^{g}\frac{V(i)}{N}\log N - \sum_{i=1}^{g}\frac{V(i)}{N}\log V(i) + \sum_{i=1}^{g}\frac{V(i)}{N}\log p_i \\
&= -\sum_{i=1}^{g}G(i)\log G(i) + \sum_{i=1}^{g}G(i)\log p_i \\
&= \sum_{i=1}^{g}G(i)\log\frac{p_i}{G(i)} \tag{4.6}
\end{aligned}
$$

The formula in (4.6) is related to the well-known Kullback-Leibler divergence, denoted here as $KLD(G, p)$. Therefore, we have that for large population sizes N,

$$-\frac{1}{N}\log\mu(N) \simeq KLD(G, p).$$

where

$$KLD(G,p) = \begin{cases} \infty & \text{there is a } j \in \Gamma \text{ such that } G(j) > 0 \text{ and } p_j = 0 \\ \sum_{i=1}^{g} G(i) \log \frac{G(i)}{p_i} & \text{otherwise} \end{cases}.$$

$$(4.7)$$

with the convention that $0 \log 0 = 0$.

<u>**Case 2:**</u> Suppose there is exactly 1 genotype that is in the boundary. Without loss of generality, suppose $G(1) \leq \varepsilon$ and $G(i) \geq \varepsilon$ for all other genotypes. This is equivalent to $V(1) \leq 50$ and $V(i) \geq 50$ for all other genotypes. Proceeding just as in Case 1, we calculate $\frac{1}{N} \log \mu(N)$. Applying Stirling's approximation to all factorials except $V_1!$ yields

$$\frac{1}{N} \log \mu(N) \simeq \log N - 1 - \frac{1}{N} \log(V(1)!) - \sum_{i=2}^{g} \frac{1}{N}(V(i) \log V(i) - V(i)) + \sum_{i=1}^{g} \frac{V(i)}{N} \log p_i$$

$$= -\frac{1}{N} \log(V(1)!) + G(1)(\log N - 1) + \sum_{i=2}^{g} G(i) \log \frac{1}{G(i)} + \sum_{i=1}^{g} G(i) \log p_i$$

$$= -\frac{1}{N} \log(V(1)!) + \frac{V(1)}{N}[\log N - 1 + \log p_1] + \sum_{i=2}^{g} G(i) \log \frac{p_i}{G(i)} \quad (4.8)$$

In the above expression, let

$$s(N, V(1), p_1) = \frac{1}{N} \log(V(1)!) + \frac{V(1)}{N}[1 - \log(p_1 N)].$$

Suppose $U(1) \geq 1$. Since $p_1 = U(1)/N_{sat}$, we have that $p_1 N = U(1)N/N_{sat} = F_1 U(1)$. This gives us that

$$s(N, V(1), p_1) = \frac{1}{N} \log(V(1)!) + \frac{V(1)}{N}[1 - \log U(1) - \log F_1].$$

Therefore, $s(N, V(1), p_1) \to 0$ as $N \to \infty$. If it is the case that $U(1) = 0$, then we have that $V(1) = 0$ so that $s(N, V(1), p_1) = 0$. Using this analysis of $s(N, V(1), p_1)$

in (4.8) gives us that

$$-\frac{1}{N}\log\mu(N) \simeq \sum_{i=2}^{g} G(i)\log\frac{G(i)}{p_i}. \qquad (4.9)$$

Case 3: For the histogram G, let $B_G = \{i \in \Gamma \,|\, G(i) \leq \varepsilon\}$. The support of the histogram is then $J_G = \Gamma - B_G$ and nonempty. Suppose the set B_G contains at least 2 elements. We can use a similar argument that was made for Case 2 to yield

$$-\frac{1}{N}\log\mu(N) \simeq \sum_{i\in J_G} G(i)\log\frac{G(i)}{p_i}. \qquad (4.10)$$

Combining this analysis yields the one-step transition cost associated to random selection, which is given by (4.10). However, p_i is not written explicitly in terms of the mutation matrix $r_{j,k}$. To this end, we can expand the terms in p_i to get

$$p_i = \frac{U(i)}{N_{sat}} = \frac{NF_iH(i) + N\sum_k(-r_{j,k} + r_{k,j})}{N\langle F, H\rangle} = \frac{F_iH(i) + \sum_k(-r_{j,k} + r_{k,j})}{\langle F, H\rangle}.$$

Therefore, we finally have the one-step cost approximation associated to random selection given by

$$KLD(r, H, G) = \sum_{i\in J_G} G(i)\log\frac{G(i)}{p_i} \qquad (4.11)$$

$$p_i = \frac{F_iH(i) + \sum_k(-r_{j,k} + r_{k,j})}{\langle F, H\rangle}.$$

Large deviations approximation for one-step random mutations

Recall the probability expression for random Poisson mutations is given by

$$Q(r, H, N) = \prod_{j,k\,|\,j\neq k} \exp(-NF_jH(j)M_{j,k})\frac{(NF_jH(j)M_{j,k})^{Nr_{j,k}}}{Nr_{j,k}!} \qquad (4.12)$$

Using this expression, we will calculate the one-step cost approximation associated to random mutations by calculating $\frac{1}{N} \log Q(r, H, N)$, which will use Stirling's formula again to approximate factorials. We then have

$$
\begin{aligned}
\frac{1}{N} \log Q(r, H, N) =& \sum_{j,k|j\neq k} \left(-F_j H(j) M_{j,k} + r_{j,k} \log N\right) \\
&+ \sum_{j,k|j\neq k} \left(r_{j,k} \log(F_j H(j) M_{j,k}) - \frac{1}{N} \log((Nr_{j,k})!)\right) \\
\simeq& \sum_{j,k|j\neq k} \left(-F_j H(j) M_{j,k} + r_{j,k} \log N\right) \\
&+ \sum_{j,k|j\neq k} \left(r_{j,k} \log(F_j H(j) M_{j,k})\right) + \log N \sum_{j,k|j\neq k} r_{j,k} \\
&- \frac{1}{N} \sum_{j,k|j\neq k} \left(Nr_{j,k} \log(Nr_{j,k}) - Nr_{j,k} + \frac{1}{2} \log(Nr_{j,k}) + \frac{1}{2} \log 2\pi\right).
\end{aligned}
$$

Simplifying the above expression, for large population sizes N, we have

$$
-\frac{1}{N} \log Q(r, H, N) \simeq \sum_{j,k|j\neq k} \left(F_j H(j) M_{j,k} - r_{j,k} \log(F_j H(j) M_{j,k}) + r_{j,k} \log r_{j,k} - r_{j,k}\right)
$$

Therefore, we have the one-step cost approximation associated to random mutations given as

$$
L(r, H) := \sum_{j,k|j\neq k} \left(F_j H(j) M_{j,k} + r_{j,k} \log \frac{r_{j,k}}{F_j H(j) M_{j,k}} - r_{j,k}\right) \tag{4.13}
$$

One-step cost of daily transitions

Combining our computations of the one-steps costs associated to random mutations and selection, we have

$$P(H_{n+1} = G \,|\, H_n = H) \simeq \sum_{r_{j,k} \neq 0} \exp(-N(L(r, H) + KLD(r, H, G))) \qquad (4.14)$$

Notice that this probability is written as a sum of exponentials over nonzero entries $r_{j,k}$. Therefore, when evaluating the asymptotic behavior of the one-step probabilities for fixed histograms H and G, the exponential decay rate of $P(H_{n+1} = G \,|\, H_n = H)$ is given by $RF(H, r^*, G)$ where r^* is the minimizer of the function $RF(H, r, G) :=$ $L(r, H) + KLD(r, H, G)$ over all possible mutation matrices $[r_{j,k}]$. This is precisely the content of the following key theorem, which gives the one-step cost function $C(H, G)$ in terms of the optimal intermediary mutation matrix linking the histogram H to G.

Theorem 4.4.1. *Let $ftr(S) \subset S \times S$ be the set of all feasible transitions, and fix any pair of histograms H and G in S. Let $MUT = MUT(H, G)$ be the compact convex set of all $(g \times g)$ matrices r with coefficients $0 \leq r_{i,j} \leq 1$ verifying $r_{i,j} = 0$ whenever $M_{i,j} = 0$, and such that*

$$p(j) = \frac{1}{< F, H >}(F_j H(j) - r_{j,.} + r_{.,j}) > 0 \quad \text{for all } j = 1, \dots, s$$

where $r_{i,.}$ and $r_{.,j}$ are the resp. sums of the ith row and j^{th} column of the matrix r. On the set MUT, define the function $RF(H, r, G)$ by

$$RF(H, r, G) = \sum_{j,k} [\, r_{j,k} \log(r_{j,k}/F_j H(j) M_{j,k}) - r_{j,k} + F_j H(j) M_{j,k} \,]$$

$$+ \sum_j G(j) \log(G(j)/p(j))$$

where $\sum_{j,k}$ is restricted to the j,k such that $M_{j,k} > 0$ and the $\sum_j$ excludes all the

j such that $H(j) = G(j) = 0$. Then $RF(H, r, G)$ is a convex function of r on the

compact convex set MUT.

When (H, G) is in $ftr(S)$, the value of $C(H, G)$ is finite, and given by the variational

formula

$$C(H, G) = \min_{r \in MUT} RF(H, r, G)$$

When (H, G) is not in $ftr(S)$, we have $C(H, G) = +\infty$.

An explicit derivation of $C(H, G)$ then involves a minimization of $RF(H, r, G)$. We want to avoid the cases in which $C(H, G) = \infty$, which introduces natural constraints on $RF(H, r, G)$ so that we only consider transitions $H \to G$ that are possible.

Constraint 1: For feasibility of daily emergence of mutants of type j, we must have that the number of j-cells after growth is at least the number of emmigrants of type j; that is, $NF_j H(j) \geq \sum_k Nr_{j,k}$. This yields the constraint

$$F_j H(j) - \sum_k r_{j,k} \geq 0. \tag{4.15}$$

Constaint 2: In order to have a finite cost during daily selection, if $G(j) \neq 0$, we must satisfy $NF_j H(j) > \sum_k Nr_{j,k} - \sum_k Nr_{k,j}$, which yields the constraint

$$F_j H(j) - \sum_k r_{j,k} + \sum_k r_{k,j} > 0. \tag{4.16}$$

This constraint states that if we choose at least 1 j-cell during random selection, we must have at least 1 j-cell present before selection and after the growth and mutation steps.

Constraint 3: If $H(j) = 0$ or $H \to G$ is not a supported transition,

$$r_{j,k} = 0. \tag{4.17}$$

The function $RF(H, r, G)$ represents the cost of transitioning from the histogram H to the histogram G via the intermediary normalized mutation matrix r. The one-step cost function $C(H, G)$ is then the cost of transitioning from the histogram H to the histogram G via the *optimal* intermediary mutation step, which yields the most-likely mutation step resulting in this transition. Calculation of the one-step cost function immediately yields the trajectory cost function $\lambda(w, T)$ of a histogram trajectory w of length T. Consequently, fast numerical computation of $C(H, G)$ is necessary when generating optimal trajectories linking two distinct histograms. For interior histograms, we have an explicit formula for $C(H, G)$ using Taylor expansions.

Theorem 4.4.2. *Consider any two interior histograms H and G in S^o, and let $q(j) = F_j H(j)/ < F, H >$. When the sum of all mutation rates $M_{j,k} := mQ_{j,k}$ is small, the one-step transition cost $C(H, G)$ has an explicit Taylor expansion of any finite order with respect to the mutation rates $M_{j,k}$. The first order expansion of $C(H, G)$ is given by*

$$C(H, G) \sim \sum_j G(j) \log(G(j)/q(j)) + m \sum_{j,k} Q_{j,k} F_j H(j)[\, 1 - E_{j,k} \,]$$

where

$$E_{j,k} = \exp(G(k)/F_k H(k) - G(j)/F_j H(j))$$

and this expression provides a very accurate explicit evaluation of $C(H, G)$ for mutation rates $m \leq 10^{-6}$.

Proof. Let $\Gamma = \{1, 2, \ldots, g\}$ and H and G be interior histograms. Notice that $RF(H, r, G)$ is a convex differentiable function of r. We write this minimization as $C(H, G) = \min_r RF(H, r, G)$ subject to the constraints given by (4.15)–(4.17). To calculate $C(H, G)$, we will assume that none of the inequality constraints are saturated. Then, we will solve the system

$$\frac{\partial}{\partial r_{i,n}} RF(H, r, G) = 0 \text{ for all } (i, n) \in \Gamma \times \Gamma \text{ with } i \neq n.$$

The only constraint required then is (4.15) for each $j \in \Gamma$. Taking the derivative of $RF(H, r, G)$ for all $(i, n) \in \Gamma \times \Gamma$ with $i \neq n$ gives

$$\frac{\partial}{\partial r_{i,n}} RF(H, r, G) = \log \frac{r_{i,n}}{F_i H(i) M_{i,n}} - \sum_{j \in \Gamma} \frac{G(j)}{p_j} \frac{\partial p_j}{\partial r_{i,n}}. \tag{4.18}$$

where we have

$$\frac{\partial p_j}{\partial r_{i,n}} = \begin{cases} 0 & i \neq j \text{ and } n \neq j \\ \frac{-1}{\langle F, H \rangle} & i = j \text{ and } n \neq j \\ \frac{1}{\langle F, H \rangle} & i \neq j \text{ and } n = j \\ 0 & i = n \end{cases} \tag{4.19}$$

Using (4.19) in (4.18) and setting the system equal to 0 gives the following solution:

$$\log \frac{r_{i,n}}{F_i H(i) M_{i,n}} = \frac{-G(i)/p_i + G(n)/p_n}{\langle F, H \rangle} \tag{4.20}$$

Set $A_j = p_j \langle F, H \rangle$. We then have

$$A_j < F_j H(j) + \sum_k r_{k,j} < F_j H(j) + \sum_{k \neq j} F_k H(k) = \langle F, H \rangle.$$

66

When the mutation rate $m \to 0$, we have that all entries $M_{j,k} \to 0$ at rates proportional to m and all $r_{j,k} \to 0$. We then have the limit

$$\lim_{m \to 0} A_j = F_j H(j) > 0. \tag{4.21}$$

Plugging the above into (4.20), we get the first-order result for mutation matrices $M_{j,k} < 10^{-6}$

$$r_{i,n} = F_i H(i) M_{i,n} E_{i,n} \tag{4.22}$$

$$E_{i,n} = \exp\left(-\frac{G(i)}{F_i H(i)} + \frac{G(n)}{F_n H(n)}\right). \tag{4.23}$$

The above gives the optimal mutation frequencies for fixed interior histograms H and G operating under the assumption that the constraints on $r_{j,k}$ are not saturated. For the constraint (4.15), we want for each $j \in \Gamma$,

$$F_j H(j) - \sum_k r_{j,k} > 0.$$

Using the optimized values of $r_{j,k}$, the non-saturation condition must verify for all j

$$\sum_{k | M_{j,k} \neq 0} M_{j,k} \exp\left(\frac{G(k)}{F_k H(k)}\right) < \exp\left(\frac{G(j)}{F_j H(j)}\right). \tag{4.24}$$

In order to complete a first-order computation of the cost function $C(H, G)$, we need to obtain a first-order approximation of the terms $\log p_j$, which utilizes the optimized values of $r_{j,k}$. Recall that with the optimized values of $r_{j,k}$, we have that

$$p_j = \frac{F_j H(j)}{\langle F, H \rangle} + \frac{1}{\langle F, H \rangle} \sum_k (F_k H(k) E_{k,j} M_{k,j} - F_j H(j) E_{j,k} M_{j,k}).$$

As we can see, p_j is comprised of a zero-order term and a term of order $m \leq 10^{-6}$, which is the mutation rate. We will denote the zero-order term as $q_j =$

67

$F_j H(j)/\langle F, H \rangle$. We can then write p_j as

$$p_j = q_j + \sum_k (q_k E_{k,j} M_{k,j} - q_j E_{j,k} M_{j,k})$$

$$= q_j \left(1 - \sum_k E_{j,k} M_{j,k} + \frac{1}{p_j} \sum_k p_k E_{k,j} M_{k,j} \right).$$

We can then write a first-order approximation for $\log p_j$ as

$$\log p_j = \log q_j + v_j \tag{4.25}$$

$$v_j = -\sum_k E_{j,k} M_{j,k} + \frac{1}{F_j H(j)} \sum_k F_k H(k) E_{k,j} M_{k,j} \tag{4.26}$$

where v_j is of order $m \leq 10^{-6}$ and $\sum_j q_j v_j = 0$.

Finally, we use the first-order approximations of $\log p_j$ and the mutation frequencies $r_{j,k}$ in order to get a first-order approximation for the cost function $C(H, G)$. We proceed by decomposing $RF(H, r, G)$ as follows:

$$RF(H, r, G) = RF_1 + RF_2$$

$$RF_1 = \sum_{j,k} \left(F_j H(j) M_{j,k} - r_{j,k} + r_{j,k} \log \frac{r_{j,k}}{F_j H(j) M_{j,k}} \right)$$

$$RF_2 = \sum_j G(j) \log \frac{G(j)}{p_j}$$

First, we compute RF_1 using the optimal values of $r_{j,k}$. This yields

$$RF_1 = \sum_{j,k} \left(F_j H(j) M_{j,k} - r_{j,k} + r_{j,k} \log \frac{r_{j,k}}{F_j H(j) M_{j,k}} \right)$$

$$= \sum_{j,k} F_j H(j) M_{j,k} \left(1 - \frac{r_{j,k}}{F_j H(j) M_{j,k}} + \frac{r_{j,k}}{F_j H(j) M_{j,k}} \log \frac{r_{j,k}}{F_j H(j) M_{j,k}} \right)$$

$$= \sum_{j,k} F_j H(j) M_{j,k} \left(1 - E_{j,k} + E_{j,k} \log E_{j,k} \right) \tag{4.27}$$

68

Notice that the coefficients of $M_{j,k}$ in RF_1 are always nonnegative.

Finally, we calculate RF_2. In this case, we use the optimized values of $r_{j,k}$ along with the first-order approximation of $\log p_j$. This yields

$$-\sum_j G(j) \log p_j = -\sum_j G(j) \log q_j + \sum_j \left(G(j) \sum_k E_{j,k} M_{j,k} \right)$$
$$-\sum_j \left(\frac{G(j)}{F_j H(j)} \sum_k F_k H(k) E_{k,j} M_{k,j} \right).$$

Plugging this into RF_2 gives us

$$RF_2 = \log\langle F, H \rangle + \sum_j G(j) \log \frac{G(j)}{F_j H(j)} \tag{4.28}$$
$$+ \sum_j \left(G(j) \sum_k E_{j,k} M_{j,k} \right) - \sum_j \left(\frac{G(j)}{F_j H(j)} \sum_k F_k H(k) E_{k,j} M_{k,j} \right).$$

This gives a first-order approximation of $C(H, G)$ given by (4.27) and (4.28), which can be simplified further. Write $C(H, G) = C_0(H, G) + Z(H, G)$ where

$$C_0(H, G) = \log\langle F, H \rangle + \sum_j \log \frac{G(j)}{F_j H(j)}$$
$$Z(H, G) = \sum_{j,k} \left(G(j) E_{j,k} M_{j,k} - \left(\frac{G(j) F_k H(k)}{F_j H(j)} \right) E_{k,j} M_{k,j} \right)$$
$$+ \sum_{j,k} \left(F_j H(j) M_{j,k} (1 - E_{j,k} + E_{j,k} \log E_{j,k}) \right)$$

We can write the terms $Z(H, G) = \sum_{j,k} M_{j,k} Z_{j,k}$ where

$$Z_{j,k} = F_j H(j)(1 - E_{j,k} + E_{j,k} \log E_{j,k}) + G(j)E_{j,k} - \frac{G(k)F_j H(j)}{F_k H(k)} E_{j,k}$$

$$= F_j H(j) - F_j H(j)E_{j,k} + F_j H(j)E_{j,k} \log E_{j,k} + G(j)E_{j,k} - \frac{G(k)F_j H(j)}{F_k H(k)} E_{j,k}$$

$$= F_j H(j) - F_j H(j)E_{j,k} + F_j H(j)E_{j,k} \left(\frac{-G(j)}{F_j H(j)} + \frac{G(k)}{F_k H(k)} \right)$$

$$+ G(j)E_{j,k} - \frac{G(k)F_j H(j)}{F_k H(k)} E_{j,k}$$

$$= F_j H(j)(1 - E_{j,k}).$$

Therefore, the formula for the cost function $C(H, G)$ when H and G are interior histograms is given by

$$C(H, G) = \log\langle F, H \rangle + \sum_j G(j) \log \frac{G(j)}{F_j H(j)} + \sum_{j,k} F_j H(j)M_{j,k}(1 - E_{j,k}) \quad (4.29)$$

$$M_{j,k} = mQ_{j,k}$$

$$E_{j,k} = \exp\left(\frac{-G(j)}{F_j H(j)} + \frac{G(k)}{F_k H(k)} \right)$$

This formula is valid as long as the constraints on $r_{j,k}$ are indeed not saturated. The nonsaturation inequality is given by

$$\sum_k M_{j,k} \exp\left(\frac{G(k)}{F_k H(k)} \right) < \exp\left(\frac{G(j)}{F_j H(j)} \right) \quad \text{for all } j. \quad (4.30)$$

$\square$

This type of approximation will need more complicated but achievable extensions to compute $C(H, G)$ when H and G are boundary histograms with some frequencies $H(j)$ and/or $G(k)$ equal to zero. Since we will focus on interior histograms,

we will only consider the above formula. Since we used Stirling's formula and imposed constraints on $RF(H, r, G)$, the histograms H and G must satisfy the following nonsaturation and boundary conditions, respectively:

$$\sum_k mQ_{j,k} \exp\left(\frac{G(k)}{F_k H(k)}\right) < \exp\left(\frac{G(j)}{F_j H(j)}\right) \text{ for all } j, \tag{4.31}$$

$$H(j), G(j) \geq 50/N \text{ for all } j \in \Gamma. \tag{4.32}$$

4.4.2 Large deviations for random histogram trajectories

Now that we have an explicit form for the one-step cost function, we can state a large deviations result for the random histogram trajectories. Let $\Omega(T) = S^{1+T}$ be the set of all histograms sequences $\mathbf{w} = [w_0 \ldots w_T]$ of finite length T, and define the path space Ω as the union of all the $\Omega(T)$ for $T \in \mathbb{N}$. The set $\Omega(T)$ is a compact metric space for the usual Euclidean distance in $(R^g)^T$. The interior and the closure of any subset $A \subset \Omega(T)$ are denoted by A^o and $\bar{A}$, respectively. For any histogram trajectory $\mathbf{w} \in \Omega$, we will define the cost function $\lambda(\mathbf{w}, T) \geq 0$ by the additive formula

$$\lambda(\mathbf{w}, T) = C(w_0, w_1) + C(w_1, w_2) + \ldots + C(w_{T-1}, w_T) \tag{4.33}$$

which is a lower-semicontinuous function on each path space $\Omega(T)$. Now that we have an explicit formula for the one-step cost function given by (4.29), we can now establish a large deviations principle and perform the key minimizations that appear in the following two key theorems.

Theorem 4.4.3. *For any set of paths $A \subset \Omega(T)$, define the rate functional $\Lambda(A) \geq 0$*

by the formula

$$\Lambda(A) = \inf_{\mathbf{w} \in A} \lambda(\mathbf{w}, T).$$

Then the random trajectory of population histograms $\mathbf{H} = [H_0 \, H_1 \, \ldots \, H_T]$ *verifies the large deviations limit*

$$\Lambda(A^o) \leq \liminf_{N \to \infty} \frac{1}{N} \log[\, P(\mathbf{H} \in A)\,] \leq \limsup_{N \to \infty} \frac{1}{N} \log[\, P(\mathbf{H} \in A)\,] \leq -\Lambda(\bar{A}).$$

In particular, whenever $\Lambda(A^o) = \Lambda(\bar{A})$, *one has*

$$\lim_{N \to \infty} \frac{1}{N} \log[\, P(\mathbf{H} \in A)\,] = -\Lambda(A).$$

The relation $\Lambda(A^o) = \Lambda(A) = \Lambda(\bar{A})$ *is always true when* A *has "thin boundary", i.e. when* A *and* A^o *have the same closure* $\bar{A}$, *which is certainly the case when* A *is an open set.*

Intuitively, this says that for large classes of subsets A of the path space Ω and for N large, we have $P(\mathbf{H} \in A)$ is roughly equivalent to $\exp(-N\Lambda(A))$. Hence for $\Lambda(A) > 0$ and large N, the events $\mathbf{H} \in A$ are rare events. The calculation of $\Lambda(A)$, which gives the exponential decay rate of these probabilities, is linked to the cost function $\lambda(\mathbf{w}, T)$ of a trajectory $\mathbf{w}$. However, once the unique cost-minimizing path is obtained, we get the following useful tube result well-documented in many situations (see [2]).

Theorem 4.4.4. *Within the space* $\Omega(T)$ *of histogram trajectories, consider any closed subset* A *having thin boundary such that* $\Lambda(A) > 0$. *Assume that there is a unique cost minimizing path* $\mathbf{w}^*$ *in* A *such that*

$$\lambda(\mathbf{w}^*, T) = \Lambda(A) = \inf_{\mathbf{w} \in A} \lambda(\mathbf{w}, T).$$

Let $U \subset \Omega(T)$ be any fixed tube of arbitrary small radius around this optimizing path $\mathbf{w}^*$, and let $\mathbf{H}$ be the random histogram trajectory $[H_0 \ldots H_T]$. Then, the conditional probabilities $P(\mathbf{H} \in U \mid \mathbf{H} \in A)$ must tend to 1 as population size $N \to \infty$.

For large N in the above theorem, the rare event $(\mathbf{H} \in A)$ can essentially be realized only by histograms trajectories $\mathbf{H}$ which are quite close to the cost minimizing trajectory $\mathbf{w}^*$ in A. This is the basic mathematical reason why for a large population size N, specific rare evolutionary events A can only be realized by population evolutions following a narrowly defined path in the fitness landscape, namely the cost minimizing path $\mathbf{w}^*$ just defined. Furthermore, the preceding two theorems allow one to answer an important question in many general settings: what is the most likely transition pathway linking a fixed initial point to a desired target point? We address this question in Section 5.2.2.

Chapter 5

Applications of Large Deviations Principles

In Chapter 4, we reviewed and established some large deviations principles in a number of settings. However, once one establishes a large deviations principle that is applicable to a specific stochastic system, what types of rare events would one investigate? For these rare events, how would one go about finding the element that minimizes the Cramer transform so that estimates can be made on the probabilities of these rare events? The rare events on which we focus are transition pathways linking a fixed initial point to a desired target state. Implicit in this transition path problem is the time it takes to reach the target state. Therefore, applying the large deviations principles we established involves minimizing the Cramer transform (cost function) over all possible pathways where the initial and terminal points are fixed *and* all possible times in which the system can reach the target. This double

minimization problem yields a function of the initial and target points and is related to the *quasi-potential* in the theory of large deviations of SDEs developed by Friedlin and Wentzell [17], which is central to applying large deviations principles on long timescales. Furthermore, the minimizing path gives the most likely transition and time the system takes in order to reach the target state.

In this chapter, we will accomplish this double minimization for Gaussian diffusions with delay, which yields a fully explicit formula for the minimizing path and rate functional. For populations of E. Coli, we will state a theorem that mirrors the Friedlin-Wentzell large deviations framework for SDEs which will allow us to calculate most likely evolutionary trajectories linking an initial histogram to a target histogram. We then perform this minimization using interior histograms.

5.1 Gaussian Diffusions with Delay

Recall that a Gaussian diffusion with delay X_t is a stochastic process that verifies the linear delay SDE defined by (1.1). We showed that this process is indeed a Gaussian process (Proposition 3.1.1). Once we center this process, we can apply Theorem 4.3.2 and Proposition 4.3.4 by minimizing the Cramer transform over a set of paths. Since we are interested in finding most likely transition pathways $f \in C([0, T], \mathbb{R}^d)$ such that $f(0) = p \in \mathbb{R}^d$ and $f(T) = q \in \mathbb{R}^d$, the set of paths will be all possible paths with these constraints. Furthermore, the Cramer transform in this setting is a quadratic form so that we can use Lagrange multipliers. In this section, we will perform this minimization, which will involve the process Z_t, which is a centered version of X_t.

Then, we will provide a probabilistic interpretation using a small tube around the minimizing path.

5.1.1 Large deviation rate functional for Gaussian diffusions with delay

Recall that $X_t = m(t) + \varepsilon Z_t$ denotes Gaussian diffusion with delay under study. In this section we minimize the Cramer transform associated with Z_t. For points $p, q \in \mathbb{R}^d$ and time $T > 0$, define

$$\text{Path}(p, q; T) = \left\{ f \in C([0, T], \mathbb{R}^d) : f(0) = p, \ f(T) = q \right\}.$$

Random paths of X_t lie in $\text{Path}(p, q; T)$. To study Z_t, we must shift this space of paths by the mean $m(t)$. Define

$$C_{\mathbf{0}}([0, T], \mathbb{R}^d) = \left\{ f \in C([0, T], \mathbb{R}^d) : f(0) = \mathbf{0} \right\},$$

$$\text{Path}(\mathbf{0}, q - m(T); T) = \left\{ f \in C_{\mathbf{0}}([0, T], \mathbb{R}^d) : f(T) = q - m(T) \right\}.$$

We now minimize the Cramer transform λ associated with Z_t over $\text{Path}(\mathbf{0}, q - m(T); T)$. The Cramer transform is linked to the covariance operator R of Z_t by

$$\lambda(f) = \frac{1}{2} \langle R^{-1} f, f \rangle_{L^2[0,T]}$$

for paths $f \in \sqrt{R}(L^2[0, T])$. Since $\text{Path}(\mathbf{0}, q - m(T); T)$ is determined by linear constraints on f, we minimize the quadratic form $\lambda(f)$ for $f \in \text{Path}(\mathbf{0}, q - m(T); T)$ using Lagrange multiplier theory [28].

For $f \in C_{\mathbf{0}}([0,T], \mathbb{R}^d)$, define the Lagrangian

$$\mathcal{L}_{f,\mu} := \frac{1}{2}\langle R^{-1}f, f\rangle + \mu \cdot (f(T) - (q - m(T))),$$

where $\cdot$ is the usual dot product in $\mathbb{R}^d$ and $\mu \in \mathbb{R}^d$ is the Lagrange multiplier vector.
Setting the derivative $D\mathcal{L}_{f,\mu}(\varphi)$ for $\varphi \in C_{\mathbf{0}}([0,T], \mathbb{R}^d)$ equal to zero, we have

$$D\mathcal{L}_{f,\mu}(\varphi) = \lim_{\Delta \to 0} \frac{\mathcal{L}_{f+\Delta\varphi,\mu} - \mathcal{L}_{f,\mu}}{\Delta} = \langle R^{-1}f, \varphi\rangle + \mu \cdot \varphi(T) = 0,$$

yielding the condition

$$\langle R^{-1}f, \varphi\rangle = -\mu \cdot \varphi(T) = -\mu \cdot \delta_T(\varphi).$$

Here δ_T denotes the Dirac mass at time T. The minimizing path g is therefore given by

$$g = R(-\mu \cdot \delta_T). \tag{5.1}$$

The right side of (5.1) may be expressed in terms of the covariance function ρ of Z_t:

$$R(-\mu \cdot \delta_T)(s) = -\int_0^T \rho(s,u)\mu \, d\delta_T(u) = -\rho(s,T)\mu. \tag{5.2}$$

Since $g(T) = q - m(T)$, (5.2) implies

$$q - m(T) = -\rho(T,T)\mu,$$

so the Lagrange multiplier is given by

$$-\mu = \rho(T,T)^{-1}(q - m(T)).$$

The trajectory that minimizes the Cramer transform therefore takes the form

$$g^T(s) = \rho(s,T)[\rho(T,T)^{-1}(q - m(T))] \qquad (0 \leqslant s \leqslant T),$$

and has Cramer transform

$$\lambda(g^T) = \frac{1}{2}[\rho(T,T)^{-1}(q - m(T))] \cdot [q - m(T)].$$ (5.3)

Notice that $g^T = \sqrt{R}(\hat{g})$, where

$$\hat{g}(s) = k(s,T)[\rho(T,T)^{-1}(q - m(T))]$$

and k is the kernel defined by

$$(\sqrt{R}f)(s) = \int_0^T k(s,u)f(u)\,\mathrm{d}u.$$

For the Gaussian diffusion with delay $X_t = m(t) + \varepsilon Z_t$, the most likely path $h^T(s)$ realizing $X_0 = p$ and $X_T = q$ is hence given by

$$h^T(s) = m(s) + g^T(s) = m(s) + \rho(s,T)[\rho(T,T)^{-1}(q - m(T))] \qquad (0 \leqslant s \leqslant T)$$

(5.4)

and has energy

$$\lambda(h^T) = \frac{1}{2}[\rho(T,T)^{-1}(q - m(T))] \cdot [q - m(T)].$$ (5.5)

Minimizing $\lambda(h^T)$ over T produces the most likely time T of transition from $X_0 = p$ to $X_T = q$, the most likely transition path, and the associated energy. Now, if we directly apply Theorem 4.3.2 to the set $\mathrm{Path}(p,q;T)$, we would only get the large deviations bounds given by (4.4) because $\mathrm{Path}(p,q;T)$ has empty interior in $C([0,T];\mathbb{R}^d)$. However, if we place a small tube around the minimizing trajectory, we will be in the more useful case where the large deviations limit exists. Below we interpret *most likely path* in a precise probabilistic sense using this small tube.

5.1.2 Probabilistic interpretation

For any path from p to q over time interval $[0, T]$ in $\mathbb{R}^d$, the large deviations principle in Theorem 4.3.2 yields quantitative information about the probability that the process X_t remains within a small tube of the given path over $[0, T]$. To apply Theorem 4.3.2, we first shift the given tube by subtracting the mean $m(t)$ of X_t so that we may work with the centered process εZ_t. Once the large deviations principle has been applied to εZ_t, we then add $m(t)$ to recover information about X_t. Crucially, both the Cramer transform associated with Z_t and the path that minimizes it are independent of ε. The application of Theorem 4.3.2 proceeds as follows.

First assume $q \neq m(T)$. For any path $f \in \mathrm{Path}(\mathbf{0}, q - m(T); T)$ and small radius $r > 0$, define the tube

$$\mathrm{Tube}(f, r) = \left\{ \varphi \in C_{\mathbf{0}}([0, T], \mathbb{R}^d) : \sup_{0 \leqslant t \leqslant T} |\varphi(t) - f(t)| \leqslant r \right\}.$$

Since $\mathrm{Tube}(f, r)$ is the closure of its interior in $C_{\mathbf{0}}([0, T], \mathbb{R}^d)$, Theorem 4.3.2 gives

$$\lim_{\varepsilon \to 0} \varepsilon^2 \log(\mathbb{P}(\varepsilon Z^T \in \mathrm{Tube}(f, r))) = -\Lambda(\mathrm{Tube}(f, r)),$$

where Z^T denotes the set of paths generated by Z_t over $[0, T]$. In particular, for the path g^T that minimizes the Cramer transform, we have

$$\lim_{\varepsilon \to 0} \varepsilon^2 \log(\mathbb{P}(\varepsilon Z^T \in \mathrm{Tube}(g^T, r))) = -\Lambda(\mathrm{Tube}(g^T, r)) = -\lambda(g^T).$$

In this sense, $\mathrm{Tube}(g^T, r)$ is the most likely route of passage for εZ_t, and shifting $\mathrm{Tube}(g^T, r)$ by $m(t)$ yields the most likely route of passage from p to q over $[0, T]$ for X_t.

Note that $q = m(T)$ is a special case. Here, X_t will remain within a small tube around $m(t)$ with probability converging to one as $\varepsilon \to 0$. That is, the most likely transition path from p to q over $[0, T]$ is simply the path of the mean in this case.

To effectively compute the most likely transition path from p to q for X_t, we have implemented a numerical scheme in three steps:

- Solve several ODEs with delay to compute the mean path $m(t)$ of X_t and the covariance function $\rho(s, t)$ of Z_t.

- For fixed T, p, q, compute the most likely transition path $h = h^T$ from $X_0 = p$ to $X_T = q$, and its energy $\lambda(h^T)$, as given by (5.4) and (5.5).

- Compute the optimal transition time T_{opt} by minimizing $\lambda(h^T)$ over all times $T > 0$.

We explicitly describe these three steps in Section 6.1.1 and Section 6.1.2.

5.2   Genetic Evolution of E. Coli Populations

With the preceding tools, we will be able to answer a natural and important question in the context of bacterial population evolution, namely how can one reconstitute the most likely evolutionary path starting with a known initial histogram H and reaching a known terminal histogram G after an unknown number T of daily cycles. As we did in the case of Gaussian diffusions with delay, this can be accomplished by minimizing the Cramer transform (cost function) over all evolutionary paths with

initial and terminal histograms fixed. Recall that for a histogram trajectory $\mathbf{w}$ of length T, the cost function $\lambda(\mathbf{w}, T)$ is given explicitly as a sum of one-step costs. For any two *interior* histograms, the one-step cost is given Theorem 4.4.2. In this section, we will state a tube result for these optimal paths similar to the tube result in the Gaussian case. Then, we numerically compute an expression for the cost-minimizing trajectory using Lagrange multipliers and first-order Taylor expansions. In doing so, we will show that cost-minimizing paths are completely determined by their last two points.

5.2.1 Most likely evolution from initial to terminal histograms

The following tube theorem is essentially an application of Theorem 4.4.4 with the set A being all paths of length T where the initial and terminal histograms are fixed.

Theorem 5.2.1. *Fix any two population histograms H and G. Let $A(H, G, T)$ be the set of all paths $\mathbf{w} \in \Omega(T)$ verifying $w_0 = H$, $w_T = G$, and $w_n \neq G$ for all $n < T$. Assume that there is a unique path $\mathbf{w}^*$ of finite length linking H to G at minimal cost, and let T^* be the length of $\mathbf{w}^*$. Hence $\mathbf{w}^* \in A(H, G, T^*)$ and verifies*

$$\lambda(\mathbf{w}^*, T^*) = \inf_T \inf_{\mathbf{w} \in A(H,G,T)} \lambda(\mathbf{w}, T)$$

For any $\delta > 0$ and T, and any path $\mathbf{w} \in \Omega(T)$, let $U(\mathbf{w}, \delta)$ be the tube of radius δ centered at $\mathbf{w}$, and let $Q_T(\mathbf{w})$ be the conditional probability

$$Q_T(\mathbf{w}) = P\{\mathbf{H} \in U(\mathbf{w}, \delta) \mid \mathbf{H} \in A(H, G, T)\}$$

Let Q^+ be the maximum of $Q_T(\mathbf{w})$ over all T and all paths $\mathbf{w} \in \Omega(T)$. For any small enough but fixed $\delta > 0$, the difference between Q^+ and $Q_{T^*}(\mathbf{w}^*)$ then tends to 0 as

the population size $N \to \infty$. In other words, for N large enough , the most likely random evolutionary path $[H_0\, H_1\, \dots]$ linking H to G has T^* steps and is arbitrarily close to the path $\mathbf{w}^*$ linking H to G at minimal cost.

By the above theorem, we have that for large populations N, if an evolutionary path from H to G is to occur over some length of time, there is a high probability that this path will be very close to the optimal path $\mathbf{w}^*$ and will have the same length as $\mathbf{w}^*$. Thus, we now focus on computing this most likely path $\mathbf{w}^*$.

5.2.2   Numerical computation of cost minimizing histograms trajectories

The numerical computation of cost-minimizing histogram trajectories linking two given histograms is essential for concrete applications of Theorem 5.2.1 to potential bacterial evolution scenarios. To solve this challenging computational problem, we develop a fast numerical formula for generating minimizing trajectories in reverse time. Using the formula for $\lambda(\mathbf{w}, T)$ given by (4.33) and the one-step cost function given in Theorem 4.4.2, the basic idea is to minimize a *two-step cost function* using Lagrange multipliers for the case when the mutation rate $m = 0$. Using this "zero-order" solution, we then use Lagrange multipliers and Taylor expansions in m to obtain a numerical solution to the full minimization problem for small mutation rates $m \leq 10^{-6}$. Once this solution is found, we can develop algorithms to generate most likely trajectories in reverse time for a fixed initial histogram H and target histogram G. In this section, we note that any statement involving the order of a

term or solution refers to the mutation rate m.

Recall that the cost associated to an evolutionary trajectory $\mathbf{w} = [w_0 \, w_1 \, \ldots \, w_T]$ up to day T is given by the function

$$\lambda(\mathbf{w}, T) = \sum_{j=0}^{T-1} C(w_j, w_{j+1}). \tag{5.6}$$

Calculation of the Cramer set functional $\Lambda(A)$ for a set of paths A requires a minimization of $\lambda(\mathbf{w}, T)$ over all paths $\mathbf{w} \in A$. If $\mathbf{w}^* = [w_0^* \, w_1^* \, \ldots]$ is the minimizing path in A, it is not necessarily true that $C(w_j^*, w_{j+1}^*)$ is a minimizer of $C(x, y)$ over all histograms $x \in S^\circ$ for a fixed histogram $y \in S^\circ$. However, we do have that the geodesic segment $[w_j^* \, w_{j+1}^* \, w_{j+2}^*]$ of $\mathbf{w}^*$ is a minimizer of the function $C(x, y) + C(y, z)$ over all histograms $y \in S^\circ$ for fixed histograms $x, z \in S^\circ$.

With the above motivation, given a geodesic segment $[x \, y \, z]$ where $x, z \in S^\circ$ are fixed interior histograms, we compute

$$\min_{y \in S^\circ} C(x, y) + C(y, z) \qquad \text{subject to} \qquad \sum_{j=1}^{g} y(j) = 1. \tag{5.7}$$

We use Lagrange multipliers to complete the minimization. Let $L \in \mathbb{R}$ be the Lagrange multiplier associated to the constraint above. We then solve the system of g equations

$$\frac{\partial}{\partial y(j)} C(x, y) + \frac{\partial}{\partial y(j)} C(y, z) + L = 0. \tag{5.8}$$

Calculating the partial derivatives yields

$$\frac{\partial}{\partial y(j)}C(x,y) = 1 + \log \frac{y(j)}{F_j x(j)} + m \sum_k \left(Q_{j,k}E_{j,k} - \frac{F_k x(k)}{F_j x(j)}Q_{k,j}E_{k,j} \right) \tag{5.9}$$

$$\frac{\partial}{\partial y(j)}C(y,z) = \frac{F_j}{\langle F, y \rangle} - \frac{z(j)}{y(j)} + mF_j \sum_k Q_{j,k} \tag{5.10}$$

$$- \left(F_j + \frac{z(j)}{y(j)} \right) m \sum_k Q_{j,k}\hat{E}_{j,k} - \frac{z(j)}{F_j y(j)^2}m \sum_k F_k y(k)Q_{k,j}\hat{E}_{k,j}$$

$$E_{j,k} = \exp\left(-\frac{y(j)}{F_j x(j)} + \frac{y(k)}{F_k x(k)} \right)$$

$$\hat{E}_{j,k} = \exp\left(-\frac{z(j)}{F_j y(j)} + \frac{z(k)}{F_k y(k)} \right)$$

In both partial derivatives given by (5.9) and (5.10), we have terms of zero order and terms of order at most $m = 10^{-6}$. Since the mutation rate is small, we will solve the system using a first-order approximation by first solving the case when there are no mutations ($m = 0$) and then more generally for small m using the zero-order solution. Again, these approximations are valid since m is small by the implicit function theorem.

We first assume that $m = 0$. This implies that

$$\frac{\partial}{\partial y(j)}C(x,y) = 1 + \log \frac{y(j)}{F_j x(j)}$$

$$\frac{\partial}{\partial y(j)}C(y,z) = \frac{F_j}{\langle F, y \rangle} - \frac{z(j)}{y(j)}.$$

Therefore, the system (5.8) implies

$$1 + \log \frac{y(j)}{F_j x(j)} + \frac{F_j}{\langle F, y \rangle} - \frac{z(j)}{y(j)} + L = 0.$$

84

Notice that this equation can be explicitly solved for $x(j)$. This gives us

$$x(j) = \exp(L)K_j$$

$$K_j = \frac{y(j)}{F_j} \exp\left(\frac{F_j}{\langle F, y\rangle} - \frac{z(j)}{y(j)}\right)$$

Now, x is a histogram, so $\sum_{j=1}^{g} x(j) = 1$. This yields

$$1 = \exp(L)\sum_{j=1}^{g} K_j.$$

Therefore, the Lagrange multiplier must satisfy

$$\exp(L) = \frac{1}{\sum_{j=1}^{g} K_j}.$$

Hence, the histogram x must satify the equation

$$x(j) = \frac{K_j}{\sum_{l=1}^{g} K_l} \tag{5.11}$$

$$K_j = \frac{y(j)}{F_j} \exp\left(\frac{F_j}{\langle F, y\rangle} - \frac{z(j)}{y(j)}\right).$$

For each j, we call the solution given by (5.11) the *zero-order solution*.

More generally, let the mutation rate m be at most order 10^{-6}. The system (5.8) is now implicit and highly nonlinear so that an explicit solution in terms of x_j is not possible. Let $x^{(0)}(j)$ denote the zero-order solution given by (5.11). Write the first-order approximation of the solution $x(j)$ as $x(j) = x^{(0)}(j)(1 + W_j)$ where W_j is a linear combination of all the terms of order $M_{j,k}$ in the system (5.8). In this case, the condition $\sum_{j=1}^{g} x(j) = 1$ implies that $\sum_{j=1}^{g} x^{(0)}(j)W_j = 0$. Let $\hat{L}$ be a small, first-order modification of the Lagrange multiplier L. We want to solve the system

$$\log \frac{F_j x(j)}{y(j)} = L + \hat{L} + B_j + H_j$$

85

where

$$B_j = \frac{F_j}{\langle F, y \rangle} - \frac{z(j)}{y(j)}$$

$$H_j = F_j \sum_k m Q_{j,k} - \left(F_j + \frac{z(j)}{y(j)} \right) \sum_k \hat{E}_{j,k} m Q_{j,k} - \frac{z(j)}{F_j y(j)^2} \sum_k F_k y_k m Q_{k,j} \hat{E}_{k,j}.$$

Using a first-order approximation, we then have that

$$\log \frac{F_j x(j)}{y(j)} = \log \frac{F_j x^{(0)}(j)}{y(j)} + W_j$$

$$= L + B_j + W_j.$$

This is equivalent to $W_j + \hat{L} + H_j$. Let $H = (H_1, H_2, \ldots, H_g)$ be the vector of terms H_j. Our imposed condition transforms to

$$0 = \sum_{j=1}^{g} x^{(0)}(j) W_j = \hat{L} + \sum_{j=1}^{g} x^{(0)}(j) H_j$$

so that $\hat{L} = -\langle x^{(0)}, H \rangle$ and $W_j = H_j - \langle x^{(0)}, H \rangle$. Finally, the first-order approximation of the histogram x is given by

$$x(j) = (1 - \langle x^{(0)}, H \rangle) x^{(0)}(j) + x^{(0)}(j) H_j \tag{5.12}$$

$$H_j = F_j m \sum_k Q_{j,k} - \left(F_j + \frac{z(j)}{y(j)} \right) m \sum_k \hat{E}_{j,k} Q_{j,k} - \frac{z(j)}{F_j y(j)^2} m \sum_k F_k y_k Q_{k,j} \hat{E}_{k,j}$$

$$\hat{E}_{j,k} = \exp \left(-\frac{z(j)}{F_j y(j)} + \frac{z(k)}{F_k y(k)} \right).$$

The above calculations have shown a condition that all cost-minimizing paths must satisfy, which we informally present in the following theorem.

Theorem 5.2.2. *If* $\mathbf{w} \in \Omega(T)$ *is the cost minimizing path such that* w_0 *and* w_T *are fixed, then the histograms in the geodesic segment* $[w_{n-2} \, w_{n-1} \, w_n]$ *must verify*

86

the recurrence relation given by (5.12) *for all* $2 \leq n \leq T$. *Consequently, the cost minimizing histogram paths* $\mathbf{w}$ *where* $w_k \in S^{\circ}$ *for* $1 \leq k \leq T - 1$ *are completely determined by the last two points* w_{T-1} *and* w_T.

We now have an explicit formula to generate most likely evolutionary trajectories. In addition, we have a condition in which all most likely paths must obey. Notice that this condition is dependent on the last two points. With a desired fixed target, we can then generate optimal trajectories by essentially varying the penultimate point and choosing the trajectory of least cost. The numerical implementation of this method, called reverse shooting, is fully described in Section 6.2.

Chapter 6

Numerical Methods for Most Likely Trajectories

In Chapter 5, we presented explicit calculations and formulas in minimizing the Cramer transform for Gaussian diffusions with delay and stochastic evolution of bacterial populations. For Gaussian diffusions with delay, the optimal path, given by (5.4), is written explicilty as a function of the mean $m(t)$ of X_t and the covariance $\rho(s,t)$ of Z_t. Consequently, the Cramer transform is also a function of these two statistical meaures. The mean and covariance verify the delay ODEs given by (3.2) and (3.5), respectively. The delay ODE for the covariance contains a nonhomogeneous term which verifies the delay ODE (3.9). Therefore, computing most likely transition pathways for Gaussian diffusions with delay reduces to solving three delay ODEs. For bacterial populations of E. Coli, we have a condition that all most likely trajectories must satisfy for fixed terminal and penultimate histograms, which

is given by (5.12). This condition is highly dependent on the penultimate point.

In this chapter, we will describe the numerical solution of the three relevant delay ODEs for Gaussian diffusions with delay. We then explain how we numerically minimize the resulting Cramer transform. Then, we will describe the reverse shooting method used to generate most likely evolutionary trajectories linking an initial histogram to a desired target histogram. In doing so, we will show how we can choose sensible penultimate points that result in generating "good" trajectories by providing numerical evidence.

6.1 Most likely transitions for Gaussian diffusions with delay

With the most likely transition pathway being expressed a function of the mean and covariance, we need only to numerically simulate these delay ODEs. Recall that in Section 3.1.4 and Section 3.1.5, the analytical solution of the mean $m(t)$ and covariance $\rho(s,t)$ can be found using a step-by-step method. In this method, we reduced the delay ODEs to a sequence of nonhomogeneous ODEs iteratively solved on intervals of length τ where the delay terms are known. Consequently, we can use standard numerical ODE techniques to simulate these equations. We describe the technique in detail below. Then, we will explain how we can numerically minimize the Cramer transform once these delay ODEs are solved numerically.

6.1.1 Numerical solution of three delay ODEs

Each delay ODE of interest here is iteratively solved on the time intervals $J_k = [(k-1)\tau, k\tau]$ for $k = 1, 2, \ldots (1 + [T/\tau])$. For each k, this amounts to solving numerically a linear ODE with known right-hand side. For this, we use a backward Euler scheme, which is known to be stable for equations of this form [5, 19]. To compute $m(t)$, we discretize $[0, T]$ into subintervals of equal length $\Delta t = \tau/N$. Backward Euler is given by

$$m(t) - m(t - \Delta t) = [a + Bm(t) + Cm(t - \tau)]\Delta t.$$

which yields the recursive equation

$$m(t) = (I - \Delta t B)^{-1} m(t - \Delta t) + \Delta t (I - \Delta t B)^{-1}[a + Cm(t - \tau)].$$

The initial history of the mean is used to numerically compute the solution $m(t) = m_1(t)$ on the initial interval J_1. To numerically generate the solution $m(t) = m_k(t)$ on J_k, we proceed by iteration on k, using the discretized expressions just stated above. This yields a full numerical approximation of $m(t)$ on $[0, T]$. We apply a completely similar strategy to compute for each s the function $t \to \phi_s(t)$ as defined by (3.11). However both s and t will be constrained to belong to the finite grid

$$\text{Grid}(N) = \{j\tau/N : j = 1, \ldots, M \text{ and } M = N(1 + \lfloor T/\tau \rfloor)\}.$$

After the computation of $\phi_s(t)$, we generate the $F(s, t)$ values for s and t in $\text{Grid}(N)$ by the explicit formula $F(s, t) = \phi_s(t) - \Sigma H(s - t)$ where $H(s - t)$ is a Heaviside function.

We then proceed to compute $\rho(s,t)$ for s and t in $\text{Grid}(N)$. For each fixed t in $\text{Grid}(N)$, the Backward Euler discretization of the delay ODE verified by the function $s \to \rho(s,t)$ yields the recursive relation

$$\rho(s,t) = (I - \Delta s B)^{-1}\rho(s - \Delta s, t) + \Delta s(I - \Delta s B)^{-1}[C\rho(s - \tau, t) + \Sigma F(s,t)] \quad (6.1)$$

where $\Delta s = \tau/N$. The initial values $\rho(s,t) = 0$ for $s \in [-\tau, 0]$ and the recursive relation (6.1) enable the computation of $\rho(s,t)$ for $s \in J_1$. Keeping t fixed, one then uses (6.1) as above and the values of $\rho(\cdot, t)$ on J_k to compute the values of $\rho(\cdot, t)$ on J_{k+1}. Repeating this operation for each t in $\text{Grid}(N)$ finally provides $\rho(s,t)$ for s and t in $\text{Grid}(N)$.

6.1.2 Numerical minimization of the Cramer transform for Gaussian diffusions with delay

Fix $T > 0$. For the Gaussian diffusion with delay X_t, the most likely transition path h from $X_0 = p$ to $X_T = q$ and its energy $\lambda_h(T)$ have been explicitly expressed in terms of the functions $m(t)$ and $\rho(s,t)$ (see (5.4) and (5.5)). Plugging into these two formulas the values of $m(t)$ and $\rho(s,t)$ numerically computed for s and t in $\text{Grid}(N)$ immediately provides numerical approximations of $h(s)$ for s in $\text{Grid}(N)$ and of $\lambda_h(T)$ for a fixed terminal time T.

To compute the most likely time at which X_t will reach q, whenever this rare event is realized, we have to minimize $u(T) = \lambda_h(T)$ in T. So we select a large terminal time T_{large}, and we numerically minimize the function $u(T)$ on the interval $[0, T_{\text{large}}]$. If on that time interval $u(T)$ exhibits an actual minimum at T_{opt}, this gives

us an approximate most likely transition time T_{opt}. Otherwise, we set $T_{\text{opt}} = \infty$.

6.1.3 Exit path from nominally stable stationary states

As $\varepsilon \to 0$, the limit dynamics of X_t is a deterministic dynamic system x_t driven by an obvious first-order ODE with delay. Let p be a stable stationary state of x_t, and let V be a small neighborhood of p. Determining for small ε the most likely path followed by X_t to exit from V when $X_0 = p$ is a problem of practical interest in many contexts. Our numerical computation of the most likely transition path from $X_0 = p$ to $X_T = q$ with q on the boundary of V will enable us to numerically solve these types of exit problems. We illustrate this approach with the detailed study of a specific dynamical system from biochemistry, which is given in Section 2.2.

6.2 Most likely evolutionary trajectories for E. Coli populations

In light of Theorem 5.2.1, we are interested in getting probabilistic estimates for the set $A(H, G, T)$, which is the set of all paths w such that $w_0 = H, w_T = G$, and $w_n \neq G$ for all $n < T$. We can construct paths iteratively in reverse by starting at the desired target histogram G. The histogram of the preceding day, called the penultimate point, is arbitrary. For each choice of penultimate point, the remainder of the trajectory is uniquely generated by (5.12).

Two issues immediately arise in this setup however. First, for choice of penultimate point y, we seldom have that the solution (5.12) will generate a reverse trajectory that reaches the initial histogram exactly. Second, the choice of penultimate point y is arbitrary as there is currently no way to find the penultimate point resulting in the minimizing trajectory. This creates many problems in creating efficient algorithms because solving the minimization problem is related to solving Hamilton-Jacobi equations, which is computationally heavy even in a moderately-sized number of dimensions.

Theoretically, one could discretize the space of histograms S and simply let every point in S be a penultimate point. For each penultimate point, a reverse trajectory is formed and a cost is associated to it. These trajectories may or may not reach the initial histogram. For the completed trajectories, we can associate a cost to it. For the incomplete trajectories, one could design a method to essentially "complete" these trajectories and then obtain the costs of these new trajectories. Finally, the trajectory of least cost would be chosen.

Unfortunately, even though this method is computationally viable in the case $g = 3$, it becomes incredibly inefficient for $g \geq 4$. Therefore, we seek to design efficient reverse shooting methods which only a small subset of S is considered as possible penultimate points and incomplete trajectories are "completed" in a reasonable way. We do so in two explicit steps: find the first-stage rate minimizing trajectory and then find the multi-stage rate-minimizing trajectory. Once we explain the general method, we use the case when $g = 3$ to determine which penultimate points are reasonable to consider when generating reverse trajectories.

6.2.1 First-stage rate-minimizing trajectory

We form an initial minimizing trajectory by implementing the following steps.

Discretize space of histograms. We begin by generating a discretized state space of histograms $HIST$ for a chosen discretization d where for any two distinct histograms $H, G \in HIST$, we have that for all genotypes $j = 1, 2, \ldots, g$

$$|H(j) - G(j)| = n_j d$$

for some positive integer n_j.

Form mean trajectory and starting zone. For the fixed initial histogram H, we construct the unique mean trajectory interatively using Theorem 3.2.2. Call this trajectory **mtr**, which terminates at some time L. The cost associated to this trajectory is 0. For each point mtr_k on the trajectory mtr with $k = 0, 1, \ldots, L$, let V_k be a small neighborhood of mtr_k. We define the starting zone $W_{init} = \cup_k V_k$.

Choose set of penultimate points. Possible penultimate points will be chosen from a subset $PEN \subset HIST$. When calculating optimal trajectories leading to fixation of a certain genotype, the region of interest in $HIST$ is generally classified by the sets of histograms which have the required genotype frequency greater than some threshold, which we denote FTH. In realistic applications, FTH is generally taken to be 0.95 or 0.9. In our numerical examples, we take $FTH = 0.95$.

Iteratively reconstruct reverse trajectories and calculate costs. For each histogram $h_{n-1} \in PEN$, we reconstruct the geodesic segment $[h_n \, h_{n-1} \, h_{n-2}]$ using (5.12) to find h_{n-2} where $h_n = G$, the desired target histogram. We can then continue iteratively in reverse until a genotype reaches the boundary. Recall that

the approximation of the one step cost function relied on Stirling's formula, which is only valid if $h(j) \geq \varepsilon$ for all genotypes j. Furthermore, the minimization over mutation frequencies in order to obtain the one step cost assumed nonsaturation of the constraints. Therefore, the iterative procedure must stop if there is a time k such that $h_k(j) < \varepsilon$ for some genotype j or the nonsaturation condition (4.31) fails. This boundary tolerance is given by $\varepsilon = 50/N$. We denote the set of trajectories formed by the penultimate points in PEN by TR_{PEN}. Therefore, the number of trajectories in TR_{PEN} is equal to the number of penultimate points in PEN. For every trajectory $\mathbf{tr} \in TR_{PEN}$, a cost $\lambda(\mathbf{tr})$ given by (5.6) is attached to it.

Separate complete trajectories from incomplete trajectories. We want to isolate trajectories that reach the initial histogram. It is possible no trajectories in TR_{PEN} accomplish this. Therefore, let TR_{comp} be the set of complete trajectories, which we categorize as the set of trajectories that begin in the starting zone W_{init}. The remaining trajectories are classified as incomplete and collected in the set TR_{inc}.

Complete the incomplete trajectories. For each incomplete trajectory, we form a complete trajectory by concatenating a segment of the complete trajectory with the mean trajectory, which is done for each $\mathbf{tr} \in TR_{inc}$ as follows:

1. For every point tr_k on the incomplete trajectory which approximately reaches the boundary at time l, compute the one-step cost $C(mtr_j, tr_k)$ from all points on the mean trajectory mtr to the fixed point tr_k, and find the point of least one-step cost. This represents the optimal jump from the mean trajectory to the point tr_k for each $k = 0, 1, \ldots, l$. Call this point m_{j_k} for $j_k = 0, 1, \ldots, l$.

2. Now, we find the minimum one-step cost of the costs in step (1). That is, we

find

$$min_{k=1,\dots,l}C(tr_k, mtr_{j_k}).$$

This gives an optimal point to jump from the mean to the incomplete trajectory tr, call it tr_K. The cost of this jump is given as $C(tr_K, mtr_{j_K})$.

3. A new complete trajectory is formed by concatenating the partial trajectory $[mtr_0, \dots, mtr_{j_K}]$ with the partial trajectory $[tr_K, \dots, tr_l]$. Therefore, this trajectory takes the form

$$tr_{comp} = [mtr_0, \dots, mtr_{j_K}, tr_K, \dots, tr_l].$$

The cost of this trajectory is given by

$$\lambda(tr_{comp}) = C(mtr_{j_K}, tr_K) + \sum_{j=K}^{l-1} C(tr_j, tr_{j+1}).$$

These new complete trajectories are added to the set of completed trajectories TR_{comp} since they now start at the initial histogram H. We save the set of all incomplete trajectories TR_{inc} to be used in the next stage.

Find minimal cost trajectory and discard costly trajectories. In the set TR_{comp}, we find the trajectory of least cost at this stage, call it λ_{opt}. Any trajectory in the set TR_{inc} or TR_{comp} whose associated cost exceeds λ_{opt} is discarded. If the set of incomplete trajectories TR_{inc} is empty after discarding the costly trajectories, we are done and have obtained an optimal trajectory starting at the histogram H and ending at the target histogram G. Otherwise, we move on to find a multi-stage rate minimizing trajectory.

6.2.2 Multi-stage Rate Minimizing Trajectory

At this stage, we have a first-stage rate minimizing trajectory in TR_{comp} with some cost λ_{opt}. We now need to sift through the remaining trajectories in TR_{inc} to generate multi-stage rate minimizing trajectories. For each incomplete trajectory $\mathbf{tr} \in TR_{inc}$ written as $\mathbf{tr} = [tr_k, tr_{k+1}, \ldots, G]$ where tr_k is a histogram close to the boundary where the boundary tolerance is given by $\varepsilon = 50/N$, we treat tr_k at the new target point, call it H_{tar}. We then form a new set of penultimate points $PEN_{new} \subset HIST$ in order to generate new reverse trajectories stemming from H_{tar}. We then repeat the method from the previous section to get a new set of complete and incomplete trajectories. If there is a new complete trajectory $\mathbf{tr}_{new}$ whose cost $\lambda_{new} < \lambda_{opt}$, this becomes the new temporary optimal trajectory, and we replace λ_{opt} with the optimal cost λ_{new}. We continue this process until there are no more incomplete trajectories. The final optimal evolutionary trajectory is called the multi-stage rate minimizing trajectory.

In summary, generating optimal evolutionary trajectories linking an intial histogram H to a target histogram G can be done using the following steps:

1. Select a desired initial histogram H, target histogram G, and discretization level d. Generate the state space $HIST$ using d.

2. Generate the mean trajectory $\mathbf{mtr}$ starting at H using Theorem 3.2.2, and select the starting zone W_{init} by placing small neighborhoods around each point on mtr.

97

3. Choose a set of penultimate points $PEN \subset HIST$. Generate the set of reverse trajectories TR_{PEN} using the penultimate points in PEN. For each $\mathbf{tr} \in TR_{PEN}$, calculate the corresponding cost $\lambda(\mathbf{tr})$.

4. Trajectories that reach the starting zone W_{init} at some reverse iteration is placed in the set of completed trajectories TR_{comp}. The remaining trajectories are incomplete and gathered in the set TR_{inc}.

5. For each $\mathbf{tr} \in TR_{inc}$, form a complete trajectory by concatenating the mean $\mathbf{mtr}$ with a segment of $\mathbf{tr}$ at the optimal jump point from $\mathbf{mtr}$ to $\mathbf{tr}$. Add these complete trajectories to TR_{comp}. Keep the original incomplete trajectories in TR_{inc}.

6. From the set TR_{comp}, find the trajectory of least cost, say λ_{opt}.. This gives a first-stage rate minimizing trajectory. Delete any complete or incomplete trajectory whose cost exceeds λ_{opt}.

7. Each reverse trajectory in TR_{inc} was terminated at a histogram that approached the boundary. These points TAR become new target points. For each new target $G_{new} \in TAR$, repeat steps (3)-(6).

8. If a new complete trajectory emerges with cost lower than λ_{opt}, this trajectory becomes the new rate-minimizing trajectory with updated optimal cost λ_{opt}.

9. Repeat until all trajectories are complete or all incomplete trajectories have cost higher than λ_{opt}. This give a multi-stage rate-minimizing trajectory from H to G with optimal cost λ_{opt}.

6.2.3 Numerical Challenges

In the reverse shooting method, the discretization level d and choice of penultimate points PEN become key factors in finding rate-minimizing trajectories efficiently. In particular, the size of $HIST$ using a discretization d is of order $(1/d)^{g-1}$. For example, if we have 3 genotypes ($g = 3$) and use a discretization $d = 0.002$, the state space $HIST$ contains $125,751$ histograms. In the case of three genotypes, it is possible to let PEN be the entire set of $HIST$ while excluding those histograms near the boundary. In fact, numerical simulations have shown that the multi-stage step is not necessary when $g = 3$; that is, all rate-minimizing trajectories are first-stage rate-minimizing trajectories. However, this method quickly becomes infeasible when we move to four genotypes ($g = 4$). For instance, if $d = 0.005$, the state space $HIST$ has $1,373,701$ histograms. Therefore, letting PEN be nearly the entirety of $HIST$ is inefficient and causes major memory issues.

With these difficulties in mind, we can first improve the computational scheme by implementing a multi-scale method in obtaining an optimal trajectory. To do so, one would choose a coarse discretization in order to zones of promising penultimate points that may yield optimal trajectories. Near these penultimate points, one could then choose a finer discretization near these penultimate points in order to compute an overall optimal trajectory. Our conjectures that we have stated further aid in identifying these promising zones.

We can also improve computation times in the multi-stage method by picking "smart" penultimate points. We will work in the case of $g = 3$ to illustrate this since

letting PEN be all histograms away from the boundary is computationally feasible. When comparing one-steps costs from the penultimate point to the target to the actual cost of the rate-minimizing trajectory, many one-step costs are already too costly to possibly yield an optimal trajectory. This greatly reduces the number of penultimate points that may actually create optimal trajectories. We can link the choice of penultimate points to the norm of the gradient $\|\nabla_y C(y, G)\|$ with respect to the penultimate point y for a fixed target G. The cost derivatives are given by (5.9) and (5.10). Penultimate points that result in costly trajectories tend to be points in which this norm is relatively large. We will use numerical simulations to illustrate these claims.

We can further improve computational efficiency by using discretization levels of adaptive size for any given target G. This can again be linked to the norm of the gradient $\|\nabla_y C(y, G)\|$ with respect to the penultimate point y. As one would expect, a finer discretization used in the multi-stage approach will reduce the optimal cost λ_{opt}. However, after a certain level, this reduction stabilizes. Therefore, choosing a very fine discretization will increase computation times greatly while not providing a substantially more accurate estimate of λ_{opt}. We then establish a method to generate a set of penultimate points roughly centered at the penultimate point which minimizes $\|\nabla_y C(y, G)\|$, which can be found independent of the discretization level.

Finally, we can improve the computational scheme by first creating an initial complete trajectory $\mathbf{tr}_{init}$ with associated cost λ_{init} before generating reverse trajectories for each penultimate point in PEN. The computation of one complete trajectory with associated cost is computationally cheap. We can then use this complete trajectory

and associated cost to delete penultimate points whose one-step costs are larger than λ_{init}. One could create this trajectory by simply picking any single penultimate point. However, there is a way to choose a penultimate point independent of the discretization d which is a point which roughly minimizes $\|\nabla_y C(y, G)\|$. This trajectory may not result in a globally optimal trajectory, but it does provide a sensible initial trajectory to help further reduce the number of penultimate points to consider. We can also use this penultimate point to generate the set PEN of sensible possible penultimate points.

We can summarize these claims in the following three conjectures. Recall that we are assuming all histograms are interior histograms.

Conjecture 6.2.1. For any given target G, the best discretization for the choice of penultimate point will be of adaptive size; namely, the discretization cell centered around a penultimate point y should be of size $c/g(y, G)$ where

$$g(y, G) = \|\nabla_y C(y, G)\|$$

$$C(y, G) = \text{one-step cost from } y \text{ to } G$$

$$c = \text{fixed proportionality constant}$$

Conjecture 6.2.2. When N is very large (10^8), m is very small (10^{-8}), and G is close to the boundary $(G(j) \approx 100/N$ for at least one genotype $j)$, the function $g(y, Z)$ will tend to large values when the penultimate point y is close to the boundary. Consequently, in asymptotic situations with $N \to \infty$ and $m \to 0$, a trajectory that bounces back from the boundary will have a large cost and cannot be optimal.

Conjecture 6.2.3. To generate an initial trajectory $\mathbf{tr}_{int}$ independent of discretization d for a fixed target histogram $G = (G_1, \ldots, G_g)$, one can choose penultimate point y to be the solution to the linear system

$$
\begin{pmatrix}
\left(1 - \frac{1}{G_1}\right) F_1 & F_2 & F_3 & \ldots & F_g \\
F_1 & \left(1 - \frac{1}{G_2}\right) F_2 & F_3 & \ldots & F_g \\
\vdots & \vdots & \vdots & \vdots & \vdots \\
F_1 & F_2 & \ldots & \left(1 - \frac{1}{G_{g-1}}\right) F_{g-1} & F_g \\
1 & 1 & 1 & \ldots & 1
\end{pmatrix}
\begin{pmatrix}
y_1 \\ y_2 \\ y_3 \\ \vdots \\ y_{g-1} \\ y_g
\end{pmatrix}
=
\begin{pmatrix}
0 \\ 0 \\ 0 \\ \vdots \\ 0 \\ 1
\end{pmatrix}. \quad (6.2)
$$

The solution y^* is a histogram which approximately minimizes the function $g(y, G)$ so that $g(y^*, G)$ is roughly of order m. Furthermore, the solution y^* of this system can then be used in 6.2.1 to create a set of penultimate points in the following way: A point y is considered a *possible penultimate point* if $c \cdot g(y, G) \leq g(y^*, G)$ where c is a fixed proportionality constant with $0 < c < 1$.

In order to provide evidence for these claims, we look at the length of the optimal and mean trajectories, cost of the optimal trajectories, and gradient norms of the penultimate points resulting in optimal trajectories. In addition, we look for any optimal trajectories that bounce off the boundary or reach the initial zone directly by the reverse recursive formula. We provide evidence for these conjectures along with the above attributes of the optimal trajectories in Section 6.3.

For Conjectures 6.2.1 and 6.2.3, we calculated numerous examples using different target histograms and initial histograms and analyze these trajectories along with the function $g(y, G)$ and the one-step cost $C(y, G)$. We found that no trajectories

bounced off the boundary and that optimal trajectories were generated from penultimate points that were close the the minimum of $g(y, G)$. We also compared our method to the exhaustive method which uses all points as possible penultimate points in order to show the significant save in computation time. Finally, using these examples and partitioning our space of histograms into quantiles based on the function $1/g(y, G)$, we were able to find a reasonable interval of proportionality constants to use in Conjecture 6.2.3. We used a quantile percentage of 0.025 and generated most likely trajectories for various initial histograms. We found that we can actually use smaller proportionality constants to generate a set of penultimate points since only a small subset of the quantile sets could reasonably generate optimal trajectories. The proportionality constant can be chosen (by the user) so that $0.00001 \leq c \leq 0.01$ depending on the initial histogram since $g(y^*, G)$ is roughly of order m.

For Conjecture 6.2.2, we used our method to generate most likely trajectories for 1030 targets using three separate parameter sets. In all three simulations, we found that no trajectories bounced off the boundary. Furthermore, even though we used a large amount of targets, the trajectories for each parameter set were generated in approximately an hour. To further solidify this conjecture, we perform an analysis of the function $g(y, G)$ when both the target and penultimate points are near the boundary, which showed that the gradient norm is large.

At the end of Section 6.3, we finally use our three conjectures to generate most likely trajectories for four genotypes using three examples. We found that the method was very efficient even though we increased the dimension of the problem. Furthermore, none of these trajectories bounced off the boundary and penultimate points

that generated optimal trajectories were close the the approximate minimum of $g(y, G)$. We end the section by providing a very informal analysis and prediction for the case when $g = 8$.

6.3 Analysis Using Three Genotypes

In this section, we will take numerous examples using three genotypes in order to test our conjectures. We will first analyze the set of penultimate points. Then, we will explain how to obtain a sensible initial trajectory using a penultimate point that roughly minimizes the function $g(y, G)$. Next, we will demonstrate an accelerated method in obtaining most likely trajectories using various targets and initial points. We will then combine our analysis to give evidence that trajectories that bounce off the boundary are not optimal. We end the section by directly simulating the system.

6.3.1 Choosing the set PEN

To illustrate how to choose good penultimate points, we will take a specific example. The parameters for our system are given as follows:

$$N = 10^6 \qquad\qquad\qquad M = mQ$$

$$F_1 = 200 \qquad\qquad\qquad d = 0.002$$

$$F_2 = 200^{1.08} \qquad\qquad\qquad FTH = 0.95$$

$$F_3 = 200^{1.12} \qquad\qquad\qquad \varepsilon = 50/N = 5 \times 10^{-5}$$

$$m = 10^{-6} \qquad\qquad\qquad H = (1 - 100/N, 50/N, 50/N)$$

$$Q = \begin{pmatrix} 0 & 1/2 & 1/2 \\ 1/2 & 0 & 1/2 \\ 1/2 & 1/2 & 0 \end{pmatrix} \qquad G = (0.1, 0.45, 0.45), (0.05, 0.9, 0.05)$$

Recall that the gradient of the one-step cost $C(y, z)$ with respect to y for a fixed z is given by

$$\frac{\partial}{\partial y_n} C(y, z) = \frac{F_n}{\langle F, y \rangle} - \frac{z_n}{y_n} + F_n \sum_k M_{n,k}$$
$$- \left(F_n + \frac{z_n}{y_n} \right) \sum_k M_{n,k} \hat{E}_{n,k} - \frac{z_n}{F_n y_n^2} \sum_k F_k y_k M_{k,n} \hat{E}_{k,n}$$
$$\hat{E}_{n,k} = \exp \left(-\frac{z_n}{F_n y_n} + \frac{z_k}{F_k y_k} \right).$$

We investigate $1/g(y, G)$ for the targets G given above where $g(y, G)$ is the norm of the gradient with respect to y. We accomplish this by reordering the values $1/g(y, G)$ into quantiles and investigate the penultimate points in each quantile set. We can then compare the penultimate points making up the quantile sets to the penultimate point that resulted in the optimal trajectory. This will help to greatly reduce the penultimate points we consider when generating optimal trajectories. This will also

give evidence to why choosing penultimate points near the boundary will yield costly trajectories.

For these targets, we will calculate quantile values and corresponding quantile sets using the percentage $p = 1/40 = 0.025$. Denote the quantile values q_j with $1 \leq j \leq 39$ and by convention $q_0 = 0$ and $q_{40} = 1$. Rearrange the values $1/g(y, G)$ into bins of the form $Quant_k$ where

$$Quant_k = \{x : q_k < 1/g(y, Z) < q_{k+1}\}$$

for $0 \leq k \leq 39$. Notice that $Quant_0$ corresponds to penultimate points in which $1/g(y, G)$ is small, meaning that $g(y, G)$ is large. Similarly, $Quant_{39}$ corresponds to penultimate points in which $1/g(y, G)$ is large, meaning that $g(y, G)$ is small. Since we would like to compare the one-step cost to the function $1/g(y, G)$, we want to keep track of the values on the function on these sets. Thus, define the sets C_k and $Grad_k$ where

$$C_k = \{C(y, G) : y \in Quant_k\}$$

$$Grad_k = \{1/g(y, G) : y \in Quant_k\}.$$

Using this reordering, we will focus on the sets $Quant_0$ and $Quant_{39}$.

Target Point $G = (0.1, 0.45, 0.45)$

Recall that when finding the optimal trajectory, we first create an initial trajectory using as penultimate point the solution to 6.2. In this case, the trajectory using this point yielded the optimal trajectory, which is shown in Figure 6.5. In fact, the one-step cost $C(y, G)$ for all penultimate points was already more costly than this initial

106
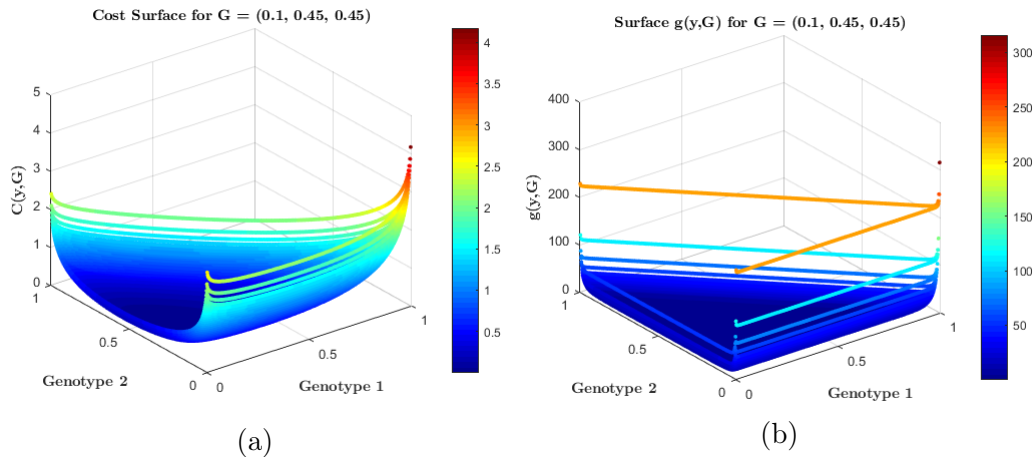
Figure 6.1: The cost surface $C(y, G)$ and gradient norm surface $g(y, G)$ for the target $G = (0.1, 0.45, 0.45)$.

trajectory. Figures 6.1-6.4 investigate the behavior of the one step cost $C(y, G)$ and $g(y, G)$ in order to see which penultimate points yield possible optimal trajectories.

In Figure 6.1, we have the two full surfaces of the one-step cost $C(y, G)$ and $g(y, G)$ as a function of the penultimate point y for this fixed target. The global minimum of $C(y, G)$ is 1.22×10^{-16}, and the global minimum of $g(y, G)$ is 4.27×10^{-6}. These values both occur at the penultimate point $(0.158, 0.465, 0.377)$, which is the solution to the system (6.2). In (6.1a) and (6.1b), notice the large increase in these surfaces near the boundary, in particular, the boundary points near the target G. These penultimate points are already becoming too costly to yield a possible optimal trajectory.

In Figure 6.2, we have the surfaces of $C(y, G)$ and $g(y, G)$ on the uppermost quantile $Quant_{39}$. Even on the set $Quant_{39}$ where the norm is relatively small, we see large increases in the one-step cost and function $g(y, G)$ as we move away from the point where the norm is approximately minimized.

107
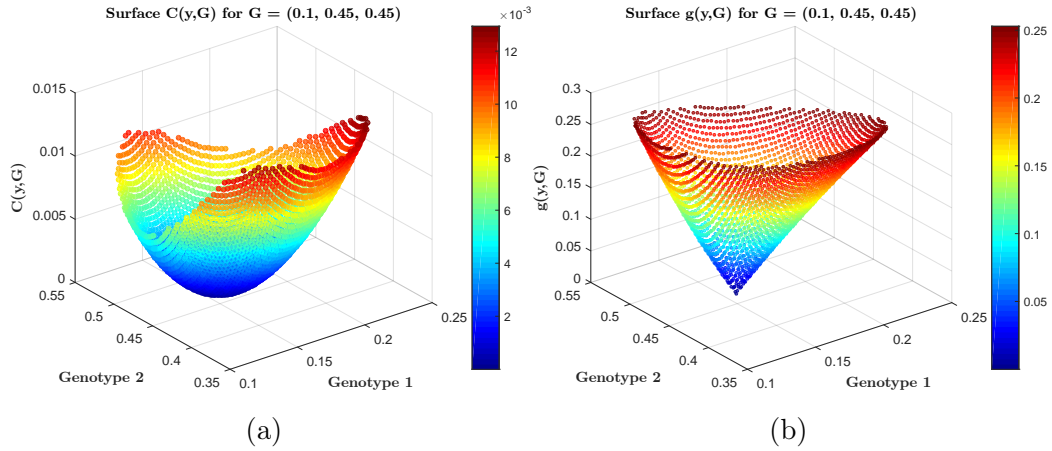
Figure 6.2: The surfaces $C(y,G)$ and $g(y,G)$ on the uppermost quantile $Quant_{39}$.
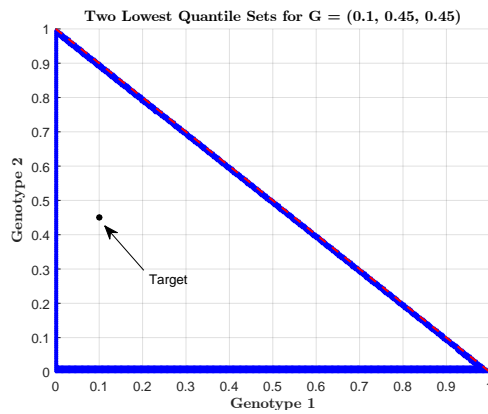
Figure 6.3: The two quantile sets $Quant_0$ and $Quant_1$ given as the blue points. The red dotted line is the boundary.

In Figure 6.3, we have the quantile sets in which the gradient is large. Noticed that these sets are comprised of points near the boundary. This shows that penultimate points near the boundary are too costly to yield optimal trajectories.

In Figure 6.4, we let every point away from the boundary in the discretized space $HIST$ be possible penultimate points. We then generated a trajectory for each point and calculated its corresponding cost. The figure shows that penultimate
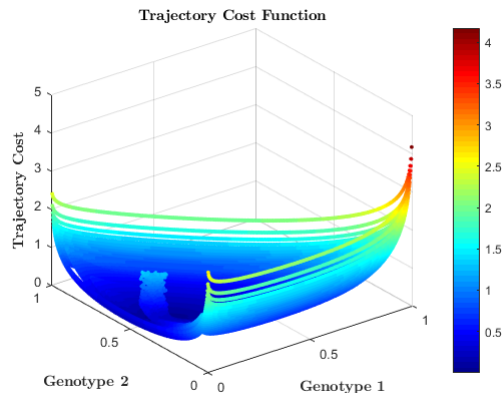
Figure 6.4: The trajectory cost surface as a function of the penultimate point.

points relatively close to the target and away from the boundary yield trajectories with low costs. These represent trajectories that have the best chance at yielding optimal trajectories.

In Figure 6.5, the optimal trajectory has cost 2.17×10^{-7} whose penultimate point is given by the solution to the system (6.2). Notice that the magenta set is roughly a disc centered at optimal penultimate point with radius 0.0998. This gives some motivation to why we consider penultimate points near the solution to the system (6.2). These points have relatively small gradient norms and one-step costs.

Target Point $G = (0.05, 0.9, 0.05)$

In this case the optimal trajectory was formed from a penultimate point in the discretized space $HIST$, not the solution to (6.2). This initial trajectory did reduce the number of possible penultimate points from approximately $125,000$ to approximately 3300. However, the optimal penultimate point was close to the solution of (6.2) and also fell in the uppermost quantile $Quant_{39}$. Figures 6.6-6.9 show that even though
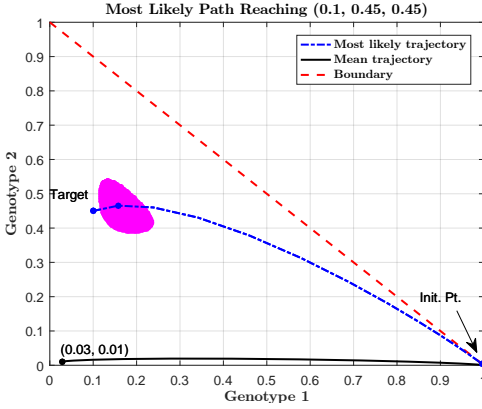
Figure 6.5: The optimal trajectory for the target point $G = (0.1, 0.45, 0.45)$. The blue trajectory is the optimal trajectory. The black trajectory is the mean. The magenta set is the set of penultimate points in $Quant_{39}$. The red dotted line represents the boundary.

G is close to a corner, the optimal trajectory did not bounce off the boundary, and the gradient norm of the points close to the boundary was large.

In Figure 6.6, we have the two full surfaces of the one-step cost $C(y, G)$ and $g(y, G)$ as a function of the penultimate point y for this fixed target. The global minimum of $C(y, G)$ is approximately 0, and the global maximum of $g(y, G)$ is 1.5×10^{-5}. These values both occur at the penultimate point $(0.0751, 0.8851, 0.0398)$, which is the solution to the system (6.2). In this case, notice the target G is relatively close to a corner. Notice the increases in these surfaces as we move away from the target, especially close to the boundary. Since the target is relatively close to a corner, it is not yet evident if boundary points near the target can be considered as possible penultimate points. This will be studied further using quantiles.

In Figure 6.7, we see that even on $Quant_{39}$, the cost and gradient norms begin increasing very quickly near the boundary. This again suggests that even though the

110
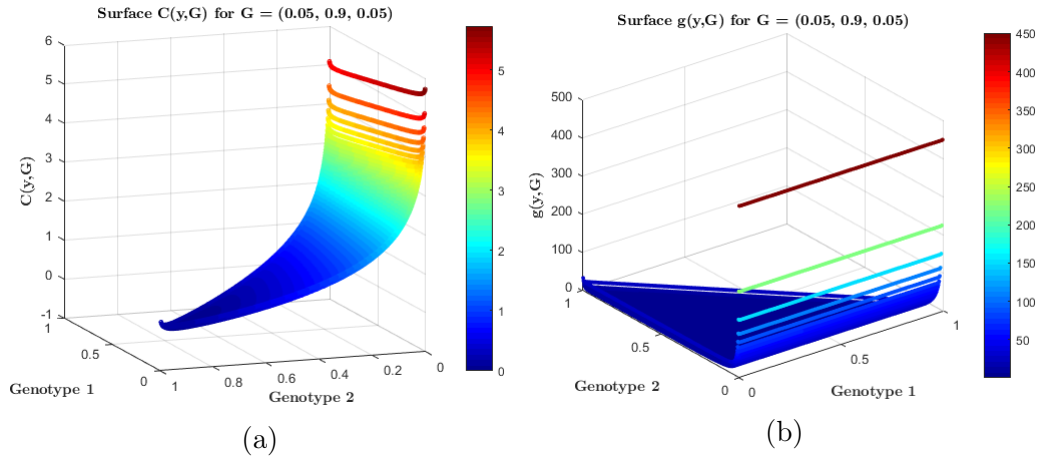
Figure 6.6: The cost surface $C(y, G)$ and gradient norm surface $g(y, G)$ for the target $G = (0.05, 0.9, 0.05)$.

target is relatively close to the boundary, boundary points to not seem to be relevant when obtaining optimal trajectories.

In Figure 6.8, we see that even though G is a point close to a corner, points that are near the boundary still result in large gradient norms. This further suggests that these penultimate points will not result in optimal trajectories.

In Figure 6.9, the cost surface was generated exactly the same as the surface in Figure 6.4. We again see that the penultimate points yielding possible optimal trajectories fall close to the target point.

In Figure 6.10, the optimal trajectory has cost 0.014 whose penultimate point is given by $(0.082, 0.878, 0.04)$, which is not a solution to (6.2) but still is a point in the set $Quant_{39}$. The initial trajectory using as penultimate point the solution to (6.2) has associated cost 0.0649. Even though this point $(0.0751, 0.8851, 0.0398)$ is an approximate minimum of $g(y, G)$, it did not yield the optimal trajectory because
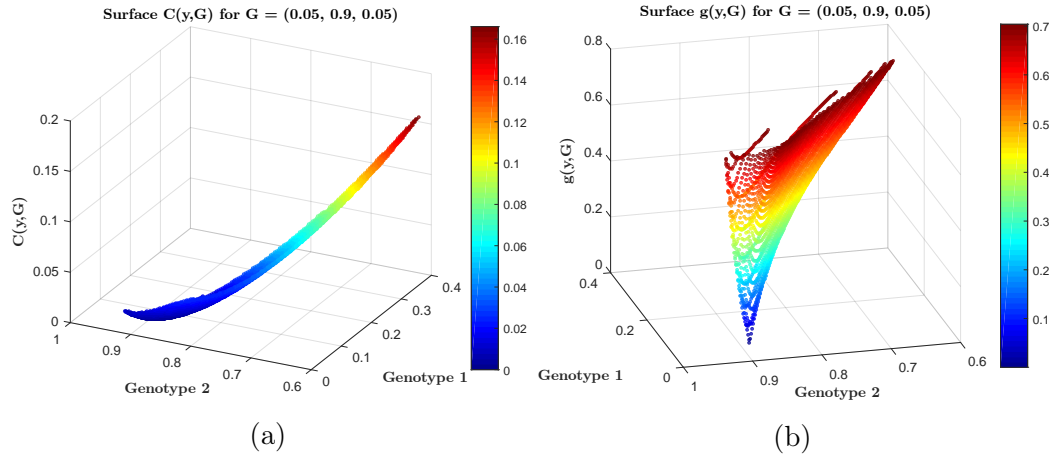
Figure 6.7: The surfaces $C(y, G)$ and $g(y, G)$ on the uppermost quantile $Quant_{39}$.

the "aim" was slightly off. This trajectory reached the boundary too quickly so that jumping from the mean to this partial trajectory became too costly. Our method essentially adjusted the "aim" of this reverse trajectory so that the optimal path used a penultimate point that was a slight adjustment to $(0.0751, 0.8851, 0.0398)$ so that the jump from the mean to this partial trajectory is less costly. This gives more motivation to why we consider penultimate points near the solution to the system (6.2). These points have relatively small gradient norms and one-step costs.

Penultimate Point Resulting From Conjecture 6.2.3

From the previous two examples, we saw that the optimal trajectory resulted from a penultimate point in which the gradient $g(y, G)$ was relatively small. Therefore, it makes sense to seek the penultimate point which results in an approximate minimum of $g(y, G)$ for a fixed target G. Notice that the derivative of $C(y, G)$ with respect to
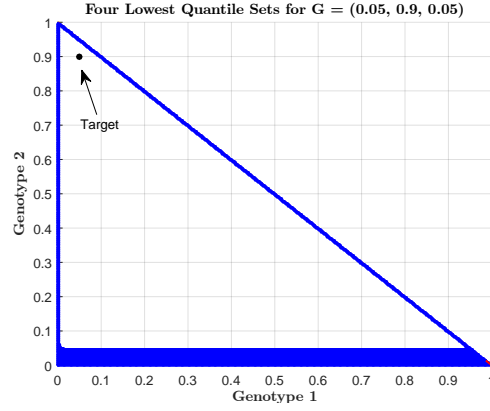
Figure 6.8: The surfaces $C(y, G)$ and $1/g(y, G)$ on the lowest quantiles $Quant_k$ for $k = 0, 1, 2, 3$.
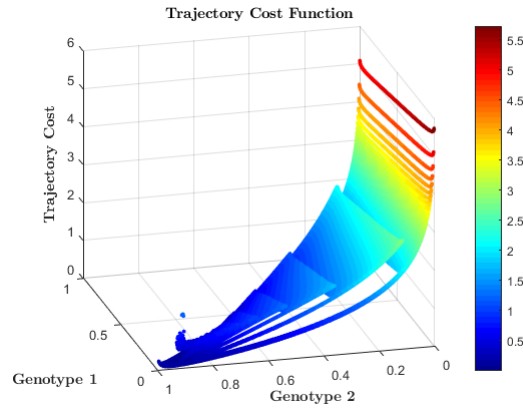
Figure 6.9: The trajectory cost surface as a function of the penultimate point.

y has terms of zero order and terms of order m. Thus, we write,

$$\frac{\partial}{\partial y_n} C(y, G) = \frac{F_n}{\langle F, y \rangle} - \frac{G_n}{y_n} + mZ$$

where Z is all terms of order m. Therefore, finding the minimizing penultimate point of $g(y, G)$ is roughly approximated by solving the system of equation

$$\frac{F_n}{\langle F, y \rangle} - \frac{G_n}{y_n} = 0$$

113

Most Likely Path Reaching (0.05, 0.9, 0.05)
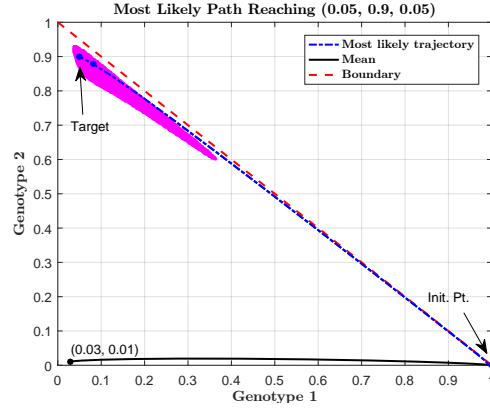
Figure 6.10: The optimal trajectory for the target point $G = (0.05, 0.9, 0.05)$. The blue trajectory is the optimal trajectory. The black trajectory is the mean. The magenta set is the set of penultimate points in $Quant_{39}$. The red dotted line represents the boundary.

for all genotypes n subject to the condition that $\sum_n y_n = 1$. This system is equivalent to

$$\sum_{k \neq n} F_k y_k + \left(1 - \frac{1}{G_n}\right) F_n y_n = 0. \tag{6.3}$$

With the condition $\sum_n y_n = 1$, we can solve the system (6.3) for all genotypes $n = 1, 2, \ldots, g - 1$, which immediately gives the system in Conjecture 6.2.3 given by (6.2).

Let y^* be the solution to (6.2). This implies that $g(y^*, G)$ is roughly of order m for targets away from the boundary, which will be small. Therefore, for interior histograms, the point y^* is a good approximation of the minimizer of the gradient $g(y, G)$. Furthermore, this point can be generated independent of the discretization of the space $HIST$ so that an intial completed trajectory can be computed immediately given that the mean trajectory has been computed. We note that we do not claim that this point will generate the optimal trajectory, especially if the target point

114

is near the boundary. However, from numerical experiments, the penultimate point resulting in the optimal trajectory will be close to the penultimate point y^*, as we saw in the two examples presented. Therefore, we can use this point in Conjecture 6.2.1 in order to generate a set of possible penultimate points *without generating the entire state space $HIST$*.

Notice that in our two examples we presented, the most likely trajectory was either generated directly from the penultimate point y^* or fell very close to y^*. In addition, most of the penultimate points in the uppermost quantile $Quant_{39}$, the set of points in which the gradient norm is small, will not generate optimal paths. This suggests that we could have chosen a smaller quantile percentage. However, one main reason for this may have been that many reverse trajectories are aiming back towards the initial histogram. If we change the initial histogram, we may have to adjust the number of penultimate points chosen. We investigate this further in Section 6.3.2.

Comparing exhaustive method with acceleration method

For the target $(0.1, 0.45, 0.45)$, the optimal trajectory was generated directly from the penultimate point obtained fom the system given by (6.2). Therefore, the exhaustive method and acceleration method will work equally well here. However, in the case of the target $(0.05, 0.9, 0.05)$, the exhaustive method yielded an optimal trajectory with 26 steps and a cost of 0.014. The penultimate point that yields this optimal trajectory is $(0.082, 0.878, 0.04)$. This trajectory also took about an hour to generate since there

were many incomplete trajectories to filter through. Using the acceleration method yielded an optimal trajectory with 26 steps and a cost of 8.716×10^{-4}. The penultimate point yielding the optimal trajectory here is $(0.0771274, 0.883092, 0.039871)$, which we wrote out with many decimals to show the precision. The optimal trajectory took 2 seconds to obtain. A penultimate point of this form is unattainable with a direct exhaustive method. We were able to keep the precision of the approximate gradient-minimizing point by perturbing this minimizer to generate new points until the gradient norm threshold is reached. By doing so, the optimal trajectory reached the starting zone *without having to jump to the mean in reverse time*. Any method that requires a very fine discretization to reach this precision would be computationally heavy. This is the main advantage of our method. We will now compute many optimal paths with various initial histograms to showcase the method.

6.3.2   Examples using acceleration technique

When using the acceleration technique, we first find the approximate minimizer of the norm of the gradient, which is given by Conjecture 6.2. The minimizer will give a very small gradient norm (usually of order $m \approx 10^{-6}$ for targets away from boundary). In order to test good proportionality constants, we will consider penultimate points whose gradient norm is at most 2. This will generate a lot of penultimate points. We can then analyze the gradient norm of the penultimate point that results in the optimal trajectory. We can then use these results to suggest good threshold values for the gradient norm used in generating the set of penultimate points. We will choose many initial and target points to test and summarize the results in a table.

116

Note that the optimal trajectories in each case were generated in less than a minute, even with a large gradient norm threshold. The system parameters for all initial points and target points are given below:

$$N = 10^6 \qquad\qquad M = mQ$$

$$F_1 = 200 \qquad\qquad m = 10^{-6}$$

$$F_2 = 200^{1.08} \qquad\qquad d = 0.002$$

$$F_3 = 200^{1.12} \qquad\qquad FTH = 0.95$$

$$Q = \begin{pmatrix} 0 & 1/2 & 1/2 \\ 0 & 0 & 1 \\ 0 & 0 & 0 \end{pmatrix} \qquad\qquad \varepsilon = 50/N = 5 \times 10^{-5}$$

Notice that in the above parameter set, the mutations are irreversible, which is realistically more reasonable than our previous examples.

Initial histogram $(1 - 2\varepsilon, \varepsilon, \varepsilon)$

The histogram in this example is a "typical" histogram when analyzing bacterial evolution. The initial population will contain cells of only the ancestor genotype. Experiments with this initial population are then used to derive information about the system (genotype fixation, fixation times, etc.) Our initial histogram starts with a small population of genotype 2 and 3 cells so that the initial histogram is not a boundary histogram. The optimal trajectories for various targets are given in Figures [6.11a, 6.11b]. Using the acceleration technique resulted in all 6 trajectories reaching the initial zone W_{init} without having to jump to the mean. The mean trajectory has

117
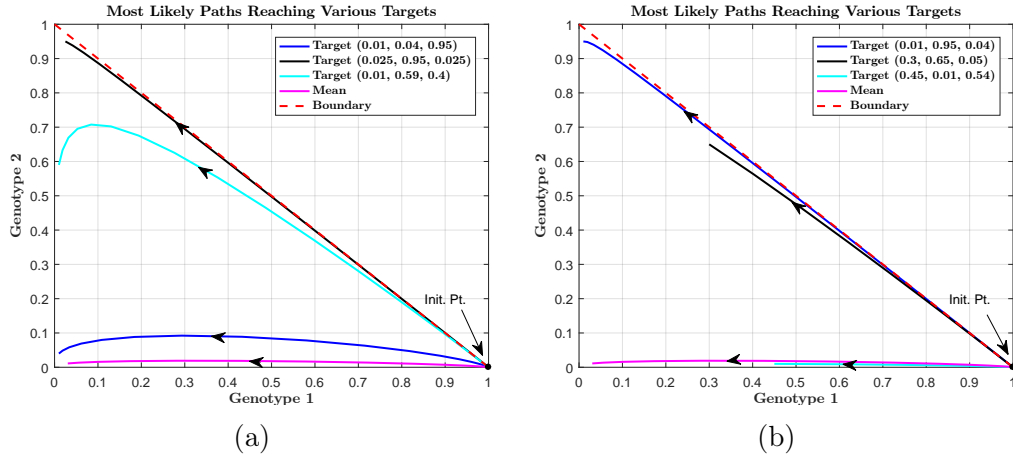
Figure 6.11: Most likely paths reaching various targets using the initial histogram $(1 - 2\varepsilon, \varepsilon, \varepsilon)$.

22 steps.

Table 6.1 shows the number of time steps in the optimal trajectory, the cost of the trajectory, the value of the norm of the gradient of the best penultimate point, and the overall approximate minimum of the norm of the gradient. As we can see, the value of the norm of the gradient of the best penultimate point was much smaller than the threshold we set in generating the penultimate set. When generating reverse trajectories from a target point, these trajectories are wanting to travel towards the bottom right of the triangle, which represents starting histograms in which the ancestor genotype is heavily dominant. Therefore, when the initial histogram is of this type, the gradient norm threshold can be chosen much smaller than our threshold of 2.

Targets	(0.01, 0.04, 0.95)	(0.025, 0.95, 0.025)	(0.01, 0.95, 0.04)
Time	23	26	24
Cost	1.68×10^{-7}	0.002	0.0026
Pen. Grad	1.07×10^{-6}	0.0641	0.1362
Grad. Min.	1.07×10^{-6}	4.8×10^{-5}	2.95×10^{-5}

Targets	(0.01, 0.59, 0.4)	(0.3, 0.65, 0.05)	(0.45, 0.01, 0.54)
Time	27	16	15
Cost	0.0024	0.0009	3.54×10^{-7}
Pen. Grad	0.0663	0.0055	2.67×10^{-5}
Grad. Min.	2.04×10^{-6}	2.28×10^{-5}	2.67×10^{-5}

Table 6.1: Attributes of most likely trajectories for initial histogram $(1 - 2\varepsilon, \varepsilon, \varepsilon)$.

Initial histogram $(0.6 - \varepsilon, 0.4 - \varepsilon, 2\varepsilon)$

The initial histogram here represents an initial situation in which the weaker geno-types are heavily dominant. As stated before, since trajectories are wanting to travel in reverse time towards the bottom right of the triangle, optimal trajectories in this case are more likely to be trajectories that are concatenated with the mean. Thus, the optimal transition will involve staying on the mean for a time before jumping away from the mean at the optimal time. Furthermore, since the initial histogram has a formidable amount of genotype 2 cells, the mean trajectory will actually first fixate at genotype 2 and then fixate at genotype 3. Furthermore, a portion of the mean reaches the boundary in route to fixating at genotype 3 so that some mean points will not be valid points to use when concatenating trajectories. The trajectories are shown in Figure [6.12a, 6.12b]. The mean trajectory has 54 steps.

In Table 6.2, notice here that the gradient norm of the best penultimate point is larger than it was for the previous example. Since the initial histogram is not heavily dominant in the ancestor genotype, we need a larger set of penultimate points in order
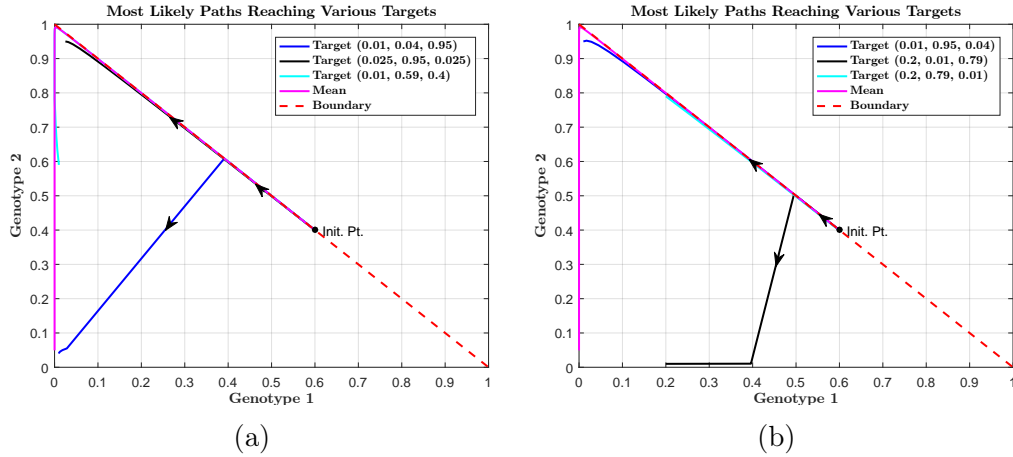
Figure 6.12: Most likely trajectories for various targets using the initial histogram $(0.6 - \varepsilon, 0.4 - \varepsilon, 2\varepsilon)$.

to find an approximate optimal trajectory. However, the loss in computation time is minimal because a large number of trajectories will "overshoot" the initial histogram, making these histograms too costly very quickly.

Initial histogram $(0.4, 0.3, 0.3)$

The initial histogram here represents an initial situation in which the distributions of each genotype are approximately equal. With the prominence of the dominant genotype (genotype 3) in the initial histogram, the mean trajectory will fixate quickly to the dominant genotype. Therefore, optimal trajectories will tend to jump away from the mean immediately in order to avoid this fixation. The trajectories are shown in Figure [6.13a, 6.13b]. The mean trajectory has 15 steps.

Table 6.3 shows that the gradient norm of the optimal penultimate point is large in comparison with the previous examples. Again, this is because the initial histogram is

Targets	(0.01, 0.04, 0.95)	(0.025, 0.95, 0.025)	(0.01, 0.95, 0.04)
Time	8	12	12
Cost	0.0077	0.0012	0.0023
Pen. Grad	0.5129	0.1257	0.1102
Grad. Min.	1.07×10^{-6}	4.8×10^{-5}	2.95×10^{-5}

Targets	(0.01, 0.59, 0.4)	(0.2, 0.01, 0.79)	(0.2, 0.79, 0.01)
Time	39	4	6
Cost	0.0086	0.0129	0.0024
Pen. Grad	0.3505	0.3453	0.0593
Grad. Min.	2.04×10^{-6}	1.05×10^{-5}	1.21×10^{-4}

Table 6.2: Attributes of most likely trajectories for the initial histogram $(0.6-\varepsilon, 0.4-\varepsilon, 2\varepsilon)$.

Targets	(0.01, 0.04, 0.95)	(0.025, 0.95, 0.025)	(0.01, 0.95, 0.04)
Time	13	11	12
Cost	0.0082	0.1894	0.1781
Pen. Grad	0.4408	0.6087	0.4753
Grad. Min.	1.07×10^{-6}	4.8×10^{-5}	2.95×10^{-5}

Targets	(0.01, 0.59, 0.4)	(0.2, 0.01, 0.79)	(0.2, 0.79, 0.01)
Time	7	5	6
Cost	0.0535	0.1246	0.2507
Pen. Grad	0.3091	0.8054	1.0879
Grad. Min.	2.04×10^{-6}	1.05×10^{-5}	1.21×10^{-4}

Table 6.3: Attributes of most likely trajectories using the initial histogram $(0.4, 0.3, 0.3)$.

far away from the bottom-right of the triangle. Optimal trajectories will then require costly penultimate jumps in order to avoid traveling towards this area in reverse time. Again, the computation time loss is minimal because many trajectories "overshoot" the initial histogram.
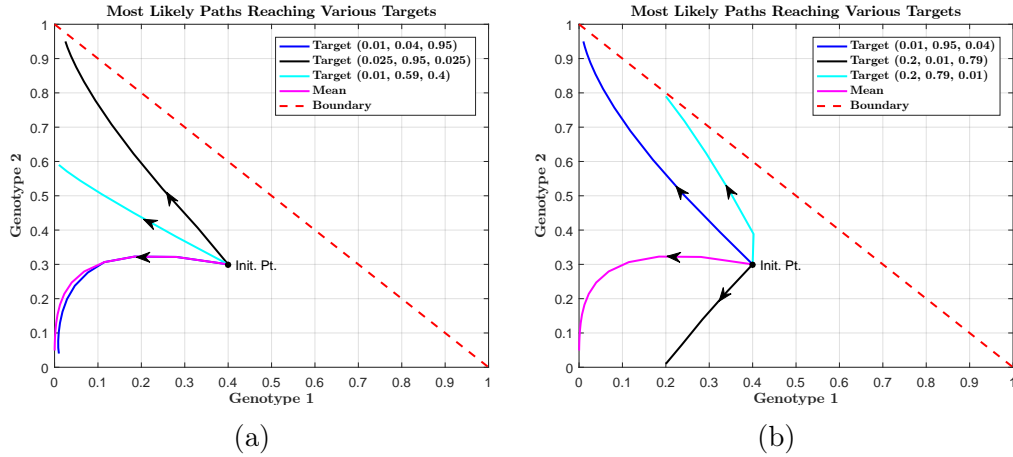
Figure 6.13: Most likely trajectories using the initial histogram $(0.4, 0.3, 0.3)$.

Initial histogram $(0.5 - \varepsilon, 2\varepsilon, 0.5 - \varepsilon)$

The initial histogram here represents an initial situation in which the ancestor and dominant genotypes are prominent. This situation can be thought of as a subsituation of the case when the initial histogram is $(1 - 2\varepsilon, \varepsilon, \varepsilon)$ because in that situation, the mean trajectory eventually reached a point in which the ancestor and fittest genotype were highly dominant. With this initial histogram, the mean will fixate very quickly again to the fittest genotype. The trajectories are shown in Figure [6.14a, 6.14b]. The mean trajectory has 6 steps.

In Table 6.4, the gradient norm is again relatively large in comparison with the previous examples. In this case, since the system on average fixates very quickly to the fittest genotype, it is very costly for optimal trajectories reaching other targets to break away from this behavior. Thus, penultimate points with relatively large gradients are required. This corresponds to having the probability of such targets being reached by the system essentially 0.
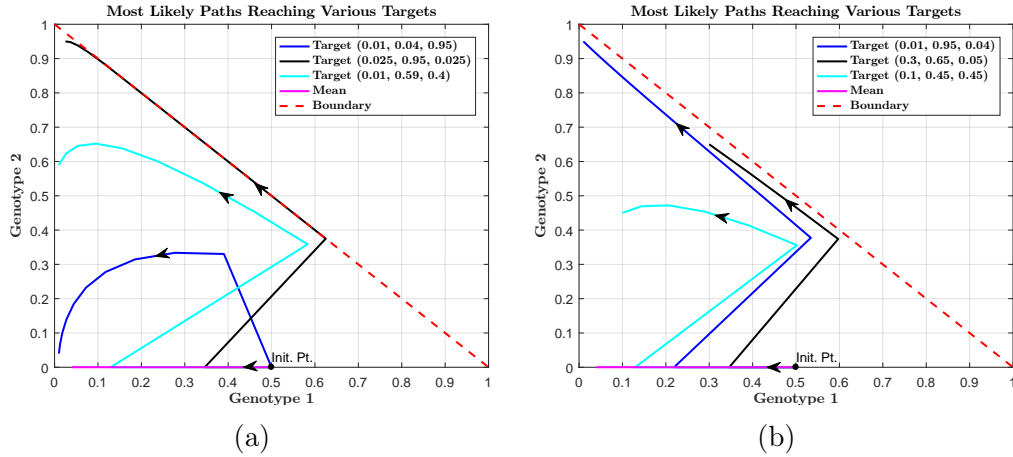
Figure 6.14: Most likely trajectories using the initial histogram $(0.5 - \varepsilon, 2\varepsilon, 0.5 - \varepsilon)$.

6.3.3   Evidence supporting Conjecture 6.2.2

Recall that Conjecture 6.2.2 claims that for targets that are near the boundary, penultimate points that are also close to the boundary have large gradient norms so that for large populations and small mutation rates, trajectories that bounce off the boundary cannot be optimal. In order to test this claim, we simulated most likely trajectories for 1030 targets using three different parameter sets where the initial histogram is fixed at $(1 - 2\varepsilon, \varepsilon, \varepsilon)$. The targets are shown in Figure 6.15. The only difference among the parameter sets are the growth rate vectors F. The parameters

123

Targets	(0.01, 0.04, 0.95)	(0.025, 0.95, 0.025)	(0.01, 0.95, 0.04)
Time	11	13	13
Cost	0.0163	0.0582	0.0516
Pen. Grad	0.3411	0.2096	0.9858
Grad. Min.	1.07×10^{-6}	4.8×10^{-5}	2.95×10^{-5}

Targets	(0.01, 0.59, 0.4)	(0.3, 0.65, 0.05)	(0.1, 0.45, 0.45)
Time	13	6	10
Cost	0.0124	0.007	0.0053
Pen. Grad	0.2323	0.4306	0.0663
Grad. Min.	2.04×10^{-6}	2.28×10^{-5}	1.82×10^{-6}

Table 6.4: Attributes of the most likely trajectories using the initial histogram $(0.5 - \varepsilon, 2\varepsilon, 0.5 - \varepsilon)$.

are given below.

$$N = 10^6 \qquad\qquad M = mQ$$

$$m = 10^{-6} \qquad\qquad d = 0.002$$

$$FTH = 0.95 \qquad\qquad \varepsilon = 50/N = 5 \times 10^{-5}$$

$$Q = \begin{pmatrix} 0 & 1/2 & 1/2 \\ 0 & 0 & 1 \\ 0 & 0 & 0 \end{pmatrix}$$

The growth vectors used in each simulation, denoted $F^{(1)}, F^{(2)}$, and $F^{(3)}$, respectively, are $F^{(1)} = [200; 200^{1.08}; 200^{1.12}]$, $F^{(2)} = [200; 200^{1.04}; 200^{1.08}]$, and $F^{(3)} = [200; 200^{1.1}; 200^{1.15}]$.

Each round of simulations took approximately an hour to complete. Using 1030 different targets, this implies our method to find most likely trajectories took approximately 3.5 seconds per target, which again provides further evidence of the efficiency of our algorithm. Furthermore, there were no most likely trajectories that bounced
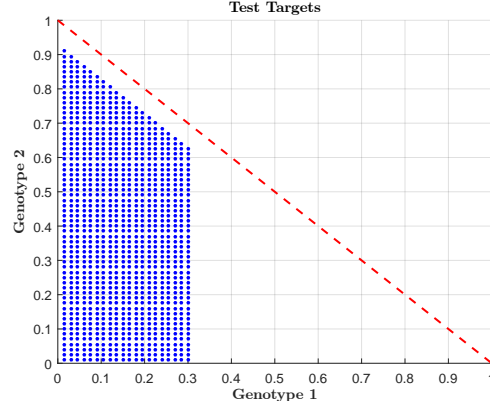
Figure 6.15: The 1030 targets used to test if most likely trajectories bounced off the boundary.

off the boundary. In order to see why this is the case, we will informally analyze the gradient norm $g(y, G)$ when the target is close to the boundary.

Let N be sufficiently large, and without loss of generality let G be a fixed target close to the boundary so that $G(n) \approx 100/N$ for exactly one genotype n. Recall that the norm of the gradient of the one step cost function with respect to the penultimate point is given by

$$
\frac{\partial}{\partial y_n} C(y, G) = \frac{F_n}{\langle F, y \rangle} - \frac{G_n}{y_n} + F_n \sum_k m Q_{n,k}
$$

$$
- \left(F_n + \frac{G_n}{y_n} \right) \sum_k m Q_{n,k} \hat{E}_{n,k} - \frac{G_n}{F_n y_n^2} \sum_k F_k y_k m Q_{k,n} \hat{E}_{k,n}
$$

$$
\hat{E}_{n,k} = \exp \left(-\frac{G_n}{F_n y_n} + \frac{G_k}{F_k y_k} \right)
$$

Without loss of generality, suppose that y is a penultimate point that is also close to the boundary so that $y(j) \approx 100/N$ for exactly one genotype j. Note that it is possible that $n = j$. Notice that $\frac{\partial}{\partial y_n} C(y, G)$ has a zero-order term and term of order m. The term of greatest influence in the terms of order m are the exponential terms

125

$\hat{E}_{n,j}$ and $\hat{E}_{j,n}$. Notice that the zero-order term in m, by our assumption, is of order N. The exponential terms are roughly of order $\exp(N)$. Even when m is small, a term of order $m \exp(N)$ will greatly influence the norm of the gradient. Therefore, the norm of the gradient will roughly have order at least $N + m \exp(N)$ for penultimate points near the boundary. Even if it is the case that $n = j$, we still have that the norm of the gradient will roughly be of order N. Therefore, for targets and penultimate points close to the boundary, the gradient norm is large.

The above argument gives reason why bouncing trajectories are not optimal. When a trajectory approaches the boundary, the gradient norm of the one-step cost is growing very quickly so that one-step costs will also grow very quickly. Consequently, these trajectories become too costly too quickly.

6.3.4 Direct simulation of the system

Using the parameters in the previous section with an initial histogram of $(1-2\varepsilon, \varepsilon, \varepsilon)$, we directly simulate the system to see if we approximately reach any of the six targets that we used for this initial histogram. We expect the system to fixate at genotype 3 eventually. However, since the optimal trajectory that reached $(0.45, 0.01, 0.54)$ has such a low cost, we expect to actually observe realizations that come close to this target. We say that a trajectory approximately reaches a target if there is a time in which the concentration of every genotype is within 0.01 of the target $(0.45, 0.01, 0.54)$. We simulate $10,000$ trajectories for 100 days. The relevant trajectories are given in Figure 6.16.
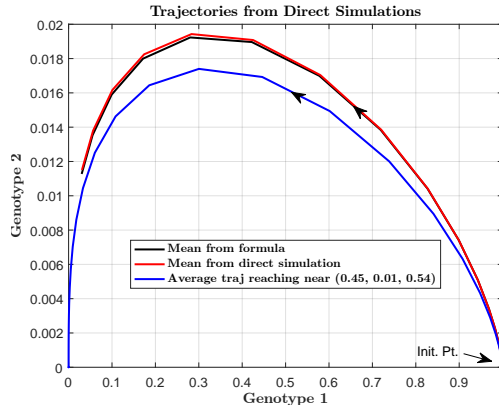
Figure 6.16: Direct simulation of system along with example trajectories.

In Figure 6.16, from the $10,000$ trajectories simulated, 623 approximately reached the target $(0.45, 0.01, 0.54)$. The average of these trajectories is given in blue, which approximately reaches the target on average in 17 days. The cost of the blue trajectory is 5.67×10^{-7}. The optimal trajectory we calculated for this target had 15 steps with a cost of 3.54×10^{-7}. We also see that the mean trajectory from the direct simulation and the mean trajectory we calculated using the conditional expectation are close. Furthermore, the mean trajectory from the direct simulation reached fixation of genotype 3 on day 22, which is precisely the number of steps we had in our mean trajectory. We note that no other targets (other than the fixation target $(0.01, 0.04, 0.95)$) were approximately reached, which is expected since the cost we calculated of such trajectories would give an approximate probability very close to 0.

6.3.5 Concluding analyses

Based on the numerous examples in this section, we have presented a wealth of evidence to support our conjectures. In Conjecture 6.2.1, we see that an increase in

the gradient norm associated to a penultimate point requires a finer discretization in order to obtain a sensible optimal trajectory. This became relevant for targets near the boundary, especially near corner points, as the gradient norm increases as we move towards the boundary, which is the content of Conjecture 6.2.2. In all of the optimal trajectories, even for targets away from the boundary, the penultimate point always involved a relatively small step from the target. Near boundaries and corners, the steps become smaller, which supports the need for very fine discretizations for these targets. Though we would need a very fine discretization for these points, we can adjust for this because having a target located near a corner/boundary reduces the direction in which we can reverse shoot. Thus, when implementing Conjecture 6.2.3, we can be more restrictive when generating our set of penultimate points. Finally, our direct simulation example above suggests that the optimal trajectory we are generating from our scheme is indeed the most likely transition pathway of the system.

Chapter 7

Numerical Examples

A common issue when establishing large deviations principles is implementability. We explicitly applied these principles and developed methods in Chapters 5 and 6 to generate most likely ways in which systems achieve rare events. In order to demonstrate these methods, we will now compute escape trajectories from a neighborhood of a metastable state of the corepressive toggle switch using the approximation given by (2.6). We will also compute most likely evolutionary trajectories when there are 4 genotypes present.

7.1   Corepressive Toggle Switch

Recall that the corepressive toggle switch is given by the chemical langevin equation (2.4), a nonlinear system. Here, we focus on the problem of optimal escape

from neighborhoods of metastable states. We fix a neighborhood of $(x_{\text{low}}, y_{\text{high}})$ (Figure 7.1, black curve) and ask: What is the most likely route of escape from this neighborhood for (2.4)? In Section 2.2.1, we computed a linear noise approximation of (2.4) that is valid near $(x_{\text{low}}, y_{\text{high}})$, which is given by (2.6). Since this linear noise approximation is a Gaussian diffusion with delay, the framework of the present paper applies to it. We use this framework to compute most likely routes of escape for the linear noise approximation and thereby obtain (approximate) most likely routes of escape for (2.4).

In Figure 7.1, we show examples of exit paths directly simulated from the chemical langevin equation. We simulated 1000 trajectories over the time interval $[0, 5]$. We then chose three sample trajectories that exited the disk D and extracted a segment from each of them. The blue, red, and magenta trajectory segments begin near the metastable state (small black disk) at the coordinates $(0.0817, 1.0668)$, $(0.0673, 1.1233)$, and $(0.1272, 1.0733)$, respectively, and cover time intervals $[2.799, 3.399]$, $[3.099, 3.599]$, and $[1.699, 2.299]$. The history of each simulated trajectory over the time interval $[0, 5]$ is taken to be fixed at $(x_{\text{low}}, y_{\text{high}})$ over the time interval $[-\tau, 0]$. Trajectories have been generated using Euler-Maruyama with time step $\Delta t = \tau/1000 = 0.001$. Parameters: $\beta = 0.73$, $k = 0.05$, $\gamma = \ln(2)$, $\tau = 1$, $N = 30$.

We are now in position to apply the large deviations framework of our paper to (2.6). Before doing so, we perform a preliminary numerical calculation and comment on the role of trajectory histories.

We numerically compute the stationary points of (2.5). We work with the parameter set $\beta = 0.73$, $k = 0.05$, $\gamma = \ln(2)$, and $\tau = 1$, a parameter set for which (2.5)
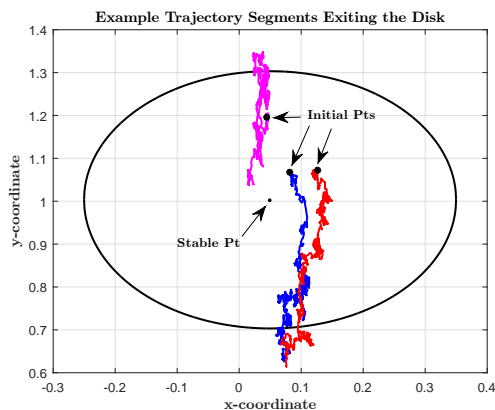
Figure 7.1: Sample trajectory segments of (2.4) in a neighborhood of the metastable state $(x_{\text{low}}, y_{\text{high}})$.

has two stable stationary states and one saddle stationary state. We find these states by setting the drift expressions in (2.5) equal to zero along with $x(t - \tau) = x$ and $y(t - \tau) = y$. Approximate solutions can be found numerically using many well-known iterative methods. The two stable stationary states are approximately $(v, w) \approx (0.0498, 1.0033)$ and $(1.0033, 0.0498)$. The stationary saddle is approximately $(0.3306, 0.3306)$.

Notice that since the Gaussian diffusion (2.6) contains delay, one must specify a trajectory history over the time interval $[-\tau, 0]$ in order to properly initialize the equation. Trajectory history will influence the evolution of the mean of the Gaussian diffusion with delay and will therefore affect the computation of optimal large deviations trajectories. In general, this history may be deterministic or random. For our current study, we work with deterministic histories and take them to be constant on $[-\tau, 0]$. See Figure 7.2 for examples of the evolution of the mean of the Gaussian

131

diffusion using various histories. Finally, note that although the process $\xi(t)$ is Gaussian, it will not be centered if the history is not identically zero. To be consistent with the notation of Section 5.1.1, we write the process that locally approximates the delay chemical Langevin equation as $m(t) + \varepsilon Z_t$, where $m(t) = \mathbb{E}[\xi(t)]$, $\varepsilon = \frac{1}{\sqrt{N}}$, and Z_t satisfies (2.6) with no small parameter ($N = 1$) and history zero.

7.1.1 Optimal escape trajectories and exit points - analysis

We now apply our large deviations framework to the Gaussian diffusion that approximates the delay chemical Langevin equation (2.4) near (v, w). We begin with an analytical view and then follow with numerical simulation.

We find the most likely exit path with constant initial history $m(0)$ that exits the disk

$$D = \left\{ (z_1, z_2) : (z_1 - v)^2 + (z_2 - w)^2 \leqslant R^2 \right\}.$$

(We choose $R = 0.3$ for the numerical computations in Section 7.1.2 so that the neighborhood of (v, w) has size of order one but remains bounded away from the separatrix.) To find this optimal path, we first find the path of least energy that exits D at a preselected point $q \in \partial D$ and at a preselected time T. We then optimize over T and q. For fixed exit time T and exit point $q \in \partial D$, the optimal escape path and associated energy are given by

$$h(s) = \rho(s, T) \left[\rho(T, T)^{-1}(q - m(T)) \right] + m(s)$$

$$\lambda_h(T, q) = \frac{1}{2} \left[\rho(T, T)^{-1}(q - m(T)) \right] \cdot (q - m(T))$$

using (5.4) and (5.5). Here, s ranges over $[0, T]$ and $\rho(s, t)$ is the covariance matrix of Z_t at times $s, t \in [0, T]$. Note that we are using the terms "exit time" and "escape path" loosely since we do not impose the *a priori* condition that h remain inside D until it reaches q at time T.

In order to optimize over q and T, we first fix T and optimize $\lambda_h(T, q)$ over points $q \in \partial D$. Notice that $\lambda_h(T, q)$ is a classical quadratic form on $\mathbb{R}^2$ for fixed T, so we apply standard minimization techniques to find the minimizer $\hat{q}(T)$ analytically. The minimization problem for fixed T is

$$\min_q \lambda_h(T, q) \quad \text{subject to} \quad (q_1 - v)^2 + (q_2 - w)^2 = R^2. \tag{7.1}$$

Using a Lagrange multiplier $\mu \in \mathbb{R}$, define the Lagrangian

$$L_\mu(q) := \lambda_h(T, q) - \mu((q_1 - v)^2 + (q_2 - w)^2 - R^2).$$

Calculating the gradient $\nabla_q(L_\mu(q))$ and setting the gradient equal to zero yields the equation

$$\rho(T, T)^{-1}(q - m(T)) = 2\mu(q - (v, w)^*). \tag{7.2}$$

Notice that if $m(T) = (v, w)^*$, then (7.2) becomes an eigenvalue problem for $\rho(T, T)^{-1}$. In this case, the optimal exit point $\hat{q}(T)$ is such that $\hat{q}(T) - (v, w)^*$ is the eigenvector of $\rho(T, T)^{-1}$ corresponding to the smallest eigenvalue, and the energy of the optimal path that exits D at time T is proportional to this smallest eigenvalue.

This observation has two implications. First, if the history of the linear noise process is taken to be $m(t) = (v, w)^*$ on $[-\tau, 0]$, then we will have $m(t) = (v, w)^*$

133

for all $t \geqslant 0$ as well. In this case, minimizing $\lambda_h(T, q)$ over T and q to find the optimal escape time T_{opt} and the optimal escape point $\hat{q}(T_{\mathrm{opt}})$ amounts to minimizing the smallest eigenvalue of $\rho(T, T)^{-1}$ over T. Since (2.6) is essentially an Ornstein-Uhlenbeck process with delay, we expect the smallest eigenvalue of $\rho(T, T)^{-1}$ to decrease monotonically toward a limiting value as $T \to \infty$. See Figure 7.4 for numerical evidence. There exists no minimizer of $\lambda_h(T, q)$ in this case, as we would have $T_{\mathrm{opt}} = \infty$.

Second, regardless of the initial history of the linear noise process, $m(T) \to (v, w)^*$ as $T \to \infty$ for the parameters we have selected. Consequently, (7.2) is approximately an eigenvalue problem for large values of T, so for such T the optimal exit point $\hat{q}(T)$ will be such that $\hat{q}(T) - (v, w)^*$ is close to the eigenvector of $\rho(T, T)^{-1}$ corresponding to the smallest eigenvalue.

7.1.2 Numerical results

We compute the optimal path of escape, the optimal exit time T_{opt}, and the optimal exit point $\hat{q}(T_{\mathrm{opt}}) \in \partial D$ for the linear noise process (2.6) that approximates the toggle switch (2.4) in the disk D. Along the way, we discuss interesting related computations.

Parameter selection. We set $\beta = 0.73$, $k = 0.05$, $\gamma = \ln(2)$, and $\tau = 1$ for the toggle switch. System size for the linear noise approximation (2.6) is $N = 1000$. The history of the linear noise process is taken to be the constant position $(0.0453, 1.1323)$ over the time interval $[-\tau, 0]$. We choose $R = 0.3$ for the radius of D so that this

134

neighborhood of (v, w) has size of order one but remains bounded away from the separatrix.

Optimization algorithm. To compute the optimal escape path, exit time, and exit point, we execute the following algorithm.

- Simulate the mean and covariance equations for a sufficiently large T_{large} using step sizes $\Delta t = \Delta s = \tau/500$.

- Discretize the boundary of the disk D using discretization $\Delta r = 0.006$ of $[-R, R]$.

- For each time $t_j = (j - 1)\Delta t \in [0, T_{\text{large}}]$ and each point q_k on the discretized boundary of the disk, compute the optimal trajectory that exits at time t_j through q_k as well as the energy $E_{j,k}$ of this trajectory.

- Minimize over the entries of the matrix E in order to find the optimal exit time and exit point (and hence the overall optimal path of escape).

Mean and covariance. We first compute the mean and covariance of the linear noise process. Figure 7.2 (blue curves) illustrates the evolution of the mean for our parameter set. As expected, the mean converges to the stationary state (v, w) (moved to $(0, 0)$ in Figure 7.2) regardless of the history of the mean. It is important to choose T_{large} sufficiently large so that the covariance matrix $\rho(T_{\text{large}}, T_{\text{large}})$ has stabilized and the mean is close to the stationary state. Fig. 7.3 and Fig. 7.4 provide evidence that this stabilization occurs by time $T = 20$ for our parameter set. In particular, the variances of the two components of Z_t stabilize to the vectory $(0.0567, 1.1409)$ by time

135
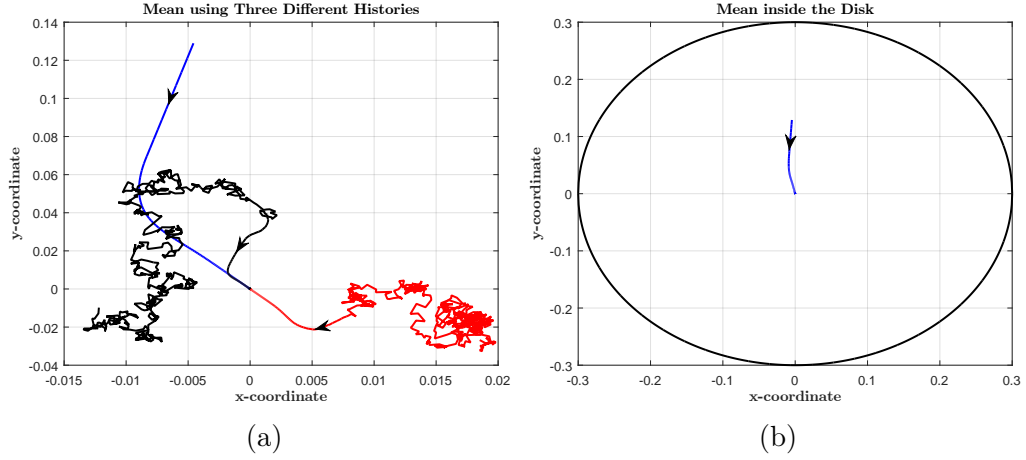
Figure 7.2: Evolution of the mean of the linear noise process. **(7.2a)** Blue curve: evolution of the mean using the constant history $(0.0453, 1.1323)$ (or $(-0.0046, 0.1289)$ in local coordinates). Red and black curves: evolution of the mean using trajectory segments of (2.4) for histories. **(7.2b)** Another view of the blue curve from Fig. 7.2a.

20 (Fig. 7.3). Fig. 7.4 illustrates that the smallest eigenvalue of $\rho(t,t)^{-1}$ stabilizes as well to 0.874.

Numerical optimization results.

We first examine the behavior of optimal paths and optimal path energies for fixed exit times. Fig. 7.5a illustrates the behavior of optimal path energy as a function of exit point over the upper half of ∂D for the fixed exit time $T = 10$. Note that optimal path energy is minimized near the top of ∂D. Fig. 7.5c depicts three different optimal escape paths for fixed escape time $T = 20$ and three different exit points. Notice that these trajectories follow the mean for some time before breaking away toward their respective exits. This behavior should not occur for the optimal exit time T_{opt} and the optimal exit point $\hat{q}(T_{\text{opt}})$. Energy values associated with the red, magenta, and blue trajectories are 0.0413, 0.4527, and 0.4661, respectively. Fig. 7.5d (blue
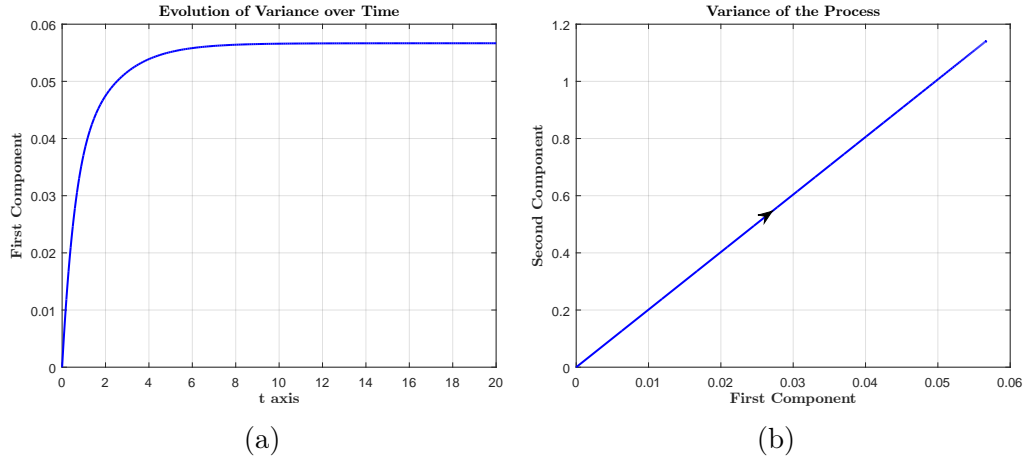
Figure 7.3: Evolution of the variances of the two components of Z_t over time. **(7.3a)** The variance of the first component. **(7.3b)** Linear relationship between variances of the first and second components.

curve) illustrates the overall optimal escape trajectory. This trajectory exits at time $T_{\text{opt}} = 1.482$ and exit point $\hat{q}(T_{\text{opt}}) = (0.0384, 1.3031)$ with energy 0.0348. Observe that the overall optimal escape trajectory diverges from the mean immediately.

Fig. 7.6 depicts overall optimal escape trajectories using three different constant initial histories. Notice that if the initial history is located in the lower half of D, then the overall optimal escape trajectory exits through the lower half of ∂D. This happens for the upper half of D as well. This behavior is natural, since moving 'across' the stationary state should not be energetically optimal. For the initial history corresponding to the blue curve in Fig. 7.6, the optimal escape path that exits through the bottom half of ∂D does so through $(0.0162, -0.2996)$ (in local coordinates) at exit time ∞ with energy 0.0394. This energy is strictly larger than that of the blue curve in Fig. 7.6 (0.0348). The energy associated with the red, magenta, and blue trajectories is 0.0389, 0.0074, and 0.0348, respectively.

137
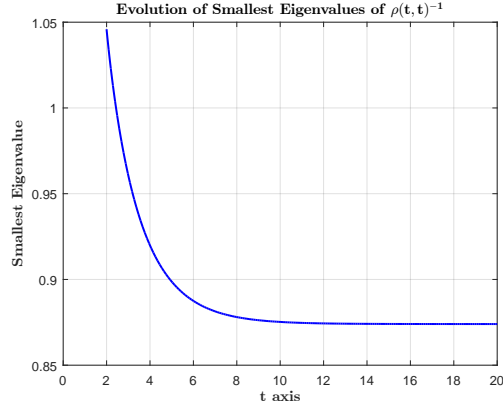
Figure 7.4: The smallest eigenvalue of the covariance matrix $\rho(t,t)^{-1}$ stabilizes to approximately 0.874 by time 20.

7.2   E. Coli Populations with 4 Genotypes

Generating the entire state space for higher dimensional problems $(g \geq 4)$ become computationally heavy even for moderate discretizations. In fact, for a given discretization level d and number of genotypes g, the state space of histograms will contain $\begin{pmatrix} 1/d + g - 1 \\ g - 1 \end{pmatrix}$ different histograms, which is of order $(1/d)^{g-1}$. Consequently, generating one optimal trajectory reaching a fixed target could take many hours to find. We will show the significant save in computation time with 4 genotypes using the target histograms $(0.02, 0.03, 0.9, 0.05)$, $(0.02, 0.9, 0.03, 0.05)$, and $(0.1, 0.4, 0.45, 0.05)$. The system parameters are given below:
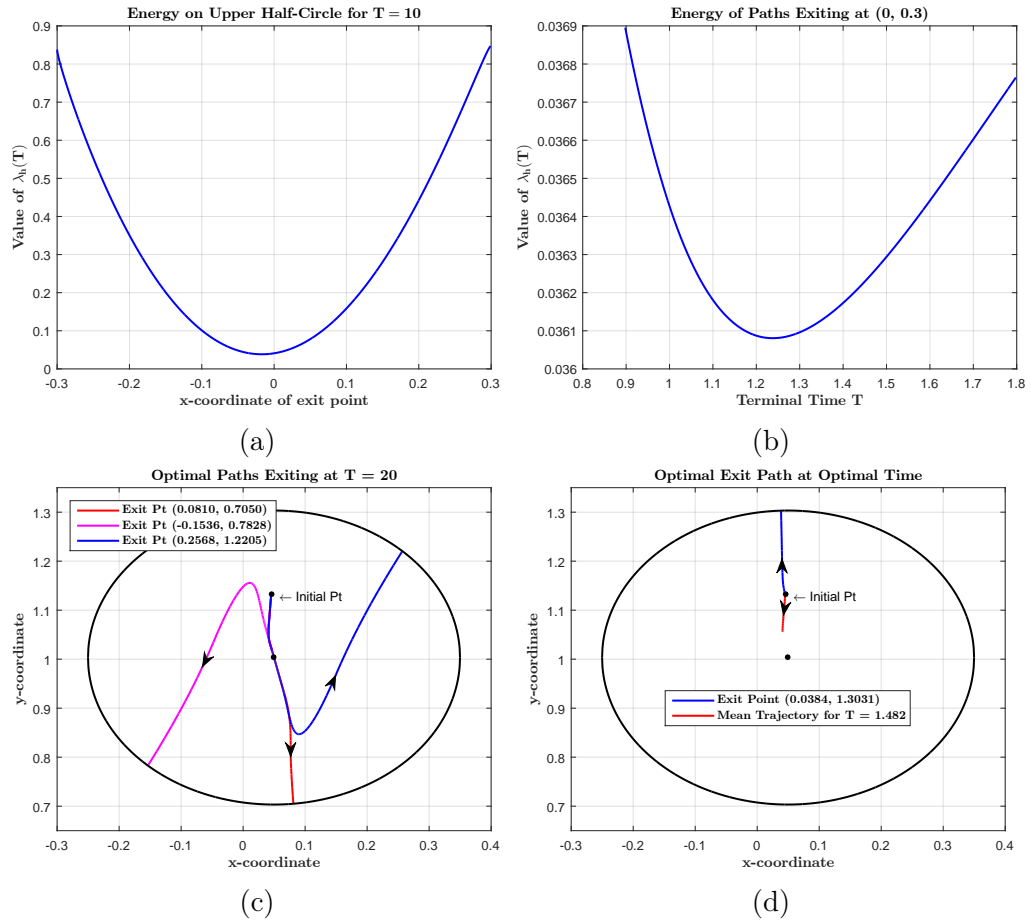
Figure 7.5: Optimal exit data. **(7.5a)** Energy of the optimal exit path at time $T = 10$ as a function of chosen exit point on the upper half of ∂D. The energy is minimized near the top of D. **(7.5b)** Energy of the optimal exit path as a function of exit time T for fixed exit point $(0, 0.3)$ (the top of D in local coordinates). **(7.5c)** Three different optimal escape paths for fixed escape time $T = 20$ and three different exit points. **(7.5d)** Overall optimal escape trajectory.

139
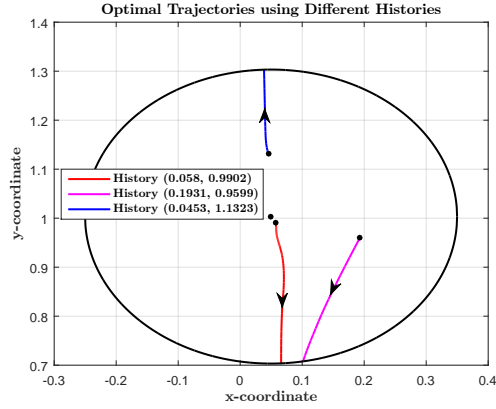
Figure 7.6: Optimal escape trajectories from D for the linear noise process using three different constant initial histories.

$$N = 10^6 \qquad\qquad\qquad \varepsilon = 50/N = 5 \times 10^{-5}$$

$$F_1 = 200 \qquad\qquad\qquad F_2 = 200^{1.06}$$

$$F_3 = 200^{1.08} \qquad\qquad\qquad F_4 = 200^{1.12}$$

$$M = mQ \qquad\qquad\qquad m = 10^{-6}$$

$$Q = \begin{pmatrix} 0 & 1/3 & 1/3 & 1/3 \\ 0 & 0 & 1/2 & 2/3 \\ 0 & 0 & 0 & 1 \\ 0 & 0 & 0 & 0 \end{pmatrix} \qquad\qquad d = 0.002$$

$$FTH = 0.95 \qquad\qquad \text{Initial Histogram} = (1 - 3\varepsilon, \varepsilon, \varepsilon, \varepsilon)$$

Using these parameters, the number of histograms in the discretized state space is approximately 21 million, which would take hours to generate assuming one had sufficient memory to hold this amount of data. The optimal trajectories are shown in Figures 7.7-7.9. The trajectories, respectively, were generated in approximately

140
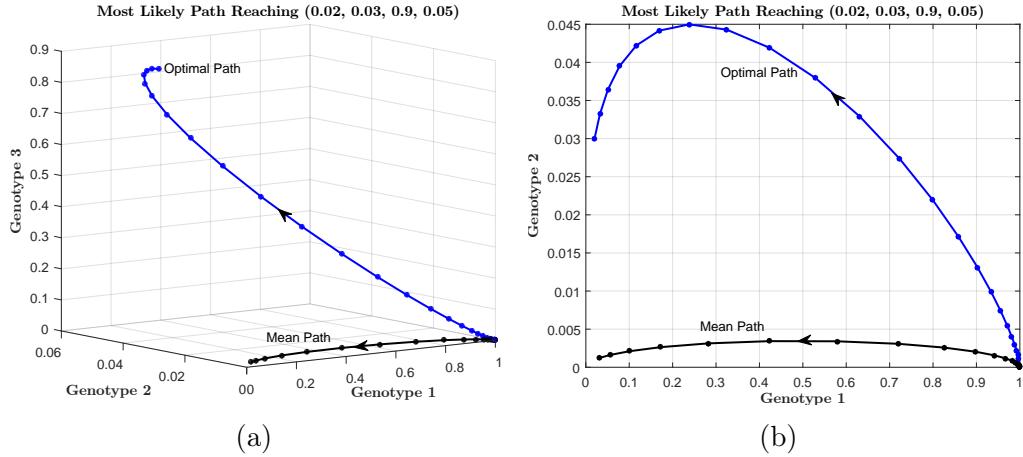
Figure 7.7: The optimal trajectory reaching the given target and the mean trajectory with $g = 4$. The left panel is the projection of these trajectories to the first three genotypes. The right panel is the projection of these trajectories to the first two genotypes.

1.5 minutes, 13 minutes, and 6.5 minutes. For all three examples, we generated the set of possible penultimate points using a gradient threshold of 0.5. By doing so in each of the three examples, the number of histograms in each of the penultimate sets make up only $0.01\%, 0.01\%$, and 0.06% of the entire discretized space of histograms, respectively. Furthermore, the size of these sets did not grow significantly when computing optimal trajectories for $g = 3$ and $g = 4$. This is the main factor contributing to computational efficiency.

In Figure 7.7, the mean trajectory has 22 steps, and the most likely trajectory reaching $(0.02, 0.03, 0.9, 0.05)$ has 26 steps with a cost of 0.001. The penultimate point that generates the optimal trajectory is $(0.032, 0.033, 0.894, 0.040)$. This trajectory reaches the initial zone in reverse time.

In Figure 7.8, the optimal trajectory has 16 steps with a cost of 0.0067. Notice
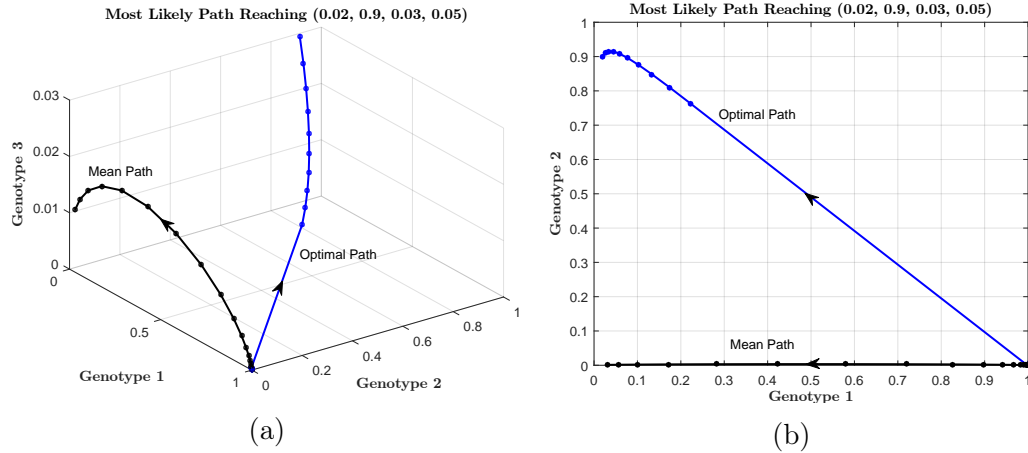
141

Figure 7.8: The optimal trajectory reaching the given target and mean trajectory with $g = 4$. The left panel is the projection of these trajectories to the first three genotypes. The right panel is the projection of the trajectories to the first two genotypes.

that the optimal trajectory makes a large jump from the mean point $(0.9981, 2.45 \times 10^{-4}, 4.16 \times 10^{-4}, 0.0012)$ to the point $(0.2331, 0.7624, 0.0020, 0.0125)$ generated from the reverse trajectory using the penultimate point $(0.02574, 0.91031, 0.02523, 0.03872)$. In particular, it is less costly to make a large jump than to bounce off the boundary.

In Figure 7.9, the optimal trajectory has 25 steps with a cost of 0.0016. The penultimate point that generates the optimal trajectory is $(0.14243, 0.406767, 0.41362, 0.03718)$, which results in a trajectory that reached the initial zone in reverse time.

7.2.1 Brief analysis and prediction for higher dimensions

As stated in Section 1.1, the future goal is to apply these large deviations techniques to analyze genotypic data gathered by Dr. Tim Cooper and Dr. Robert Azevedo in the Biology Lab at the University of Houston which involves at most $g = 8$
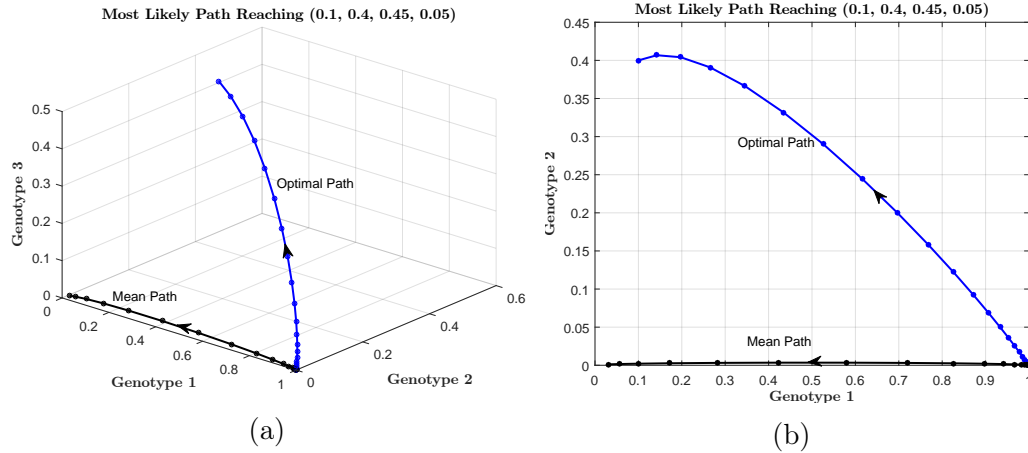
Figure 7.9: The optimal reaching the given target and mean trajectory with $g = 4$. The left panel is the projection of the trajectories to the first three genotypes. The right panel is the projection of the trajectories to the first two genotypes.

genotypes, which will appear in a later paper. We can however do a rough analysis on what we can expect based on our examples for 3 and 4 genotypes. Generating the set of penultimate points for $g = 8$ would not introduce a significant increase in computation time since it is related to the norm of the gradient and not directly to the number of genotypes and the dimension of the space. Generating the sets of penultimate points for $g = 3$ was nearly instantaneous, and generating the set for $g = 4$ took about $3 - 4$ seconds. Therefore, generating a sensible set of penultimate points should be computationally viable for 8 genotypes. However, this may yield a large amount of penultimate points. In addition, since we may need to use our multi-stage approach in order to obtain the optimal trajectory, filtering through the trajectories generated from the penultimate set may require a lengthy computation.

Now, notice that in the cases of $g = 3$ and $g = 4$, the length of the mean trajectory was 22 steps. We expect that the mean using similar initial points in higher

dimensions will have roughly the same number of steps. The optimal trajectories became slightly longer when increasing dimension, which may have some relation to the additon of a genotype in the population. Therefore, we would expect an increase in dimension to cause an increase in the length of optimal trajectories. However, it is reasonable to predict that optimal trajectories will not be significantly longer than the mean trajectory. The large deviations principle we have established states that as $N \to \infty$, the Markov chain trajectory will converge to the mean trajectory. This mean trajectory fixates at the strongest genotype exponentially quickly. Therefore, for a rare event to reasonably occur, we would expect it to happen relatively quickly. Finally, none of the optimal trajectories we generated bounced off the boundary. As stated in our conjectures, we would then expect that no optimal trajectories would require bouncing off the boundary. With this rather rough discussion in mind, we fully expect to be able to implement this method using at most 8 genotypes.

Chapter 8

Conclusions and Future Work

We have seen that large deviations principles and concepts can be used to derive quantitative information for a given stochastic model that would be otherwise difficult to observe directly through experimentation or simulation. Namely, one can derive most likely ways in which systems can achieve rare events along with estimations on the probabilities that these events can occur. In addition, the area of large deviations raises many interesting questions and problems in both theory and applications. On one hand, if one desires to use large deviations techniques on a particular system, a large deviations principle would need to be established first. This would involve many classical theoretical concetps. On the other hand, once a principle is established, implementation and application of this principle requires clever and efficient algorithms in order to calculate rare events. One hopeful direction of future work is to apply large deviations techniques to other systems of interest in biology.

Even though we have successfully applied and implemented large deviations principles for the two systems in this dissertation, there are still many interesting problems to address in future work. For Gaussian diffusions with delay, we calculated optimal trajectories for a fixed delay. With the importance of delay in biochemical systems, we would like to better understand the influence of delay on optimal transitions. We would also like to address the accuracy of the linear noise approximation we used in locally modeling the corepressive toggle switch. In addition, if better approximations arise, can we develop a large deviations framework for this better approximation which roughly mirrors our work in this dissertation?

For genetic evolution of bacterial populations, we implemented the large deviations principles for three and four genotypes. Naturally, we would like to extend this to more genotypes with the ideal case being $g = 8$. This is certainly a nontrivial extension that would raise questions involving computation times and implementation. This would more than likely require parallel processing.

Bibliography

[1] E. Aurell and K. Sneppen. Epigenetics as a first exit problem. *Phys Rev Lett*, 88:048101, 2002.

[2] R. Azencott, M. I. Freidlin, and S. R. S. Varadhan. *Large deviations at Saint-Flour*. Probability at Saint-Flour. Springer, Heidelberg, 2013.

[3] C. T. H. Baker and E. Buckwar. Numerical analysis of explicit one-step methods for stochastic delay differential equations. *LMS J. Comput. Math.*, 3:315–335 (electronic), 2000.

[4] N. Q. Balaban, J. Merrin, R. Chait, L. Kowalik, and S. Leibler. Bacterial persistence as a phenotypic switch. *Science*, 305:1622–1625, 2004.

[5] A. Bellen and M. Zennaro. *Numerical methods for delay differential equations*. Numerical Mathematics and Scientific Computation. The Clarendon Press, Oxford University Press, New York, 2003.

[6] F. Bouchet, T. Grafke, T. Tangarife, and E. Vanden-Eijnden. Large deviations in fast-slow systems. *J. Stat. Phys.*, 162(4):793–812, 2016.

[7] F. Bouchet, J. Laurie, and O. Zaboronski. Langevin dynamics, large deviations and instantons for the quasi-geostrophic model and two-dimensional Euler equations. *J. Stat. Phys.*, 156(6):1066–1092, 2014.

[8] T. Brett and T. Galla. Stochastic processes with distributed delays: Chemical langevin equation and linear-noise approximation. *Physical Review Letters*, 110(25), 2013.

[9] T. Çağatay, M. Turcotte, M. Elowitz, J. Garcia-Ojalvo, and G. Süel. Architecture-dependent noise discriminates functionally analogous differentiation circuits. *Cell*, 139(3):512–522, 2009.

[10] H. Chernoff. A measure of asymptotic efficiency for tests of a hypothesis based on the sum of observations. *Ann. Math. Statistics*, 23:493–507, 1952.

[11] T. F. Cooper, S. K. Remold, R. E. Lenski, and D. Schneider. Expression profiles reveal parallel evolution of epistatic interactions involving the crp regulon in escherichia coli. *PLoS Genet*, 4(2):e35, 2008.

[12] T. F. Cooper, D. E. Rozen, and R. E. Lenski. Parallel changes in gene expression after 20,000 generations of evolution in escherichia coli. *Proceedings of the National Academy of Sciences*, 100(3):1072–1077, 2003.

[13] H. Cramér. Sur un nouveau théoreme-limite de la théorie des probabilités. *Actualités scientifiques et industrielles*, 736(5-23):115, 1938.

[14] C. Davidson and M. Surette. Individuality in bacteria. *Annual Review of Genetics*, 42:253–268, 2008.

[15] E. Dupin, C. Real, C. Glavieux-Pardanaud, P. Vaigot, and N. M. Le Douarin. Reversal of developmental restrictions in neural crest lineages: Transition from schwann cells to glial-melanocytic precursors in vitro. *Proceedings of the National Academy of Sciences*, 100(9):5229–5233, 2003.

[16] A. Eldar and M. Elowitz. Functional roles for noise in genetic circuits. *Nature*, 467(7312):167–173, 2010.

[17] M. I. Freidlin and A. D. Wentzell. *Random perturbations of dynamical systems*, volume 260 of *Grundlehren der Mathematischen Wissenschaften [Fundamental Principles of Mathematical Sciences]*. Springer, Heidelberg, third edition, 2012. Translated from the 1979 Russian original by Joseph Szücs.

[18] T. S. Gardner, C. R. Cantor, and J. J. Collins. Construction of a genetic toggle switch in *Escherichia coli*. *Nature*, 403(6767):339–342, 2000.

[19] N. Guglielmi. Delay dependent stability regions of Θ-methods for delay differential equations. *IMA J. Numer. Anal.*, 18(3):399–418, 1998.

[20] C. Gupta, J. M. López, R. Azencott, M. R. Bennett, K. Josić, and W. Ott. Modeling delay in genetic networks: From delay birth-death processes to delay stochastic differential equations. *J Chem Phys*, 140:204108, 2014.

[21] E. He, O. Kapuy, R. A. Oliveira, F. Uhlmann, J. J. Tyson, and B. Novák. Systems-level feedbacks make the anaphase switch irreversible. *Proc Natl Acad Sci USA*, 108:10016–10021, 2011.

[22] M. Hegreness, N. Shoresh, D. Hartl, and R. Kishony. An equivalence principle for the incorporation of favorable mutations in asexual populations. *Science*, 311(5767):1615–1617, 2006.

[23] D. J. Higham. An algorithmic introduction to numerical simulation of stochastic differential equations. *SIAM Rev.*, 43(3):525–546 (electronic), 2001.

[24] T. Hong, J. Xing, L. Li, and J. J. Tyson. A simple theoretical framework for understanding heterogeneous differentiation of cd4$^+$ t cells. *BMC Syst Biol*, 6:66, 2012.

[25] T. B. Kepler and T. C. Elston. Stochasticity in transcriptional regulation: origins consequences, and mathematical representations. *Biophys J*, 81:3116–3136, 2001.

[26] R. Korona, C. H. Nakatsu, L. J. Forney, and R. E. Lenski. Evidence for multiple adaptive peaks from populations of bacteria evolving in a structured habitat. *Proceedings of the National Academy of Sciences*, 91(19):9037–9041, 1994.

[27] R. E. Lenski and M. Travisano. Dynamics of adaptation and diversification: a 10,000-generation experiment with bacterial populations. *Proceedings of the National Academy of Sciences*, 91(15):6808–6814, 1994.

[28] D. G. Luenberger. *Optimization by vector space methods.* John Wiley & Sons, Inc., New York-London-Sydney, 1969.

[29] H. Maamar and D. Dubnau. Bistability in the bacillus subtilis k-state (competence) system requires a positive feedback loop. *Molecular Microbiology*, 56(3):615–624, 2005.

[30] H. Maamar, A. Raj, and D. Dubnau. Noise in gene expression determines cell fate in bacillus subtilis. *Science*, 317(5837):526–529, 2007.

[31] X. Mao. *Stochastic differential equations and their applications.* Horwood Publishing Series in Mathematics & Applications. Horwood Publishing Limited, Chichester, 1997.

[32] X. Mao and S. Sabanis. Numerical solutions of stochastic differential delay equations under local Lipschitz condition. *J. Comput. Appl. Math.*, 151(1):215–227, 2003.

[33] J. C. Meeks, E. L. Campbell, M. L. Summers, and F. C. Wong. Cellular differentiation in the cyanobacterium nostoc punctiforme. *Archives of Microbiology*, 178(6):395–403, 2002.

[34] D. Nevozhay, R. M. Adams, E. Van Itallie, M. R. Bennett, and G. Balázsi. Mapping the environmental fitness landscape of a synthetic gene circuit. *PLoS Comp Biol*, 8:e1002480, 2012.

[35] E. M. Ozbudak, M. Thattai, H. N. Lim, B. I. Shraiman, and A. van Oudenaarden. Multistability in the lactose utilization network of *Escherichia coli. Nature*, 427:737–740, 2004.

[36] S. H. Rice. *Evolutionary theory: mathematical and conceptual foundations*. Sinauer Associates Sunderland, MA, 2004.

[37] G. Süel, R. Kulkarni, J. Dworkin, J. Garcia-Ojalvo, and M. Elowitz. Tunability and noise dependence in differentiation dynamics. *Science*, 315(5819):1716–1719, 2007.

[38] G. M. S uel, J. Garcia-Ojalvo, L. M. Liberman, and M. B. Elowitz. An excitable gene regulatory circuit induces transient cellular differentiation. *Nature*, 440:545–550, 2006.

[39] A. Veliz-Cuba, C. Gupta, M. R. Bennett, K. Josić, and W. Ott. Effects of cell cycle noise on excitable gene circuits. arXiv:1605.09328, 2016.

[40] P. B. Warren and P. R. ten Wolde. Chemical models of genetic toggle switches. *J Phys Chem B*, 109:6812–6823, 2005.

[41] W. Zhang, V. Sehgal, D. M. Dinh, R. B. Azevedo, T. F. Cooper, and R. Azencott. Estimation of the rate and effect of new beneficial mutations in asexual populations. *Theoretical population biology*, 81(2):168–178, 2012.